Stability and dynamics of chiral magnetic structures in ferro- and antiferromagnets

Mariia N. Potkina

Faculty of Physical Sciences
University of Iceland
2022

Stability and dynamics of chiral magnetic structures in ferro- and antiferromagnets

Mariia N. Potkina

Dissertation submitted in partial fulfillment of a
Philosophiae Doctor degree in Chemistry

Advisor
Prof. Hannes Jónsson

PhD Committee
Prof. Hannes Jónsson
Prof. Valery M. Uzdin
Dr. Pavel F. Bessarab

Opponents
Dr. Gísli Hólmar Jóhannesson
Prof. Sergei Egorov

Faculty of Physical Sciences
School of Engineering and Natural Sciences
University of Iceland
Reykjavik, April 2022

Stability and dynamics of chiral magnetic structures in ferro- and antiferromagnets
Chiral magnetic structures
Dissertation submitted in partial fulfillment of a *Philosophiae Doctor* degree in Chemistry

Faculty of Physical Sciences
School of Engineering and Natural Sciences
University of Iceland
Dunhaga 5
107, Reykjavik
Iceland

Telephone: 525-4700

Bibliographic information:
Mariia N. Potkina, 2022, *Stability and dynamics of chiral magnetic structures in ferro- and antiferromagnets*, PhD dissertation, Faculty of Physical Sciences, University of Iceland, 104 pp.

ISBN 978-9935-9630-2-4

Printing: Háskólaprent
Reykjavik, Iceland, April 2022

Abstract

Reduction of the size of magnetic bits for data storage, transfer and processing of information down to the nanoscale would lay the foundation for large advances in information technology, both in terms of processing speed and energy efficiency. Such a development requires analysis of the stability of localized magnetic states with respect to thermal fluctuations and random external influences. In the dissertation, these issues are investigated in the framework of harmonic transition state theory. The lifetime of skyrmions and antiskyrmions, two examples of chiral magnetic structures, is calculated using various values of materials parameters, such as the ratio of the lattice constant to the skyrmion size. The energy barrier for skyrmion collapse is found to approach the Belavin-Polyakov lower bound of the energy of a topological soliton in the σ-model, and the entropy contribution to the pre-exponential factor in the Arrhenius rate expression for the lifetime is found to approach a constant. As a result, the skyrmion lifetime can, for large enough number of spins, correspond to thermal stability at room temperature even without magnetic dipole–dipole interaction. Calculations of skyrmions in antiferromagnets are also presented, and their properties compared with skyrmions in corresponding ferromagnets. The rates of skyrmion collapse and escape through the boundary of a track, as well as the binding to and collapse at a non-magnetic impurity, are calculated as a function of an applied magnetic field. The lifetime of antiskyrmions in an Mn–Pt–Sn tetragonal Heusler material has been calculated using an atomic scale representation including nearly a million spins. The long lifetime observed experimentally at room temperature is found to result from energetic effects rather than entropic effects in this system. The properties of antiskyrmions in ferromagnetic and antiferromagnetic thin films are analyzed using an energy conserving transformation of skyrmion spin configuration and vectors in the extended Heisenberg Hamiltonian. The dynamics as well as thermal stability of antiskyrmions and corresponding skyrmions can easily be compared using the transformation.

Útdráttur

Smækkun seguleininga fyrir gagnageymslu leggur grunninn að miklum framförum í upplýsingatækni, bæði hvað varðar hraða og orkunotkun. Slík þróun krefst greiningar á stöðugleika staðbundinna segulástanda með tilliti til varmaorku og tilviljunarkenndra utanaðkomandi áhrifa. Í ritgerðinni eru þessi atriði rannsökuð með því að nota virkjunarástandskenninguna innan kjörsveifilsnálgunarinnar. Líftími skyrmeinda er reiknaður út fyrir ýmis gildi á hlutfallinu milli grindarfastans og stærðar skyrmeindarinnar. Orkuþröskuldurinn fyrir eyðingu skyrmeindar nálgast Belavin-Polyakov neðri mörk á orku stakeindar í σ-líkaninu og óreiðuframlagið til forveldisstuðulsins í Arrhenius líkingunni stefnir á fasta. Þar af leiðandi Líftími skyrmeindar getur skrymeind verið nægjanlega stöðug við stofuhita ef hún samanstendur af nægjanlega stórum fjölda spuna, jafnvel þótt tvískauts-tvískauts víxlverkun sé ekki tekin með í reikninginn. Gerðir eru útreikningar á skyrmeindum í andseglandi efnum og eiginleikar þeirra bornir saman við skyrmeindir í samseglandi efnum. Hraðafastinn fyrir eyðingu skyrmeindar inni í efninu, sem og brotthvarf skyrmeindar í gegnum jaðra segulefnisins og binding við óseglandi óhreinindi, er reiknaður sem fall af álögðu segulsviði. Líftími andskyrmeinda við stofuhita í Mn–Pt–Sn Heusler efni hefur verið reiknaður út með því að nota atómskala líkan sem inniheldur næstum milljón spuna. Niðurstöður reikninganna sýna að sá langi líftími sem hefur verið ákvarðaður með mælingum á tilraunastofu stafar af hárri virkjunarorku frekar en entrópíuáhrifum í þessu kerfi. Eiginleikar andskyrmeinda í samseglandi og andseglandi þunnum húðum eru greindir með vörpun á spunavigrum og útvíkkuðum Heisenberg Hamilton virkja. Auðvelt er að bera saman færslueiginleika sem og varmafræðilegan stöðugleika andskyrmeinda og samsvarandi skyrmeinda með þessari vörpun.

Table of Contents

List of Figures

List of Original Articles

Articles included in this thesis:

Article I: Potkina M. N., Lobanov I. S., Jónsson H., Uzdin V. M., 2022, Lifetime of skyrmions in discrete systems with infinitesimal lattice constant, *JMMM* **549**, *168974.*

Article II: Potkina M. N., Lobanov I. S., Jónsson H., Uzdin V. M., 2020, Skyrmions in antiferromagnets: Thermal stability and the effect of external field and impurities, *J. Appl. Phys.* **127**, *213906.*

Article III: Potkina M. N., Lobanov I. S., Tretiakov O. A., Jónsson H., Uzdin V. M., 2020, Stability of long-lived antiskyrmions in the Mn-Pt-Sn tetragonal Heusler material, *Phys. Rev. B* **102**, *134430.*

Other articles published during PhD study but not included in this thesis:

Article IV: Lobanov I. S., Potkina M. N., Jónsson H., Uzdin V. M., 2017, Truncated minimum energy path method for finding first order saddle points, *Nanosystems: Physics, Chemistry, Mathematics* **8(5)**, *586.*

Article V: Uzdin V. M., Potkina M. N., Lobanov I. S., Bessarab P. F., Jónsson H., 2018, The effect of confinement and defects on the thermal stability of skyrmions, *Phys. B: Condens. Matter* **549**, *6.*

Article VI: Uzdin V. M., Potkina M. N., Lobanov I. S., Bessarab P. F., Jónsson H., 2018, Energy surface and lifetime of magnetic skyrmions, *JMMM* **459**, *236.*

Article VII: Varentsova A. S., Potkina M. N., von Malottki S., Heinze S., Bessarab P. F., 2018, Interplay between size and stability of magnetic skyrmions, *Nanosystems: Physics, Chemistry, Mathematics* **9(3)**, *356.*

Article VIII: Denisov K. S., Rozhansky I. V., Potkina M. N., Lobanov I. S., Lähderanta E., Uzdin V. M., 2018, Topological Hall effect for electron scattering on nanoscale skyrmions in external magnetic field, *Phys. Rev. B* **98**, *214407.*

Article IX: Vlasov S. M., Bessarab P. F., Lobanov I. S., Potkina M. N., Uzdin V. M., Jónsson H., 2020, Magnetic skyrmion annihilation by quantum mechanical tunneling, *New J. Phys.* **22**, *083013.*

Article X: Varentcova A. S., von Malottki S., Potkina M. N., Kwiatkowski G., Heinze S., Bessarab P. F., 2020, Toward room-temperature nanoscale skyrmions in ultrathin films, *npj Comput. Mater.* **6**, *193.*

Article XI: Potkina M. N., Lobanov I. S., Uzdin V.M., 2020, Nonmagnetic impurities in skyrmion racetrack memory, *Nanosystems: Physics, Chemistry, Mathematics* **11(6)**, *628.*

Article XII: Potkina M. N., Lobanov I. S., Uzdin V.M., 2020, Fine energy structure of a magnetic skyrmion localized on a nonmagnetic impurity in an external magnetic field, *Phys. Compl. Syst.* **1(4)**, *165.*

Article XIII: Lobanov I. S., Potkina M. N., Uzdin V.M., 2021, Stability and Lifetimes of Magnetic States of Nano-and Microstructures (Brief Review), *JETP Lett.* **113**, *801.*

Acknowledgments

First of all, I would like to thank Prof. Hannes Jónsson for supervision, support and helpful discussions on my thesis work. It was my great fortune to work with him. I also thank Prof. Valery Uzdin, Dr. Igor Lobanov and Dr. Pavel Bessarab for friutfull collaboration. I would also like to extend my thanks to my parents for supporting me during my PhD study.

1 Introduction

The internal structure, dynamics, and stability of magnetic states are the most important problems of fundamental nanomagnetism and new technologies in spintronics. Here, fundamental problems are a decrease in the characteristic sizes of magnetic elements, an increase in the rate of magnetic recording and information transfer, and energy efficiency of developed systems. The operation of any device based on magnetic materials is accompanied by magnetization reversal processes and changes in the magnetic states of a system as a whole or its parts. These processes depend on the spatial sizes of elements. On one hand, the reduction of these sizes allows changing the magnetic state by a weaker action; on the other hand, magnetic states become less stable in this case. The interaction with a thermal bath can lead to their spontaneous change and loss of information contained in the magnetic configuration. Thus, the theoretical calculation of the stability of magnetic states to thermal fluctuations and random perturbations, which can be quantitatively estimated by the lifetimes of magnetic states, becomes of primary importance. In particular, it is desirable for magnetic memory that the lifetime of the corresponding magnetic states be tens of years at room temperature. The spatial size of an individual bit should be as small as possible, from one to several tens of nanometers. The development of magnetic carriers where such localized structure can exist is a complex problem of great theoretical and applied interest.

One of the approaches to this problem is the use of "topological" magnetic textures with a nonzero "topological charge" q (Belavin and Polyakov, 1975; Bogdanov and Yablonskii, 1989). The topological charge for quasi-two-dimensional systems with a continuous magnetization distribution has the form

$$q = \frac{1}{4\pi} \iint \mathbf{S}(\mathbf{r}) \cdot \left[\frac{\partial \mathbf{S}(\mathbf{r})}{\partial x} \times \frac{\partial \mathbf{S}(\mathbf{r})}{\partial y} \right] dx\,dy,$$

where $\mathbf{S}(\mathbf{r})$ is the three-dimensional unit vector directed along the magnetization at the point $\mathbf{r}$. The topological charge is an integer indicating how many times the vector $\mathbf{S}(\mathbf{r})$ wraps the unit sphere. It is conserved under the continuous variation of the magnetization and, thus, the transition from the state with $q \neq 0$ to the state with $q = 0$, e.g., ferromagnetic, under the continuous variation of the magnetization is impossible. This should ensure the "topological protection" of magnetic structures against thermal fluctuations (Nagaosa and Tokura, 2013) and makes them promising candidates for the development of a new-generation superdense and fast magnetic memory, elements of artificial neural networks, and other spintronic devices (Finocchio et al., 2016; Fert et al., 2017). However, the topological protection in real magnetic systems, where magnetic moments are localized at sites of a discrete crystal lattice, can be treated only within an approximate description, and the problem of the numerical calculation of lifetimes of

such magnetic states arises. The hierarchy of scales characteristic of magnetic systems makes the problem of estimating the lifetime very difficult for stochastic simulation. The rates of oscillations of individual magnetic moments forming magnetic states even at a nanoscale can be 10–20 orders of magnitude higher than the rates of transitions between the states themselves (Krause et al., 2009). For this reason, the lifetimes and rates of magnetic transitions at temperatures of practical interest cannot be adequately calculated by numerically solving the dynamic equations for magnetic moments and using standard Monte Carlo methods. However, transition state theory for magnetic degrees of freedom can be used (Coffey et al., 2001; Bessarab et al., 2012). This statistical approach implies the consideration of the multidimensional energy surface of the system as a function of the parameters specifying the directions of all magnetic moments in the system and the search for local minima on it corresponding to the ground and metastable states of the system, and with the minimum energy paths (MEPs) giving the most probable mechanisms of magnetic transitions. Maxima along MEPs correspond to first-order saddle points on the energy surface, which determine energy barriers between states. An expression corresponding to the Arrhenius law for rates of magnetic transitions can be obtained in the harmonic approximation where the shape of the energy surface at the minima and saddle point is approximated by a harmonic function of all variables. This approach was first used to calculate rates of chemical reactions (Hänggi et al., 1990) and diffusion of atoms on the surface at epitaxial growth (Voter, 1985) and is currently one of the most accepted methods for estimating the rates of magnetic transitions in nanostructures (Fiedler et al., 2012; Bessarab et al., 2013b; Desplat et al., 2018; Varentcova et al., 2020). Although this theory is successfully used to analyze the stability of topological magnetic structures, a number of fundamental problems remain unstudied, indicating the necessity of further development of the theoretical method itself and its applications to particular magnetic structures. Some of these problems are discussed in this work.

The problem of construction of the energy surface of the system and search for MEPs between locally stable states on it is considered in Chapter 2. In addition to the "nudged elastic band method" and string method, we describe the method of truncated MEP that allows the search for first-order saddle points on surfaces with millions of degrees of freedom and, thus, the calculation of microstructures with atomic resolution (Lobanov et al., 2017) and the minimum mode following method for magnetic systems (Müller et al., 2018) that makes it possible to seek first-order saddle points if only the initial state is specified and the final state is unknown. Using the last method, one sometimes can find mechanisms of transition to surprising final states, although it is more complex than algorithms used in cases where the final state is known. Methods of the calculation of the pre-exponential factor in the Arrhenius law for lifetimes of magnetic structures are also described in Chapter 2. Although an analytical expression for the pre-exponential factor can be obtained in the harmonic approximation of transition state theory, this expression includes the determinant of the Hessian matrix at saddle points and local minima on the energy surface. Its calculation for the energy surface with the dimension equal to or larger than a million is a difficult problem, but it can be solved if interactions are short range and the Hessian matrix is sparse (Lobanov and Uzdin, 2021). Chapter 3 presents connection between lattice and micromagnetic Heisenberg model. Chapter 4 presents the results of calculations of energy barriers and lifetimes of skyrmions

with different sizes in ferro- and antiferromagnetic media, skyrmions on magnetic tracks, in the presence of nonmagnetic impurities and external magnetic field, as well as comparison of dynamical properties and stability of skyrmions and antiskyrmions. Chapter 5 presents conclusions.

2 Transition state theory

2.1 Calculation of minimum energy paths and energy barriers

To describe quasi-two-dimensional topological magnetic structures, we use the generalized Heisenberg model, where the energy surface is described by the expression

$$E = -\sum_{\langle i,j \rangle} (J\mathbf{S_i} \cdot \mathbf{S_j} + \mathbf{D_{ij}} \cdot [\mathbf{S_i} \times \mathbf{S_j}]) - \sum_i (\mu \mathbf{S_i} \cdot \mathbf{B} + KS_{i,z}^2), \quad (1)$$

Here, $\mathbf{S_i}$ is the three-dimensional unit vector directed along the magnetic moment at the i-th site, J is the Heisenberg exchange parameter, $\mathbf{D_{ij}}$ is the Dzyaloshinskii–Moriya vector, $\mathbf{B}$ is the magnetic field perpendicular to the plane of the system, is the anisotropy constant same at all sites of the lattice, and μ is the magnetic moment same at all sites of the lattice. The parameters J and $\mathbf{D_{ij}}$ are assumed nonzero only for moments at neighboring sites. The anisotropy axis $\mathbf{e_z}$ is perpendicular to the plane of the system.

The magnetic configuration is specified by the set of all vectors $\mathbf{S_i}$. The energy surface is the energy functional of all variables that specify the directions of $\mathbf{S_i}$. Such variables can be polar θ_i and azimuth ϕ_i angles specifying the direction of each vector. If the number of sites is 10^6 (which corresponds to, e.g., a 1000×1000 square lattice), the dimension of the energy surface is $2 \cdot 10^6$. Near the poles, where $\theta_i = 0, \pi$, the angle ϕ_i is poorly defined, which complicates the calculations. To solve this problem, one can use the stereographic projection (Rybakov et al., 2015) or take orthogonal matrices as coordinates (Ivanov et al., 2020). Below, we present the results of calculations in Cartesian coordinates in the tangential space to the $\|\mathbf{S_i}\| = 1$ manifold. In this case, Lagrange multipliers should be introduced to correctly define the Hessian matrix (Lobanov and Uzdin, 2021). Expression (1) does not include the energy of the magnetic dipole–dipole interaction, which can play a significant role for the stabilization of topological microstructures (Büttner et al., 2018). According to calculations in (Lobanov et al., 2016), this contribution for nanostructures can be taken into account by renormalizing the anisotropy parameter with the same form of MEPs. All methods discussed below are also applicable to systems with the explicit inclusion of the dipole contribution, although numerical calculations of large systems are more laborious because of the long-range character of the interaction. Local minima on the energy surface corresponding to the ground and metastable states can be sought using standard methods such as the conjugate gradient method (Ivanov et al., 2020) or the Newton method and its derivatives. It is more difficult to find first-order saddle points corresponding to the maximum along one direction and to the minimum in all other directions, but just these points determine energy barriers between locally stable states. Saddle points can be

found as the maximum along the MEP that connects locally stable magnetic states. If these states are known a priori, the following computational methods can be used.

2.1.1 Geodesic Nudged Elastic Band (GNEB) Method

A path is approximated by a discrete set of images of states of the system, $p_0, \dots p_N$, which are attributed to points on the energy surface, where p_0 and p_N correspond to the initial and final locally stable states, respectively. The distance along the path is called the coordinate of the reaction. The geodesic between p_0 and p_N is often taken as the initial approximation for the path. The tangent vector τ^n is defined at each point p_n of the path by means of the following procedure (Henkelman et al., 2000). The vector $\hat{\tau}^n$ is specified in the segments of increasing and decreasing energy along the path as

$$\hat{\tau}^n = \begin{cases} \tau_+^n, & E(p_{n+1}) > E(p_n) > E(p_{n-1}), \\ \tau_-^n, & E(p_{n+1}) < E(p_n) < E(p_{n-1}), \end{cases}$$

where $\tau_+^n = p_{n+1} - p_n$ and $\tau_-^n = p_n - p_{n-1}$. If $E(p_n)$ is the local maximum or minimum along the path, then $\hat{\tau}^n$ is defined as the weighted sum of τ_+^n and τ_-^n, which is continuously transformed to the above relations when the energy along the path varies monotonically. The unit vector along $\hat{\tau}^n$ is taken as the tangent vector τ^n. Images are connected by artificial "springs," which prevent their falling to minima on the energy surface. The stiffness of springs in most of the variants of the GNEB method is chosen the same for all images. However, an increase in the stiffness of springs for images located near the maximum of the energy along the path increases the stability of algorithms, particularly quasi-Newton ones. In this case, the image with the maximum energy "attracts" the other images of the system, ensuring better resolution near a saddle point, which is of main interest for estimating the stability to thermal fluctuations (Henkelman et al., 2000; Ivanov et al., 2020). The forces of elasticity should be comparable with the energy gradient in order to ensure convergence to the MEP. Further, the system of images is relaxed under the action of the projection of forces of elasticity f_n on the tangent to the path and the projection of the energy antigradient on the direction orthogonal to the path:

$$F_n = -\nabla E(p_n) + (\nabla E(p_n) \cdot \tau^n)\tau^n + f_s \cdot \tau^n,$$

where $f_n = k[|p_{n+1} - p_n| - |p_n - p_{n-1}|]$ and $|p_{n+1} - p_n|$ is the distance between the $(n+1)$th and nth images along the path. Springs ensure an almost uniform distribution of images along the path in the equilibrium state. In the subspace orthogonal to the tangent to the path, images are located at the minimum and, therefore, have the maximum statistical weights among nearby states. The introduction of artificial nudging springs explains the term "nudged elastic band method." In the GNEB method, it is taken into account that the length of the vectors $\mathbf{S_i}$ is constant; consequently, tangent vectors to the path are projected on the tangent subspace to magnetic moments. This method can be used within collective magnetism models when the magnitudes of magnetic moments are determined from self-consistent calculations at fixed orientations at each site of the lattice (Bessarab et al. (2014); Ivanov et al. (2017)). When the MEP is determined, the image with the maximum energy provides an estimate for the energy of the saddle point.

To more accurately determine this energy, one can use the "climbing image" method (Henkelman et al., 2000), which allows the exact determination of the saddle point. In this case, the image p_{max} with the maximum energy along the path is chosen, the forces of elasticity of artificial springs acting on it are removed, and an additional force equal to the energy gradient along the path is introduced for the image to move in the direction of increasing energy:

$$F_{max} = -\nabla E(p_{max}) + 2(\nabla E(p_{max}) \cdot \tau^{max})\tau^{max}.$$

The rule for optimization of other images along the path does not change and images themselves are used to determine one degree of freedom for which the energy is maximized. Since the chain of images converges to the MEP, it is a good approximation for the energy surface along the reaction coordinate near the saddle point. When the maximum energy along the path is found, the density of images on different sides of the saddle point can be different. Two or more images that climb to the saddle point can be chosen if it is necessary to study its vicinity in more detail. The GNEB method was used for the first time in (**?**) to calculate the activation barrier for the collapse of the skyrmion. Then, the GNEB method was used for a more detailed analysis of mechanisms of collapse (Lobanov et al., 2016) and for study of the interaction of skyrmions with the magnetic field, edges of an image, and defects (Uzdin et al. (2018b,a)). The GNEB method has now become a standard method for the analysis of the stability of two-dimensional systems with magnetic skyrmions (Cortés-Ortuño et al., 2017; Malottki et al., 2017; Bessarab et al., 2018) and three-dimensional topological systems (Rybakov et al., 2015; Hoffmann et al., 2020) (but it is sometimes incorrectly implemented, see (Rohart et al., 2016)).

2.1.2 String Method

This method is based on the evolution of smooth curves with an internal parameterization (strings) that leads to the MEP between locally stable initial and final states (E et al., 2002; Heistracher et al., 2018). It is similar to the GNEB method, but another algorithm is used instead of elastic springs that uniformly distribute images along the path. Images are first shifted under the action of the transverse component of the real force. Then, the path is approximated, e.g., by means of the spline interpolation; its length is determined; and the positions of images are corrected so that they are located at the same distance from each other along the path. The climbing image algorithm can also be used here to exactly determine the position of the saddle point.

2.1.3 Minimum Mode Following Method

This method can be used when only the initial state of the system corresponding to a local minimum on the energy surface is known (Müller et al., 2018; Olsen et al., 2004). It allows finding the nearest first-order saddle points determining scenarios of transition to different a priori unknown states. Beginning with the point close to the minimum, the system at each iteration step is displaced in the direction of the eigenvector of the Hessian of the energy corresponding to the minimum eigenvalue. Relaxation to the state with

the minimum energy is performed in the subspace orthogonal to this eigenvector. The search for the minimum eigenvalue does not require large computational efforts and can be performed, e.g., with the Lanczos algorithm (Golub and Loan, 2013). The calculation of the minimum mode is not necessary if two states are relaxed simultaneously, keeping the distance between them, as in the dimer method. In this case, these states are ordered along the eigenvector corresponding to the minimum mode (Henkelman and Jónsson, 1999). When the minimum eigenvalue becomes negative, the minimum mode following method implements a procedure similar to the climbing image algorithm, ensuring convergence to a firstorder saddle point. Starting with different initial states near the minimum, one can obtain several saddle points each corresponding to a certain mechanism of escape from the initial state. This method applied to magnetic systems (Müller et al., 2018) made it possible to obtain a magnetic transition corresponding to the formation of two skyrmions from one, which is accompanied by the doubling of the topological charge of the system. The activation energy of this process appeared to be comparable with the activation energy for the collapse of the skyrmion.

2.1.4 Truncated Minimum Energy Path Method

This method allows finding a part of the total path including the saddle point (Lobanov et al., 2017). The saddle point and its vicinity are important for the determination of transition rates between magnetic configurations within transition state theory. For the collapse of the skyrmion, the configuration of the state at the saddle point is an atomic-scale noncollinear structure even for micron skyrmions. This allows determining activation barriers and lifetimes of such states without the calculation of the total MEP, which is difficult to find because the size of the structure becomes large far from the saddle point and overly large computer memory is required. In this method, one of the images is separated as an anchor, e.g., with the maximum energy, and a part of the path with a fixed length including this image is considered. Some images in this part should be on one side of the crest separating the initial and final states on the energy surface and the other images should be on the other side. At the end of the path, only the transverse component of the energy gradient is set to zero. After that, the path is optimized, e.g., as in the string method, and images in the segment are redistributed. In contrast to the string method, in the truncated MEP method, images are redistributed over a part of the path around the saddle point. The anchor is not involved in the redistribution, and the image nearest to it is chosen as the anchor at the next iteration step. One of the locally stable states, e.g., the initial or final state, can be taken as the anchor. Then, its position does not change during the operation of the algorithm, but the second end of the segment should be behind the region of the transition state. This requires the qualitative understanding of the shape of the energy surface and the general structure of the transition state. In the general case, the energy surface specified by the generalized Heisenberg model is a manifold of a large dimension, which can be million and more for real topological systems considered at the atomic scale.

For the clear representation of the energy surface and understanding of possible scenarios of magnetic transitions, it is useful to plot the two-dimensional energy surface under the assumption that the directions of all magnetic moments can be specified by two parameters. Such an approach was used in (Moskalenko et al., 2016), where the

magnetization reversal in the spin spring was simulated by the motion of a domain wall in the magnetically soft magnet and the magnetic configuration was specified by the position and thickness of the domain wall. For topological magnetic structures such as skyrmions, there are analytical expressions approximately describing the profile of the skyrmion and its magnetic configuration obtained from the comparison with experimental data (Romming et al., 2015; Boulle et al., 2016; Büttner et al., 2018). These relations with a few parameters reproduce quite well locally stable skyrmion states. We assume that the magnetic configuration in the nonequilibrium state under magnetic transformations is also specified by the same set of the parameters and only their values change in the process of transition. Then, the dimension of the energy surface is equal to the number of these parameters. We consider magnetic configurations used in (Büttner et al., 2018) within the model with the continuously distributed magnetization including the magnetic dipole–dipole interaction in addition to contributions specified by Eq. (1). The structure consisting of magnetic material layers and heavy metal was calculated in the effective medium approximation with renormalized parameters. The localized topological state was specified by three variables: the radius of the skyrmion R, the thickness of its domain wall Δ, and the angle ψ between the magnetic moments at the edge of the skyrmion and the radial direction. Contributions to the energy, in particular, the dipole interaction, can be estimated analytically (Büttner et al., 2018). This allows constructing the energy surface of the system in the (R, Δ) coordinates shown in Fig. 2.1 for the following parameters: the exchange stiffness of the magnetic material $\mathscr{A} = 2.5\,\mathrm{pJ/m}$; Dzyaloshinskii–Moriya parameter $\mathscr{D} = 6.5 \cdot 10^{-4}\,\mathrm{J/m^2}$, anisotropy constant $\mathscr{K} = 0.2\,\mathrm{pJ/m}$, magnetic field $B = 0.27\,\mathrm{T}$, saturation magnetization $M_s = 0.35\,\mathrm{MA/m}$, total thickness of the sample $d = 126,4\,\mathrm{nm}$, and $\psi = 0°$. The MEP between skyrmions of different sizes is shown in Fig. 2.1 by the white line with white circles indicating images. It is seen that the radius of the skyrmion decreases first in the process of transition from the large skyrmion to the small one and then, after the passage through the saddle point, the thickness of its domain wall decreases. We note that the distances between images seem nonidentical because of different scales along the axes in Fig. 2.1.

2.2 Pre-exponential factor

Transition state theory for magnetic degrees of freedom implies that magnetic moments are classical objects with a given interaction energy, which is determined, e.g., by Eq. (1), and that magnetic transitions are slow processes compared to oscillations of individual moments, so that the Boltzmann distribution is established and maintained in the entire accessible region on the energy surface up to the transition state inclusively. Furthermore, paths on the energy surface are assumed reactive, i.e., go from the initial to final state, crossing the dividing surface only once (Bessarab et al., 2012, 2013a). Within transition state theory, the following Arrhenius law can be obtained for lifetimes of magnetic states:

$$\tau = \tau_0 \exp\left(\frac{\Delta E}{k_\mathrm{B}\mathrm{T}}\right), \tag{2}$$

where T is temperature, $\Delta E = E_s - E_m$ is the difference between the energies

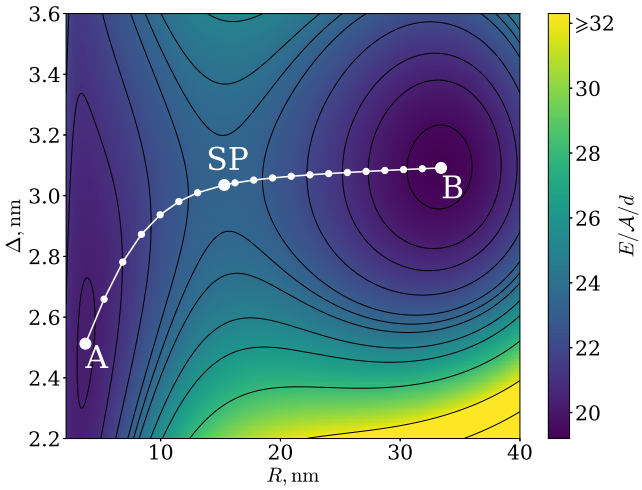

Figure 2.1. Energy surface for the system determined by the radius of a skyrmion and by the thickness of a domain wall. The minimum energy path between skyrmion states A and B stabilized by the Dzyaloshinskii–Moriya and dipole interactions, respectively.

E_s and E_m at the saddle point and in the initial state, respectively. If the harmonic approximation is used for the shape of the energy surface at the saddle point and minimum corresponding to the initial state, the pre-exponential factor τ_0 depends on the Hessians of the energy at these points. In Appendix B, we derive formulas for calculating the transition rate in the framework of the harmonic approximation to transition state theory:

$$k = \frac{1}{2\pi}\sqrt{\sum_{n=2}^{2N}\frac{\zeta_s^n}{|\zeta_s^1|}(b^n)^2}\sqrt{\frac{\det H_m}{|\det H_s|}}\exp\left(-\frac{E_s - E_m}{k_B T}\right), \tag{3}$$

where states S_m and S_s - minimum and saddle point on energy surface, E_m and E_s - corresponding energies, H_m and H_s - Hessians of energy in S_m and S_s, ζ_s^n and e^n are eigenvalues and eigenvectors of H_s, $b^n = e^n \cdot \frac{d}{dt}e^1$.

Expression (3) for the transition rate includes the ratio of determinants of the Hessian of energy at the corresponding points of the energy surface. This ratio is usually calculated as the ratio of the products of the eigenvalues of the Hessian (Fiedler et al., 2012; Bessarab et al., 2013b; Desplat et al., 2018; Varentcova et al., 2020). However, all eigenvalues of the Hessian for systems with millions of degrees of freedom cannot be determined by standard methods. For this reason, calculations of microsystems with the atomic resolution have not yet been performed. Progress has been recently achieved in this field with the use of sparseness of Hessians (Lobanov and Uzdin, 2021). The interaction between magnetic moments is shortrange; consequently, the Hessian matrix can be represented in the block tridiagonal form. The block Cholesky decomposition

(Golub and Loan, 2013) allows one to write a recurrent relation for the elements of the block diagonal corresponding to the subsystems of the initial system with one of the spatial coordinates fixed, significantly reducing the dimension of the problem. The proposed method makes it possible to calculate the determinants of Hessians for microsystems with atomic resolution.

3 Lattice and micromagnetic model

Let us now consider various contributions to energy within the framework of the generalized Heisenberg model, which is often used in describing topological magnetic structures. The energy surface is determined by the expression

$$E = E_{ex} + E_{DM} + E_K + E_{Ze} + E_{DD} \tag{4}$$

Here, E_{ex} and E_{DM} denote the contributions of the isotropic and antisymmetric exchange interactions, respectively, E_K is the energy of magnetic anisotropy, E_{Ze} is the energy of interaction with an external magnetic field, and E_{DD} - energy of magnetic dipole-dipole interaction. Let's consider each contribution to (4) in more detail.

3.1 Isotropic exchange

In the discrete model, when the magnetic moments are assumed to be localized at the sites of the crystal lattice exchange energy is

$$E_{ex} = -\frac{1}{2}\sum_{i,j} J_{i,j}\mathbf{S}_i \cdot \mathbf{S}_j, \tag{5}$$

where $\mathbf{S}_i$ is the unit vector directed along the magnetic moment at the site i. The exchange interaction parameter $J_{i,j}$ decreases with increase of the distance between the magnetic moments and will further be considered nonzero only between the nearest neighbors. However, in a number of works in which exchange integrals are chosen based on density functional calculations to describe topological magnetic structures, the parameters $J_{i,j}$ are taken into account up to 8 - 9 nearest neighbors (Heinze et al., 2011; Paul et al., 2020). In this case, the sign of the exchange parameter changes with distance and it is argued that taking into account the competition of exchange interactions significantly affects the assessment of the stability of the magnetic state (Malottki et al., 2017).

In models with a continuous distribution of magnetization $\mathbf{m}$, the contribution of the isotropic exchange interaction to the energy density is written in the form

$$\mathscr{A}(r)|\nabla \mathbf{m}|^2,$$

where

$$|\nabla \mathbf{m}|^2 = \sum_{i,j=x,y,z} \left(\frac{\partial \mathbf{m}_i}{\partial j}\right)^2.$$

Let's consider, for example, the magnetic moments of a square or triangular lattice. We will count the exchange energy from the energy of the ferromagnetic state. Then, in the case of small deviations of the directions of the magnetic moments at neighboring sites, we can write

$$E_{ex} = \frac{J}{2}\sum_{i,j}(1 - \mathbf{S_i}\mathbf{S_j}) \approx \frac{J}{4}\sum_{i,j}\varphi_{i,j}^2,$$

where $\varphi_{i,j} \approx |\mathbf{S}_i - \mathbf{S}_j|$ - angle between unit vectors $\mathbf{S}_i$ and $\mathbf{S}_j$, shown in figure 3.2.

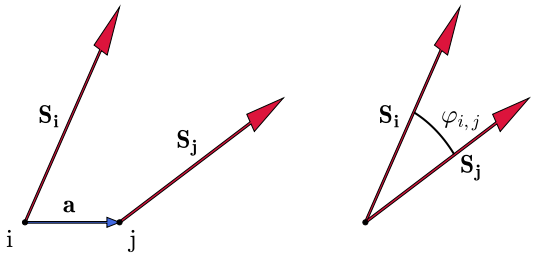

Figure 3.2. Definition of angle $\varphi_{i,j}$.

Denoting

$$\mathbf{S}_i = \mathbf{m}(\mathbf{r}), \mathbf{S}_j = \mathbf{m}(\mathbf{r}+\mathbf{a}),$$

we obtain:

$$E_{ex} = \frac{J}{4}\sum_{i,\mathbf{a}}(\mathbf{m}(\mathbf{r}) - \mathbf{m}(\mathbf{r}+\mathbf{a}))^2, \tag{6}$$

where summation over $\mathbf{a}$ is over all vectors connecting the i-th atom with its nearest neighbors (Fig. 3.3). Let's expand $\mathbf{m}(\mathbf{r}+\mathbf{a})$ in a row up to the first order:

$$\mathbf{m}(\mathbf{r}+\mathbf{a}) = \mathbf{m}(\mathbf{r}) + (\mathbf{a}\cdot\nabla)\mathbf{m}(\mathbf{r}) =$$

$$= \mathbf{m}(\mathbf{r}) + \left(a_x\frac{\partial m_x}{\partial x} + a_y\frac{\partial m_x}{\partial y}\right)\mathbf{e}_x + \left(a_x\frac{\partial m_y}{\partial x} + a_y\frac{\partial m_y}{\partial y}\right)\mathbf{e}_y + \left(a_x\frac{\partial m_z}{\partial x} + a_y\frac{\partial m_z}{\partial y}\right)\mathbf{e}_z \tag{7}$$

$$(\mathbf{m}(\mathbf{r}+a) - \mathbf{m}(\mathbf{r}))^2 \approx a_x^2\left(\frac{\partial m_x}{\partial x}\right)^2 + a_y^2\left(\frac{\partial m_x}{\partial y}\right)^2 + 2a_xa_y\frac{\partial m_x}{\partial x}\frac{\partial m_x}{\partial y} +$$

$$+a_x^2\left(\frac{\partial m_y}{\partial x}\right)^2 + a_y^2\left(\frac{\partial m_y}{\partial y}\right)^2 + 2a_xa_y\frac{\partial m_y}{\partial x}\frac{\partial m_y}{\partial y} +$$

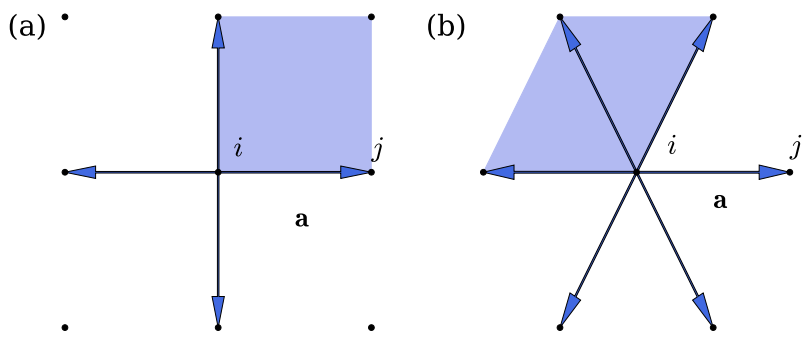

Figure 3.3. (a) Square lattice, (b) triangular lattice. Arrows show vectors **a** *connecting node i with its nearest neighbors. The filled area corresponds to the elementary cell.*

$$+a_x^2\left(\frac{\partial m_z}{\partial x}\right)^2+a_y^2\left(\frac{\partial m_z}{\partial y}\right)^2+2a_xa_y\frac{\partial m_z}{\partial x}\frac{\partial m_z}{\partial y}$$

Cross-terms containing a_xa_y will be canceled when summed after substitution in (6).

For the square and triangular lattices considered here, the sum over the nearest neighbors is $\sum a_x^2=\sum a_y^2$. We denote it by L, then

$$E_{ex}=\frac{L}{4}J\sum_i[(\nabla m_x)^2+(\nabla m_y)^2+(\nabla m_z)^2]. \tag{8}$$

Here

$$\nabla m_\alpha=\frac{\partial m_\alpha}{\partial x}\mathbf{e}_x+\frac{\partial m_\alpha}{\partial y}\mathbf{e}_y$$

$$(\nabla m_\alpha)^2=\left(\frac{\partial m_\alpha}{\partial x}\right)^2+\left(\frac{\partial m_\alpha}{\partial y}\right)^2$$

Multiply and divide the right side of the equation (8) per unit cell volume V_c:

$$E_{ex}=\frac{L}{4V_c}J\sum_i V_c[(\nabla m_x)^2+(\nabla m_y)^2+(\nabla m_z)^2]$$

For $V_c\to 0$, the sum on the right-hand side tends to the integral. We have:

$$E_{ex}=\frac{L}{4V_c}J\int[(\nabla m_x)^2+(\nabla m_y)^2+(\nabla m_z)^2]dV$$

In the model with continuous magnetization

$$E_{ex}=\mathscr{A}\int|\nabla\mathbf{m}|^2dV$$

Hence, we obtain a correspondence between the parameters of the micromagnetic and discrete models:

$$\mathscr{A} = \frac{L}{4V_c} J \tag{9}$$

For a square lattice: $L = 2a^2$, $V_c = a^2 d$ and $\mathscr{A} = \frac{J}{2d}$, for triangular: $L = 3a^2$, $V_c = \frac{\sqrt{3}}{2} a^2 d$ and $\mathscr{A} = \frac{\sqrt{3}}{2d} J$.

3.2 Antisymmetric exchange or Dzyaloshinskii-Moriya interaction

Skyrmions and other topological structures may be stabilized even in the presence of competing exchange interactions without taking into account the spin-orbit interaction (Heil et al., 2019). However, many of the topological states are chiral, i.e. do not match in space with their mirror image (Nagaosa and Tokura, 2013). The existence of these magnetic structures is explained by the presence of an antisymmetric exchange - the Dzyaloshinskii-Moriya (DM) interaction, which occurs in systems without an inversion center (Dzyaloshinsky, 1958; Moriya, 1960).

On a discrete lattice, the DM interaction energy is given by the formula

$$E_{DM} = -\frac{1}{2} \sum_{i,j} \mathbf{D}_{i,j} [\mathbf{S}_i \times \mathbf{S}_j],$$

where $\mathbf{D}_{i,j}$ - DM vector.

Let $\mathbf{D}_{i,j} = D\mathbf{d}_{i,j}$, where $\mathbf{d}_{i,j}$ is the unit vector along the DM vector, D is the DM constant. Then the energy will take the form:

$$E_{DM} = -\frac{D}{2} \sum_{i,j} \mathbf{d}_{i,j} [\mathbf{S}_i \times \mathbf{S}_j] \tag{10}$$

Since the magnetic moments are parallel in ferromagnetic (FM) ordering, the DM energy is zero, and we can say that (10) sets the DM energy with respect to the FM state.

The direction of the vector $\mathbf{d}_{i,j}$ depends on the type of inverse symmetry breaking (Moriya, 1960). In a bulk sample, for example, in compounds of MnSi cubic magnets with a B20 crystal structure without an inversion center, the DM vector is directed along the vector connecting the lattice sites (Mühlbauer et al., 2009):

$$\mathbf{d}_{i,j} = \frac{a_x}{a} \mathbf{e}_x + \frac{a_y}{a} \mathbf{e}_y$$

Let us find the relationship between the contributions from the DM interaction in the discrete model and the model with a continuous magnetization distribution. As in the case of the Heisenberg exchange, we denote

$$\mathbf{S}_i = \mathbf{m}(\mathbf{r}), \quad \mathbf{S}_j = \mathbf{m}(\mathbf{r}+\mathbf{a})$$

$$E_{DM} = -\frac{D}{2}\sum_{i,\mathbf{a}} \mathbf{d}_{i,j}[\mathbf{m}(\mathbf{r}) \times \mathbf{m}(\mathbf{r}+\mathbf{a})] \tag{11}$$

Substitute the decomposition $\mathbf{m}(\mathbf{r}+\mathbf{a})$ (7) into the mixed product:

$$\mathbf{d}_{i,j}[\mathbf{m}(\mathbf{r}) \times \mathbf{m}(\mathbf{r}+\mathbf{a})] =$$

$$\begin{vmatrix} \frac{a_x}{a} & \frac{a_y}{a} & 0 \\ m_x & M_y & M_z \\ m_x + a_x\frac{\partial m_x}{\partial x} + a_y\frac{\partial m_x}{\partial y} & m_y + a_x\frac{\partial m_y}{\partial x} + a_y\frac{\partial m_y}{\partial y} & m_z + a_x\frac{\partial m_z}{\partial x} + a_y\frac{\partial m_z}{\partial y} \end{vmatrix}$$

After summation in (11), all terms will be canceled, except for:

$$\frac{a_x^2}{a}\left(m_y\frac{\partial m_z}{\partial x} - m_z\frac{\partial m_y}{\partial x}\right) + \frac{a_y^2}{a}\left(-m_x\frac{\partial m_z}{\partial y} + m_z\frac{\partial m_x}{\partial y}\right)$$

Thus,

$$E_{DM} = -\frac{D}{2}\sum_{i,\mathbf{a}}\left[\frac{a_x^2}{a}\left(m_y\frac{\partial m_z}{\partial x} - m_z\frac{\partial m_y}{\partial x}\right) + \frac{a_y^2}{a}\left(-m_x\frac{\partial m_z}{\partial y} + m_z\frac{\partial m_x}{\partial y}\right)\right]$$

Let's multiply and divide the right side of this equation by V_c:

$$E_{DM} = \frac{DL}{2V_c a}\sum_i V_c\left[m_x\frac{\partial m_z}{\partial y} - m_y\frac{\partial m_z}{\partial x} + m_z\frac{\partial m_y}{\partial x} - m_z\frac{\partial m_x}{\partial y}\right]$$

For $V_c \to 0$, the sum on the right-hand side tends to the integral. We have

$$E_{DM} = \frac{DL}{2V_c a}\int\left[m_x\frac{\partial m_z}{\partial y} - m_y\frac{\partial m_z}{\partial x} + m_z\frac{\partial m_y}{\partial x} - m_z\frac{\partial m_x}{\partial y}\right]dV \tag{12}$$

The notations coincides with the ones introduced when describing the contribution of the Heisenberg exchange.

In the model with continuous magnetization

$$E_{DM} = \mathscr{D}\int\left[m_x\frac{\partial m_z}{\partial y} - m_y\frac{\partial m_z}{\partial x} + m_z\frac{\partial m_y}{\partial x} - m_z\frac{\partial m_x}{\partial y}\right]dV \tag{13}$$

Then the correspondence of the DM constants to the micromagnetic and discrete models has the form:

$$\mathscr{D} = \frac{DL}{2V_c a} \tag{14}$$

The energy density of a bulk DM can be written as follows (Kang et al., 2016):

$$w = \mathscr{D}\mathbf{m}\cdot\nabla\times\mathbf{m} = \mathscr{D}\begin{vmatrix} m_x & m_y & m_z \\ \frac{\partial}{\partial x} & \frac{\partial}{\partial y} & \frac{\partial}{\partial z} \\ m_x & m_y & m_z \end{vmatrix}$$

The antisymmetric exchange interaction in bulk samples leads to the formation of topological chiral structures with Bloch-type domain walls, in which the magnetic moment rotates in a direction orthogonal to the normal to the wall. A different situation is realized if the breaking of the inversion symmetry is due to the presence of a surface or interface. In this case, the DM vector is directed perpendicular to the line connecting the interacting atoms (Fert, 1991) and Néel domain walls are formed with the rotation of the magnetic moment in the plane perpendicular to the wall.

In this case

$$\mathbf{d}_{i,j} = \frac{a_y}{a}\mathbf{e}_x - \frac{a_x}{a}\mathbf{e}_y$$

$$\mathbf{d}_{i,j}[\mathbf{m}(\mathbf{r})\times\mathbf{m}(\mathbf{r}+\mathbf{a})] = \begin{vmatrix} \frac{a_y}{a} & -\frac{a_x}{a} & 0 \\ m_x & m_y & m_z \\ m_x + a_x\frac{\partial m_x}{\partial x} + a_y\frac{\partial m_x}{\partial y} & m_y + a_x\frac{\partial m_y}{\partial x} + a_y\frac{\partial m_y}{\partial y} & m_z + a_x\frac{\partial m_z}{\partial x} + a_y\frac{\partial m_z}{\partial y} \end{vmatrix}$$

After summation in (11), all terms will be canceled except those containing:
$\frac{a_y^2}{a}\left(m_y\frac{\partial m_z}{\partial y} - m_z\frac{\partial m_y}{\partial y}\right)$ and $\frac{a_x^2}{a}\left(m_x\frac{\partial m_z}{\partial x} - m_z\frac{\partial m_x}{\partial x}\right)$
Similarly to the case with the volume interaction of the DM, we obtain:

$$E_{DM} = \frac{DL}{2V_c a}\int\left(m_z\frac{\partial m_x}{\partial x} - m_x\frac{\partial m_z}{\partial x} + m_z\frac{\partial m_y}{\partial y} - m_y\frac{\partial m_z}{\partial y}\right)dV$$

$$\mathscr{D} = \frac{DL}{2V_c a},$$

Thus, the relationship between the parameters $\mathscr{D}$ and D is the same for the interface and bulk DM interaction. As a result, we obtain the ratio of the parameters for a square lattice: $\mathscr{D} = \frac{D}{ad}$, for a triangular one: $\mathscr{D} = \frac{\sqrt{3}}{ad}D$.

The DM energy density in the case of the interface DM interaction has the form (Bogdanov and Yablonskii, 1989):

$$w = \mathscr{D}\left(m_z\frac{\partial m_x}{\partial x} - m_x\frac{\partial m_z}{\partial x} + m_z\frac{\partial m_y}{\partial y} - m_y\frac{\partial m_z}{\partial y}\right) \tag{15}$$

Sometimes, two more equivalent expressions are used for the DM interaction energy density, due to the presence of an interface:

1. $w = -\mathscr{D}\mathbf{m}[[z\times\nabla]\times\mathbf{m}]$ according to (Heil et al., 2019)

$$[z\times\nabla] = \begin{vmatrix} \mathbf{e}_x & \mathbf{e}_y & \mathbf{e}_z \\ 0 & 0 & 1 \\ \frac{\partial}{\partial x} & \frac{\partial}{\partial y} & \frac{\partial}{\partial z} \end{vmatrix} = -\mathbf{e}_x\frac{\partial}{\partial y} + \mathbf{e}_y\frac{\partial}{\partial x}$$

$$[[z\times\nabla]\times\mathbf{m}] = \begin{vmatrix} \mathbf{e}_x & \mathbf{e}_y & \mathbf{e}_z \\ -\frac{\partial}{\partial y} & \frac{\partial}{\partial x} & 0 \\ M_x & M_y & M_z \end{vmatrix} = \mathbf{e}_x\frac{\partial m_z}{\partial x} + \mathbf{e}_y\frac{\partial m_z}{\partial y} - \mathbf{e}_z\frac{\partial m_y}{\partial y} - \mathbf{e}_z\frac{\partial m_x}{\partial x}$$

$$-\mathbf{m}[[z\times\nabla]\times\mathbf{m}] = -m_x\frac{\partial m_z}{\partial x} - m_y\frac{\partial m_z}{\partial y} + m_z\frac{\partial m_y}{\partial y} + m_z\frac{\partial m_x}{\partial x},$$

which results in the expression (15).

2. $w = \mathscr{D}(m_z\nabla\cdot\mathbf{m} - (\mathbf{m}\cdot\nabla)m_z)$ according to (Wang et al., 2018)

$$\nabla = \mathbf{e}_x\frac{\partial}{\partial x} + \mathbf{e}_y\frac{\partial}{\partial y} + \mathbf{e}_z\frac{\partial}{\partial z}$$

$$m_z\nabla\cdot\mathbf{m} - (\mathbf{m}\cdot\nabla)m_z = m_z\left(\frac{\partial m_x}{\partial x} + \frac{\partial m_y}{\partial y} + \frac{\partial m_z}{\partial z}\right) - m_x\frac{\partial m_z}{\partial x} - m_y\frac{\partial m_z}{\partial y} - m_z\frac{\partial m_z}{\partial z} =$$

$$= m_z\frac{\partial m_x}{\partial x} + m_z\frac{\partial m_y}{\partial y} - m_x\frac{\partial m_z}{\partial x} - m_y\frac{\partial m_z}{\partial y},$$

which also results in the expression (15).

In some cases, models are considered that include two different DM vectors in a thin magnetic film on a metal surface to describe chiral magnetic states in it (Vedmedenko et al., 2007). In tetragonal Heusler alloys Mn-Pt-Sn, an anisotropic DM interaction has been experimentally discovered, leading to the formation of an antiskyrmion lattice (Nayak et al., 2017).

The general form of the energy density of the Dzyaloshinskii-Moriya interaction may be written as a linear combination of Lifshitz invariants $\mathscr{L}_{ij}^k = m_i\partial_k m_j - m_j\partial_k m_i$, $i,j,k \in \{x,y,z\}$, $i > j$. We are considering the case $\partial_z m_i = 0$.

$\mathscr{L}_i = \mathscr{L}_{zx}^x + \mathscr{L}_{zy}^y$, $\mathscr{L}_b = \mathscr{L}_{zy}^x + \mathscr{L}_{zx}^y$, $w_{i,b} = D\mathscr{L}_{i,b}$.

3.3 Anisotropy energy

On a discrete lattice, the contributions due to magnetic anisotropy are written in the form

$$E_K = -\sum_i K(\mathbf{e}\cdot\mathbf{S}_i)^2 \tag{16}$$

where $\mathbf{e}$ is the unit vector along the anisotropy axis, K is the anisotropy constant. If $K < 0$, the “easy plane” anisotropy is realized in the system, and if $K > 0$ - “easy axis”. Although skyrmion topological states (Nagaosa and Tokura, 2013; Bordács et al., 2017) can exist in both cases, in what follows we will consider only the case of quasi-two-dimensional magnetic systems with anisotropy of the "easy axis" type with $\mathbf{e} = \mathbf{e_z}$. In this case, the anisotropy energy is given by the formula:

$$E_K = -K\sum_i S_{i,z}^2$$

If the anisotropy energy is measured from the energy in a ferromagnetic state with magnetic moments ordered along the z axis, then:

$$E_K = K\sum_i (1 - S_{i,z}^2) \tag{17}$$

Let's transit to a continuous description of the magnetization:

$$\mathbf{m}(r) = \mathbf{S}_i$$

Multiply and divide the right side of the equation (17) by V_c:

$$E_K = \frac{K}{V_c}\sum_i V_c(1 - m_z(r)^2)$$

For $V_c \to 0$, the sum on the right-hand side tends to the integral:

$$E_K = \frac{K}{V_c}\int (1 - m_z^2)dV$$

In the model with continuous magnetization

$$E_K = \mathscr{K}\int (1 - m_z^2)dV$$

Hence, we obtain the correspondence of the anisotropy parameters in the micromagnetic and discrete models:

$$\mathscr{K} = \frac{K}{V_c} \tag{18}$$

For a square lattice: $\mathscr{K} = \frac{K}{a^2 d}$, for triangular: $\mathscr{K} = \frac{2K}{\sqrt{3}a^2 d}$.

3.4 Zeeman energy of interaction with an external field

Let us consider the case when the magnetic field is directed perpendicular to the plane of the system, along the magnetization at infinity, co-directed with the z axis. The Zeeman energy of interaction with an external field of magnitude B, measured from a homogeneous ferromagnetic state for a discrete model, is represented in the following form

$$E_{Ze} = \mu B\sum_i (1 - S_{i,z}), \tag{19}$$

$$E_{Ze} = -\mu\sum_i (\mathbf{B}\mathbf{S}_i), \tag{20}$$

where μ is the magnitude of the magnetic moments, which is assumed to be the same at all lattice sites.

Let's transit to a continuous description of the magnetization:

$$\mathbf{m}(r) = \mathbf{S}_i$$

Multiply and divide the right side of the equation (19) by V_c:

$$E_{Ze} = \frac{\mu B}{V_c} \sum_i V_c (1 - m_z(r))$$

For $V_c \to 0$, the sum on the right side tends to the integral:

$$E_{Ze} = \frac{\mu B}{V_c} \int (1 - m_z(r)) dV$$

In a continuous micromagnetic model

$$E_{Ze} = M_s B \int (1 - m_z(r)) dV,$$

where the integration is over the sample volume.

From this we obtain the relationship between the magnetic moment at the site and the saturation magnetization M_s:

$$M_s = \frac{\mu}{V_c} \tag{21}$$

For a square lattice: $M_s = \frac{\mu}{a^2 d}$, for triangular: $M_s = \frac{2\mu}{\sqrt{3} a^2 d}$.

3.5 Magnetic dipole-dipole interaction

The energy of the dipole-dipole interaction in the discrete model has the form:

$$E_{DD} = \frac{\mu_0 \mu_S^2}{4\pi} \sum_{\langle i,j \rangle} \left[\frac{\mathbf{S_i} \cdot \mathbf{S_j}}{r_{i,j}^3} - \frac{3(\mathbf{S_i} \cdot \mathbf{r}_{i,j})(\mathbf{S_j} \cdot \mathbf{r}_{i,j})}{r_{i,j}^5} \right]. \tag{22}$$

Here μ_0 is a magnetic constant, the vector $\mathbf{r}_{i,j}$ is directed from the i-th to the j-th site, the summation is carried out over all pairs of spins. This interaction is long-range, in contrast to all those considered above, and its calculation for micromagnetic systems presents significant difficulties. In most cases, below we will consider small-radius skyrmions in quasi-two-dimensional systems. In this case, we can assume that the dipole interaction is taken into account through the effective anisotropy (Lobanov et al., 2016).

4 Stability of chiral magnetic structures

4.1 Stability of magnetic skyrmions at various spatial scales

Magnetic skyrmions are promising candidate for information carriers in future memory and logic devices. For realization of these ideas the thermal stability becomes a fundamental problem, since thermal fluctuations and random external effects can lead to structural breakdown and loss of data. At the moment experimentaly observed skyrmions at room temperature have micron sizes (Woo et al., 2016). Understanding of such stability and its conection with skyrmion size is a first step to constuction of compact and reliable skyrmion-based data storage. When the size of a skyrmion is increased, the direction of neighboring magnetic moments becomes more similar and the continuous magnetization model becomes more appropriate for describing the system. How does topological protection present in continuous models manifest itself in the limit of infinitesimal lattice constant in discrete models? How does stability of skyrmions change under scaling transformation? These questions are addressed in this section. We calculate the energy of the skyrmion state, the minimum energy path between the metastable skyrmion and the homogeneous ferromagnetic state, and the activation energy of the skyrmion collapse for a gradually decreasing lattice constants while the skyrmion radius is kept constant. The pre-exponential factor in the Arrhenius law for the lifetime is estimated within the harmonic approximation to transition state theory for decreasing values of the lattice constant. The parameter values for the discrete lattice model are scaled with the lattice constant in such a way as to be consistent with the same continuous micromagnetic model, and therefore to keep the size of the skyrmion and its energy unchanged.

4.1.1 Scaling laws

The energy of the magnetic system is described by a Heisenberg-like model for a two-dimensional square lattice (1). The vector of DMI $\mathbf{D_{j,k}}$ is taken to lie in the plane of the lattice and point in the direction along the vector connecting atomic sites j and k, which contributes to stabilization Bloch type skyrmions. Formally, the lattice constant does not enter into (1), but if we consider the same system with larger resolution, the parameters corresponding to this system have to be changed by definite way. As was shown in Chapter 3 one can obtain micromagnetic model with continuous distribution of magnetization in space from Heisenberg - like model (1). In this case energy counted from homogeneous ferromagnetic state can be written as

$$E = \int \omega(x)dx, \quad \omega(x) = \mathscr{A}\|\nabla \mathbf{S}\|^2 - \mathscr{D}(\mathbf{S}\cdot \mathrm{rot}\mathbf{S}) - \mathscr{K}(\mathbf{K^0}\cdot\mathbf{S}) - M_s(\mathbf{B}\cdot\mathbf{S}) \qquad (23)$$

Here integration is taken over whole $\mathbb{R}^2$ space. The exchange stiffness $\mathscr{A}$, DMI density $\mathscr{D}$, anisotropy density $\mathscr{K}$ and M_s are proportional to the exchange parameter J_{jk}, modulus DMI vector $\mathbf{D_{j,k}}$, anisotropy constant K and μ in (1). However the coefficients of proportionality depend on the type of crystal lattice, number of exchange parameters used in lattice model etc. The correspondence between continuous and lattice model is ambiguous so that different lattice models may correspond to the micromagnetic model with the same set of parameters. Nevertheless, the evolution under scaling of parameters, corresponding to some micromagnetic ones, is determined unique and depends only on the dimensionality of the system. Note, that in this paragraph the micromagnetic parameters $\mathscr{A}$, $\mathscr{D}$, $\mathscr{K}$ and M_s have the meaning of energy densities per unit area, unlike energy densities per unit volume considered in Chapter 3. Thus, their connection with discrete parameters will be given by the formulas derived in the Chapter 3 but without dividing by sample thickness d:

$$J = 2\mathscr{A}, \quad D = a\mathscr{D}, \quad K = a^2\mathscr{K}, \quad \mu = a^2 M_s$$

This relations gives us the scaling law for values of discrete parameters at different lattice constant, which correspond to the same set of micromagnetic parameters:

$$J\left(\frac{a}{N}\right) = J(a), \quad D\left(\frac{a}{N}\right) = \frac{D(a)}{N}, \quad K\left(\frac{a}{N}\right) = \frac{K(a)}{N^2}, \quad \mu\left(\frac{a}{N}\right) = \frac{\mu(a)}{N^2} \qquad (24)$$

Within the framework of the lattice model we performed the calculations using following set of dimensionless parameters at initial lattice constant: $D/J = 0.35$, $K/J = 0.16$, $\mu B/J = 0.02$. The initial cell size was chosen sufficiently large compared to skyrmion size (30×30 atoms on square lattice with periodic boundary conditions) to prevent the influence of boundary conditions on the state of the skyrmion. The lattice constant for initial system will be denoted as a_1. We will call further N as scaling parameter, which denotes the number of times a lattice constant decreases.

The parameter transformation given by Eq. (24) can be interpreted in two ways, as illustrated in Fig.4.4 (a) and Fig.4.4 (b): Either as a decrease in lattice constant as N is increased while keeping the micromagnetic parameters the same, and thereby the size of the skyrmion, or as a change in the size of the skyrmion while keeping the constant lattice fixed and thereby changing the values of the micromagnetic parameters. Calculated skyrmion profiles for these two interpretations for $N = 1,3,9$ are shown in Fig. 4.4 (a) and for $N = 1,2,3$ are shown in Fig. 4.4 (b). Parameter δ is the distance from the skyrmion center in the units of a_1. One can see that skyrmion profiles coincide at first case, and scale at N times at second one.

4.1.2 Activation energy for collapse

Fig. 4.5 shows how the energy of the skyrmion with respect to the ferromagnetic ground state depends on the scaling parameter, N. The spin configurations for $N = 1,3,9$ are

shown in the insets. For small N the energy of the skyrmion decreases with size but for sufficiently small lattice constant, when N becomes larger than 9 (which corresponds to $7 \cdot 10^4$ atoms in the supercell), the energy of the system is nearly constant and approaches the value corresponding to the energy of the continuous model.

Note that not only the total energy of the skyrmion but also each contribution to the energy in Eq. (1) is nearly constant for $N > 9$ and doesn't change after that with scaling as can be seen in the inset of Fig. 4.5 (c).

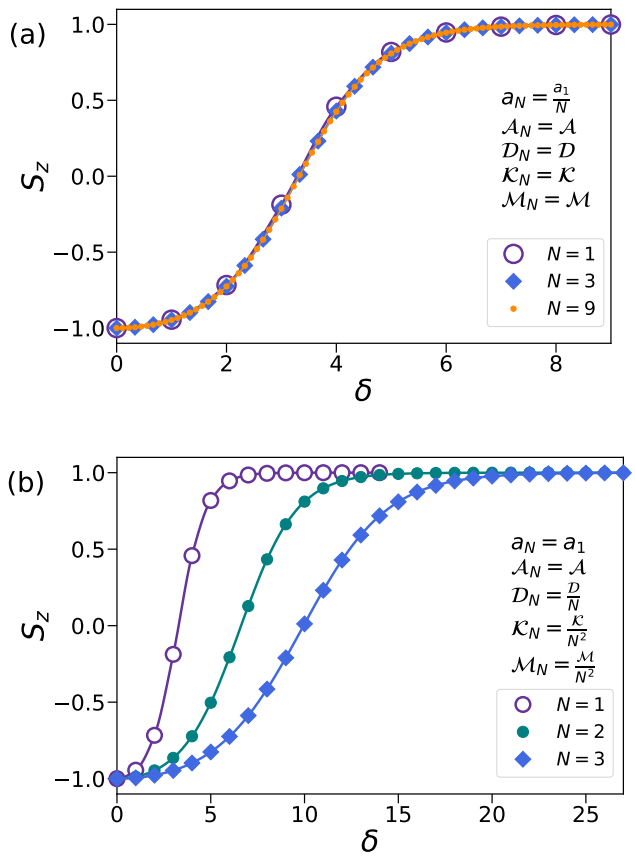

Figure 4.4. Out-of-plane component of magnetic moments for the skyrmion state as function of dimensionless distance from the skyrmion center $\delta = r/a_1$. (a) Different values of the scaling parameter N=1, 3, 9 correspond to different lattice constants but the same skyrmion size. (b) Alternatively, different values of the scaling parameter N=1, 2, 3 correspond to different skyrmiom size but the same lattice constant.

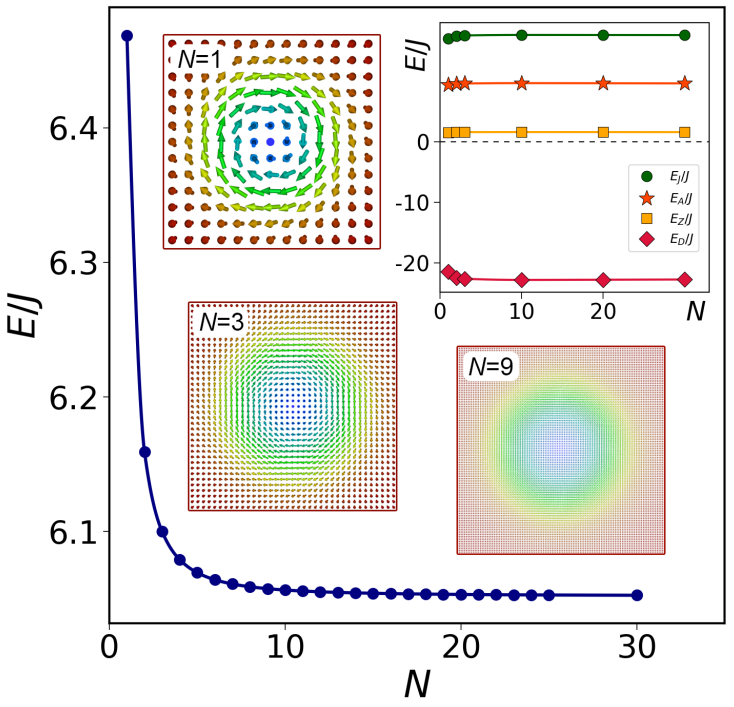

Figure 4.5. Energy of the skyrmion state as a function of scaling parameter. Insets show skyrmion configurations for N = 1, 3, 9. Right upper inset shows the exchange E_J, anisotropy E_A, Dzyaloshinskii-Moriya E_D and Zeeman E_Z contributions to total skyrmion energy as a functions of scaling parameters N.

To study the dependence of skyrmion stability on scaling parameter we calculated MEPs between the skyrmion and the FM state. The point of highest energy along the MEP, a first order saddle point on the multidimensional energy surface given by Eq. (1), minus the initial state energy gives the activation energy for the transition. For $N = 1$ the dimensionality of the energy surface is 1800, and it increases as the square of the scaling parameter, N^2. For small N, the MEP can easily be calculated using the geodesic nudged elastic band method (**?**). When N becomes large, this, however, becomes a computationally demanding task. Since the shape of the path is known it is possible to focus only on the region around the maximum and thereby reduce the effort significantly using Truncated Minimum Path Method (Lobanov et al., 2017) described in Chapter 2. This method allowed us to carry out calculations up to $N = 150$. Figure 4.6 shows the computed full MEP for N=6 and truncated MEP for N=150. The path for N=6 starts from minimum corresponding to skyrmion, and for case of N=150 it starts from some non-stationary small skyrmionic-like state. The size of transition state is much smaller than in initial skyrmionic state, which allows to not consider magnetic moments on the periphery, which are constant during transition, and therefore to use in

calculation only central part of lattice of size 200x200 spins instead of using full lattice of 4500x4500 spins.

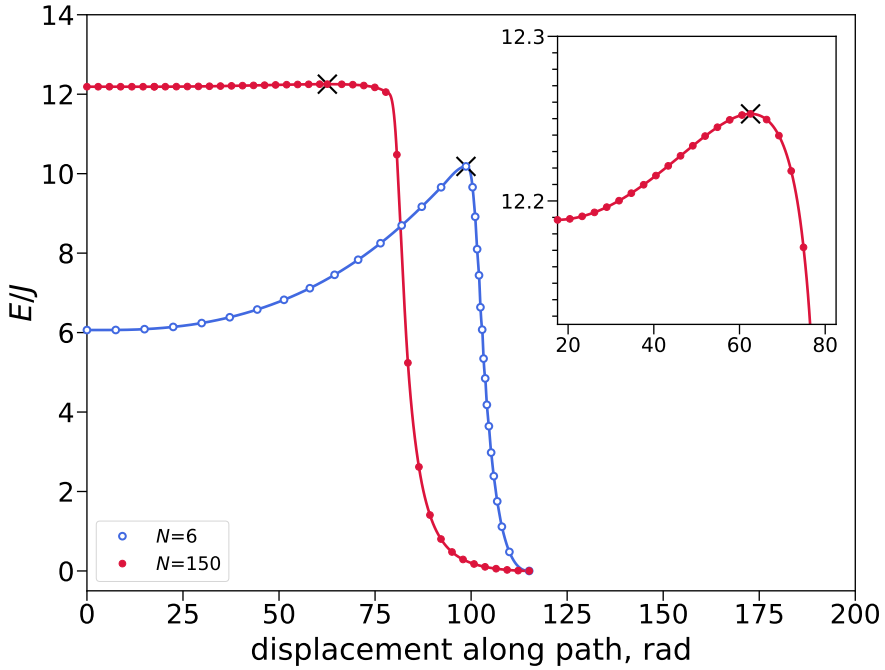

Figure 4.6. Minimum energy path for skyrmion annihilation when N=6 (blue) and part of the path when N=150 (red). Inset shows on a smaller scale in the region of the path when N=150 near the maximum. Saddle points are marked with crosses.

Skyrmion profile $S_z = \cos(\Theta(r))$ at the saddle point at different N is shown in the Fig. 4.7. For $N < 20$ magnetic moments in the neighbourhood of $r = 0$ in the saddle point are ordered under definite angle $\Theta \neq 0$. Center of symmetry for transition state is in the interstitial position. However for $N \geqslant 20$ the center of transition state is shifting to the lattice site $r = 0$.

The figure 4.8 shows the dependence of the energy barrier for skyrmion collapse on the scaling parameter. Each contribution to transition state energy, determined by the Eq. (1), is plotted in inset of Fig. 4.8.

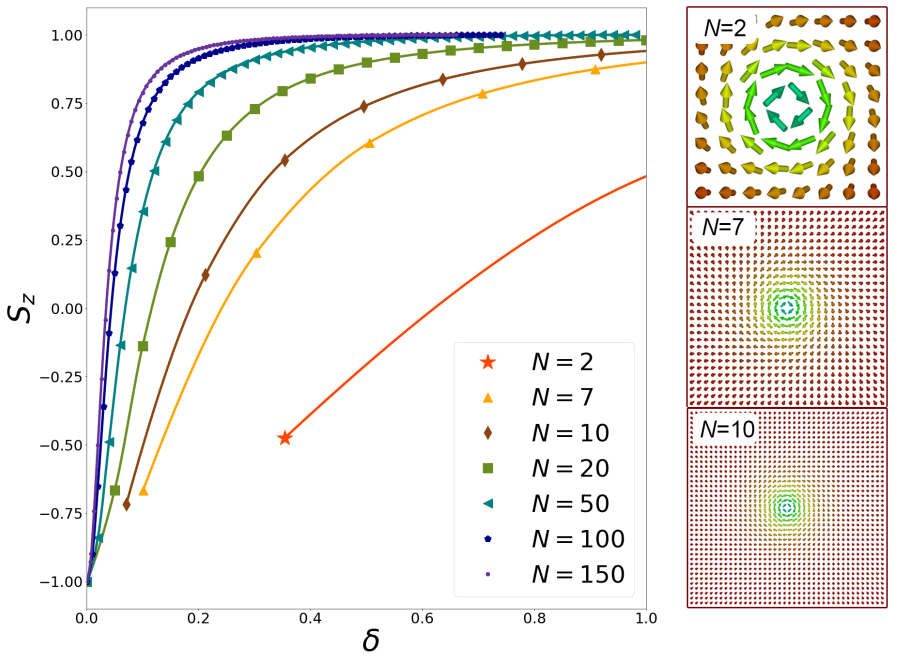

Figure 4.7. Out-of-plane component of magnetic moments for saddle point configuration for various scaling parameters. The distance is measured from the center of the skyrmion, $\delta = r/h_1$. Insets show saddle configurations for N = 2, 7, 10.

The logarithmic increase of activation energy with N takes place only up to $N < 20$. But for a larger N there is no divergence and barrier tends to a constant value. A closer look at the evolution of the central magnetic moment at the point r=0 as it passes through the saddle point shows that for $N \geqslant 20$ it jump-like changes direction on the opposite. This leads to very small relative changes in energy, since the total number of spins for such N is very large. However in continuous limit this transition changes the topological charge of the system. Such a transition mechanism agrees with the scenario of magnetization reversal of the vortex core in the disk of finite thickness. As was shown in (Thiaville et al., 2003), in the framework of the microscopic approach, magnetization reversal occurs by Bloch-point injection on the one side of the disk, passing of this singularity along the disk axis and exit from the other side.

For a large enough scaling parameter the main contribution to the energy in transition state comes from exchange interaction of magnetic moments, although small contribution from DM interaction still exists even at N=150, as it is seen in inset of Fig. 4.8. Tending of Anisotropy and Zeeman contribution to zero may be explained by the following. Profile $S_z(r)$ becomes larger with N at each r, as it is seen in Fig. 4.7. At large N directions of neibourgh magnetic moments become more similar and continious model gives good estimation of energy in discrete model. In continuous approximation Anisotropy and Zeeman contributions depend on S_z in the following

way: $\mathscr{K}\int(1-S_z^2)dx$ and $M_sB\int(1-S_z)dx$, as was shown in chapter 3, and that is why they decrease when $S_z(r)$ becomes larger.

Due to the fact that only exchange interaction remains, the transition state at large N corresponds to the σ-model soliton (Yang, 2001). According to (Belavin and Polyakov, 1975) in the continuous model with only exchange interaction the energy E of any structure with topological charge q satisfies inequality $E \geqslant 4\pi Jq$. Therefore the barrier for nucleation of any structure with $q = 1$, as in the case of skyrmion, cannot be lower than $4\pi J$. Our calculations shows that barrier is equal to this value for very large N and therefore barrier for skyrmion nucleation from FM state in the continuous case can be estimated as the energy of soliton in σ-model and skyrmion collapse goes trough the shrinking up to very small (infinitesimal in continuous case) size. Calculations for large N shows that exchange interaction gives the main contribution and the barrier approaches to this value shown in Fig. 4.8 by green dashed line.

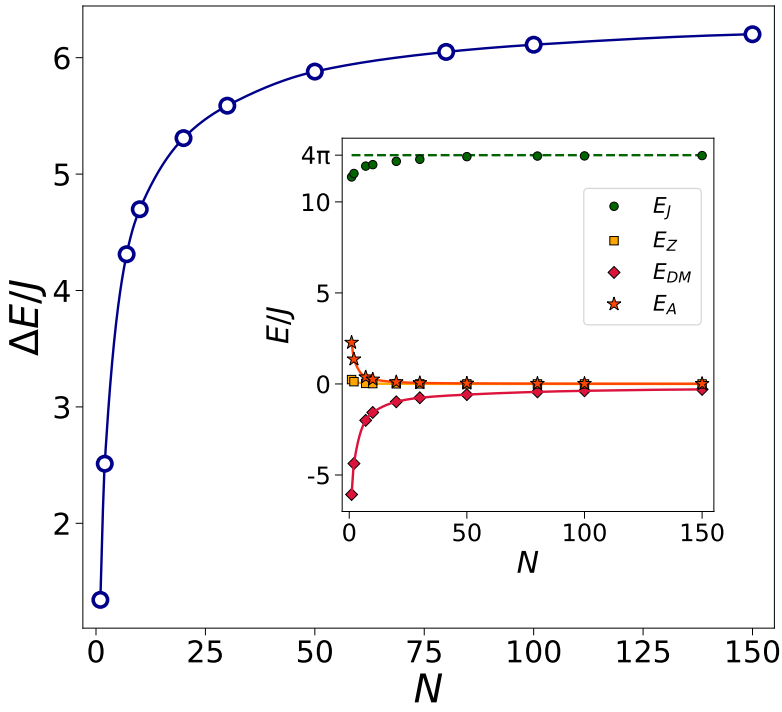

Figure 4.8. Barrier for collapse ΔE as a function of scaling parameter N. Energy contributions E_J, E_A, E_Z, E_{DM} at saddle point as a functions of scaling parameter N (inset). Exchange energy goes to 4π for large scaling parameter (denoted by green dashed line).

Obviously scaling of coordinates does not change exchange energy in continious model: $E = \mathscr{A}\int\|\nabla\mathbf{S}\|^2dx$, therefore scaling will be zero mode for transition state of

skyrmion collapse at large N. Indeed, in Fig. 4.6 at MEP at N=150 near the saddle point a flat area with tiny change in energy is visible, corresponding to the breathing mode.

Starting from N=1 the activation energy for collapse increases with scaling parameter due to variation of exchange and DM interaction (inset of Fig. 4.8). This explains why the activation energy for the magnetization reversal, which was obtained within micromagnetic calculations (Thiaville et al., 2003; Suess et al., 2018), depends on mesh size.

Although transition state energy for collapse in continuous limit does not depend on parameters of anisotropy, DMI and magnetic moment, activation energy will do because the energy of skyrmion minimum is determined by these parameters.

4.1.3 Pre-exponential factor for collapse

Our calculation shows that at first energy barrier is growing with scaling parameter but then approaches to constant value. We are interested in considering of metastable skyrmions, i.e. skyrmions with energy $E_0 > 0$. In that case energy barrier for collapse is limited by the value $\Delta E \leqslant 4\pi J$. For typical exchange parameter 25 meV we obtain energy barrier of about 300 meV, which will give exponential factor for rate of collapse at room temperature of orders 10^{-6}. Typical pre-exponential factor obtained for nanosize skyrmions is $10^{10} - 10^{12}\ s^{-1}$ (Bessarab et al., 2018). If pre-exponential factor would not vary essentially with the size of skyrmion the lifetime of even microscale skyrmions will not be larger than 10^{-4} seconds that is definitively not enough for applications. Therefore investigation of the question about evolution of pre-exponential factor with parameter N is of great importance.

In pre-exponential factor for rate constant defined by expression (3) two factors may be distinguished. The first, entropic factor f_e, is defined in the following way:

$$f_e = \sqrt{\frac{\det H_m}{|\det H_s|}}$$

and the second one, dynamical factor, is defined by expression:

$$f_d = \sqrt{\sum_{n=2}^{2N} \frac{\zeta_s^n}{|\zeta_s^1|}(b^n)^2}$$

Therefore, full pre-exponential factor is: $f_0 = \frac{1}{2\pi} f_d f_e$. The inset of Fig. 4.9 shows the dependence of logarithm of entropy term on scaling parameter N. It is seen that only because of entropy factor the pre-exponential factor decreases by 5 orders of magnitude when changing from the nano to microscale systems. Now we consider dynamical factor f_d containing the contribution from the linearized Landau-Lifshitz equation. Direct calculation demonstrates that this dynamical factor increases with scaling parameter N. Fig. 4.9 shows that this factor gives increase of one order of magnitudes of prefactor when scaling parameter N increases in 37 times. As a result the total prefactor decreases by 4 orders of magnitudes with transition from the nano to the micro scale (Fig. 4.9, inset). We used cN^d function for fitting of dynamical pre-exponential factor.

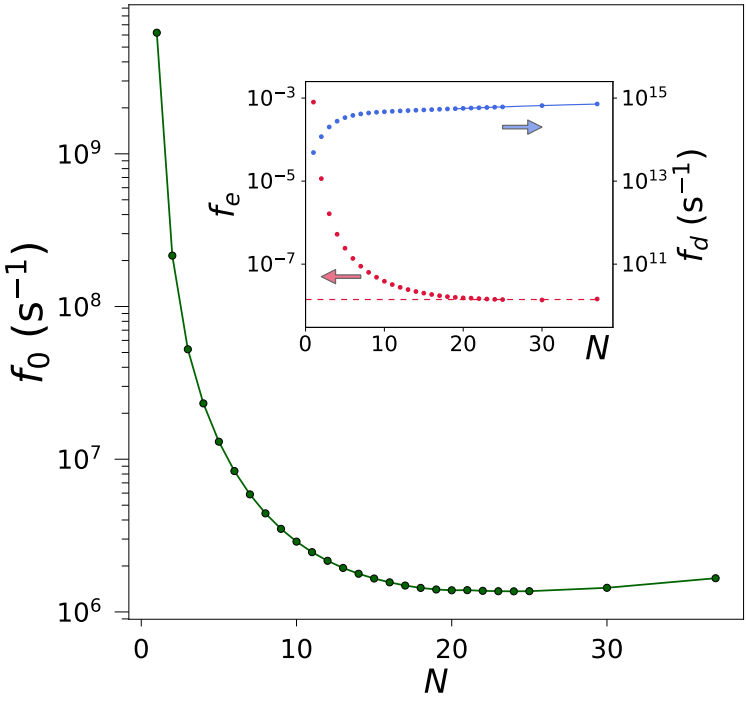

Figure 4.9. Prefactor as a function of scaling parameter N. Dynamical and entropic parts of prefactor for skyrmion collapse as a function of scaling parameter N (inset). Approximation cN^d was used for fitting of dynamical pre-exponential factor.

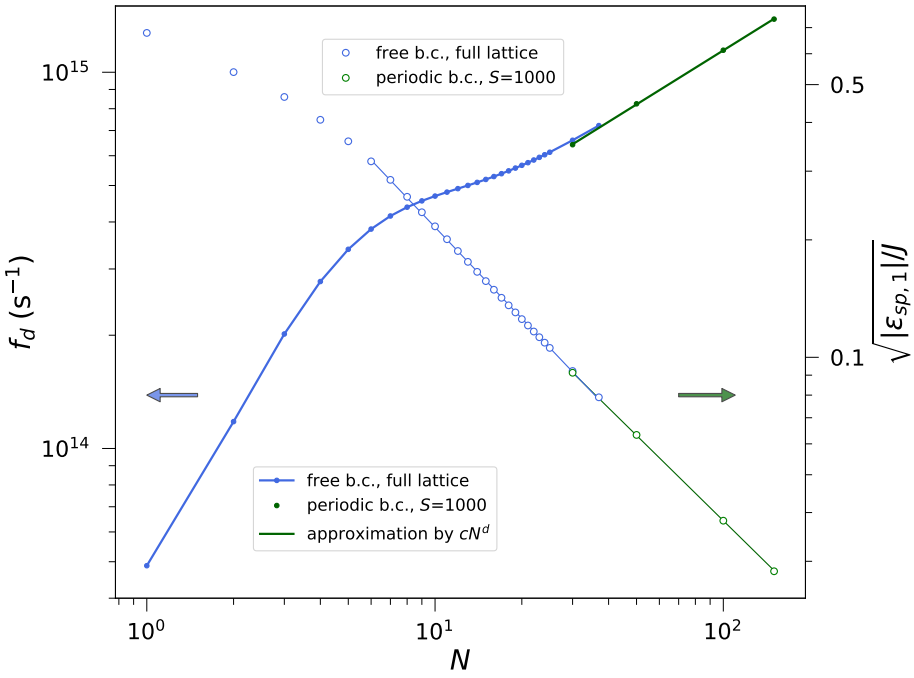

Figure 4.10. Dynamic pre-exponential factor as a function of scaling parameter N. Square root of absolute value of negative eigen value as a function of scaling parameter N and it's approximation by function cN^d, where $d \approx 0.7$. Blue curves correspond to interstitial location of center of saddle point configuration, and green curves correspond to on-atom one.

Fig. 4.10 shows dependence of dynamical prefactor on N up to N=150. For points up to N=37 we use free boundary conditions and full lattice. Saddle points for $30 < N < 150$ was obtained using TMEP method with reduced lattice size. For points $30 < N < 150$ f_d was approximated by function cN^d, which gives linear dependence in double logarithmic scale.

Note that with increase of the temperature the role of pre-exponential factor became more and more essential because in the case of equal number of zero modes in the minimum and saddle point this term is temperature independent whereas the exponent contains the ratio of activation energy and k_BT.

As a result we calculated lifetime for skyrmion collapse as a function of scaling parameter N. Fig. 4.11 shows lifetime at three temperatures: 100 K, 200 K and 300 K.

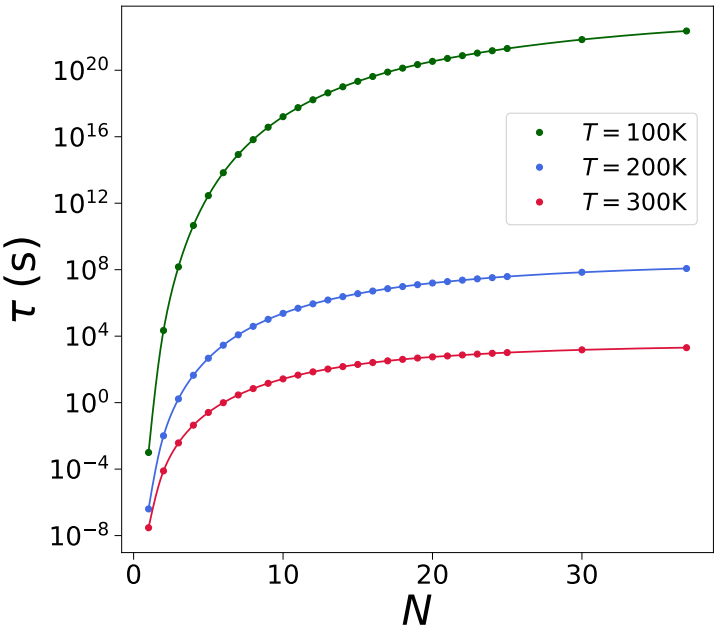

Figure 4.11. Lifetime of skyrmion at T=90 K, 100 K, 200 K, 300 K as a function of scaling parameter N. J =100 meV, $\mu = 0.2$ meV/T at N=1.

If one interprets scaling transformation as a change in the size of the skyrmion while keeping the constant lattice fixed and thereby changing the values of the micromagnetic parameters, then Fig. 4.11 shows lifetime in transition from nano- to micron scale. One can see that at such increase of skyrmion size the lifetime changes by several orders of magnitude. For example, at room temperature, it increases by 8 orders of magnitude and is about a few seconds. Only 4 orders of magnitude is due to increase of exponential factor. So the barrier is not sufficient to stabilize skyrmions at room temperature and the increase of preexponential factor becomes crucial for that. This result makes it possible to explain why microscale skyrmions can be experimentally stable at room temperature (Woo et al., 2016), while nanosized ones are usually unstable (Romming et al., 2013).

4.2 Antiferromagnetic skyrmion

In addition to quasi-two-dimensional skyrmions in thin ferromagnetic layers and multilayer systems, numerous other topological structures are of interest for fundamental magnetism and applications (Kuchkin and Kiselev, 2020). One of the promising fields is the use of ferrimagnetic and antiferromagnetic chiral materials as carriers of localized topological states. Skyrmions with a size up to 10 nm that are stable at room temperature and move under the action of the current at velocities above 1 km/s were obtained in

these systems (Caretta et al., 2018; Woo et al., 2018). Skyrmions in ferromagnetic materials move at a certain angle to the current called the Hall angle (Litzius et al., 2017); this angle in ferrimagnetic materials is much smaller and it vanishes in antiferromagnetic materials (Barker and Tretiakov, 2016; Zhang et al., 2016). In synthetic antiferromagnets consisting of ferromagnetic layers with the antiferromagnetic interlayer interaction (Duine et al., 2018), skyrmions with a size of 10 nm antiferromagnetically coupled in neighboring layers at room temperature were experimentally obtained (Legrand et al., 2020). The analysis of the stability and the estimate of lifetimes of topological states, in particular, skyrmions, in antiferromagnets can be performed within transition state theory, as for ferromagnetic materials (Bessarab et al., 2019). The comparison of the properties of such structures in ferromagnetic and antiferromagnetic materials is of particular interest. Analytical and numerical calculations show that the magnetic field provides the opposite effects on skyrmions in two types of materials: it increases the radius of the skyrmion in antiferromagnets, whereas this radius in ferromagnets decreases when the field is directed against the magnetization in the center of the skyrmion (Fig. 4.12).

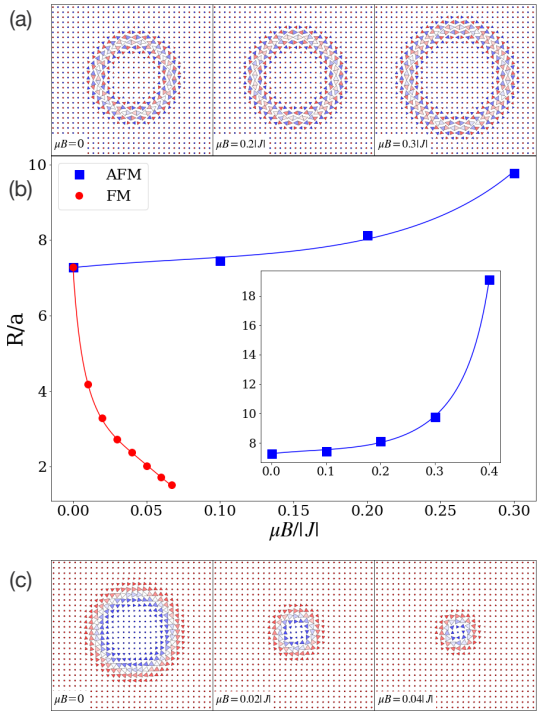

Figure 4.12. (a): AFM skyrmion in a magnetic field of $B = 0,\ 0.2$ *and* $0.3\ |J|/\mu$*. The color (red vs blue) indicates the direction of the out-of-plane component of the magnetic vector and the color intensity the magnitude. (b): Radius (in units of lattice parameter, a) of a skyrmion as a function of applied magnetic field in the AFM (blue) and the corresponding FM (red) where the sign of the exchange coupling parameter, J, and the Dzyaloshinskii-Moriya parameter, D, has been reversed. In a field of 0.07* $|J|/\mu$*, the FM skyrmion becomes unstable, but the AFM skyrmion is stable, even for significantly larger field (see inset for extended scale). While the radius of the skyrmion in an FM shrinks with applied field, it increases in an AFM. (c): FM skyrmion in a magnetic field of* $B = 0,\ 0.02$ *and* $0.04\ |J|/\mu$*. The same color code as in top panel but smaller field.*

To implement racetrack memory devices based on skyrmions, it is necessary to estimate the stability of a skyrmion on a track. Two scenarios of skyrmion decay in such system were found: inside the track through symmetrical collapse and escape through the track boundary. We consider a system of magnetic moments localized at the nodes of a square lattice track in the x–y plane. The width of the track is 60 lattice sites along the y-direction with free boundary conditions at the edges. The simulation cell contains also 60 lattice sites along the x-direction but with periodic boundary conditions applied there. Our calculations have shown that with an increase in the magnetic field, the rates of the processes of collapse of skyrmions and spontaneous escape through the edge of

the magnetic track decrease in antiferromagnetic materials and increase significantly in ferromagnets (Fig. 4.13).

Calculations within the generalized Heisenberg model specified by Eq. (4) show that the energy surfaces of ferromagnetic and antiferromagnetic systems in the absence of magnetic field are completely equivalent. In the presence of magnetic field, the energy surfaces are close to each other if the anisotropy parameter is changed quadratically in field:

$$\mathscr{K} \mapsto \mathscr{K} - \frac{(M_s B)^2}{16|\mathscr{J}|} \tag{25}$$

In this case, activation barriers should coincide. However, our calculations show that the lifetimes of skyrmions in ferromagnetic and antiferromagnetic materials are different. The reason is the different dynamics of skyrmions in these systems leading to different contributions to the pre-exponential factor in the calculated rates of magnetic transitions. The correspondence of the application of the magnetic field for antiferromagnetic media to the renormalization of the anisotropy constant in a ferromagnetic material means that the activation energy for collapse of the skyrmion in an antiferromagnetic material

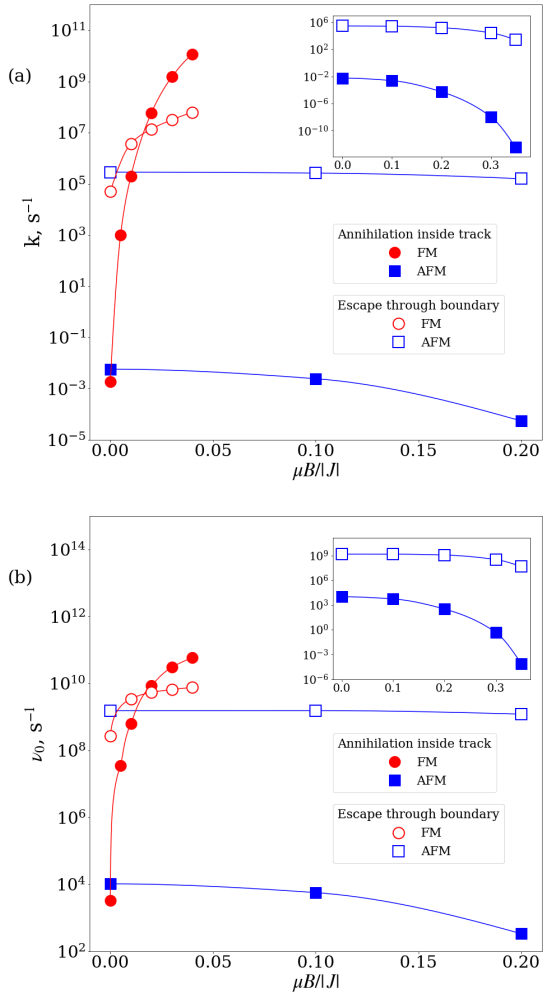

Figure 4.13. (a): Rate constant for the escape of a skyrmion through a boundary of the track and collapse inside the track as a function of an applied magnetic field at a temperature of 100 K. For a skyrmion in the AFM (blue) the effect of the field is weak, but for a skyrmion in the corresponding FM (red) the rate of annihilation increases dramatically as the strength of the applied field increases and a crossover occurs between collapse and escape, the former becoming more likely for large field. (b): Pre-exponential factor, ν_0, for the rate constants illustrated in (a). A similar variation with the field strength is seen, a decrease for the AFM but a large increase for the corresponding FM. Insets: Scale extended to larger field strength.

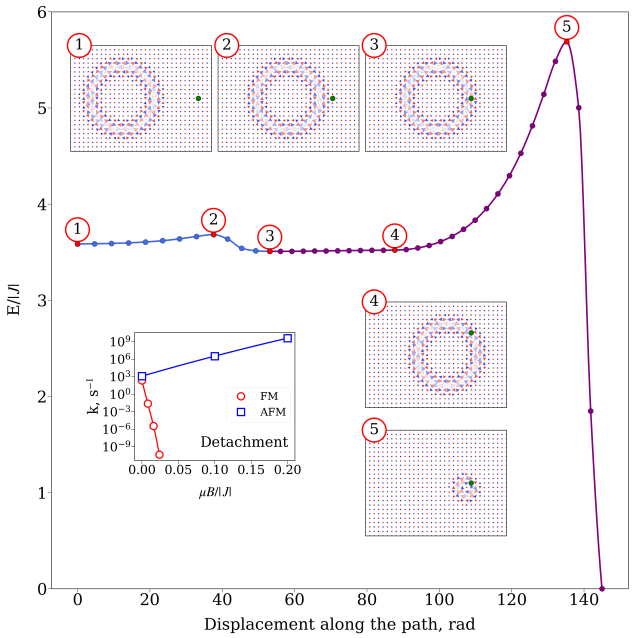

Figure 4.14. Minimum energy path for the attachment of a skyrmion to a non-magnetic impurity atom in the AFM and subsequent collapse there. The lowest energy spin configuration is when the defect is located in a region of the skyrmion where the magnetic moments have no out-of-plane component. Inset graph: Rate constant for the detachment from the impurity as a function of the applied magnetic field strength at T = 3 K. Insets 1–5: Configurations of the magnetic vectors at the various labeled points along the minimum energy path.

can be determined from existing data for ferromagnetic skyrmions without additional calculations.

An important issue for practical applications of magnetic skyrmions is the effect of impurities in the magnetic material. Figure 4.14 shows the minimum energy path for the attachment of a skyrmion in AFM to a non-magnetic substitutional atom and subsequent collapse of the skyrmion. There is a small activation energy barrier for attaching to the defect, but once that has been overcome the energy drops below that of a free skyrmion. The optimal configuration is obtained when the non-magnetic atom is located in the region where the magnetic moments have no out-of-plane component (see Fig. 4.14). This defines the optimal distance between the impurity and the center of the skyrmion. There is still a large probability that the skyrmion detaches from the impurity because the energy barrier is rather small. The impurity, however, also increases greatly the probability of collapse as the activation energy drops to a half compared to that of a free skyrmion. The impurity stabilizes the contracted skyrmion at the transition state more than the relaxed skyrmion in the initial state, thereby lowering the activation energy. Correspondingly, the lifetime drops if the skyrmion is bound

to the impurity. The skyrmion detaches more readily from an impurity in the AFM than in the corresponding FM, and this difference becomes greater as the field strength increases (see inset in Fig. 4.14). Thus an applied field has a beneficial effect for a skyrmion in the AFM by increasing the rate of detachment as well as by decreasing the rate for collapse, as shown in Fig. 4.13.

4.3 Stability of Antiskyrmion

Recently, many distinct topological structures were discovered theoretically (Kuchkin and Kiselev, 2020). They may look different but have one common feature-nontrivial topological charge. Among them skyrmion is the most studied both experimantally and theoretically in last decade. In 2017 another structure were discovered experimentally called antiskyrmion (Nayak et al., 2017), which have opposite to skyrmion topological charge. The magnetic structure of the antiskyrmion is depicted in the Fig. (4.16, a). It was shown experimentally that skyrmions and antiskyrmion can coexist in tilted field (Peng et al., 2020), and independently also these structures were found in experiment, where depending on temperature one of this structure were preferable (Jena et al., 2020). Skyrmion and antiskyrmion have many distinguishing features. For example, in contrary to antiskyrmion skyrmion has axisymmetric shape. One of the issue of skyrmion application in memory and logic devices is moving of skymion under angle (Hall angle) to the direction of spin-polarized current. In the same time value of Hall angle for antiskyrmion depends on the direction of current and may be equal to zero (Huang et al., 2017). Skyrmion and antiskyrmion have different shape and energy when taking into account dipolar interaction (Camosi et al., 2018), but this difference become the less the less the magnetization is. The reason of it is the equivalence of energy surface of skyrmion and antiskyrmion in the absence of dipolar interaction, that will be shown in next section. This fact yields in the same lifetime for two structures.

The lifetimes of the antiskyrmion in the Mn–Pt–Sn Heusler alloy were studied in the harmonic approximation of transition state theory. We used the same scaling approach as in section 4.1, i.e. calculations were performed for a series of states described by the discrete model with different lattice constants and different numbers of magnetic moments. The model parameters were chosen such that all systems correspond to the same continuous model. If the lattice constant is reduced by a factor of N, the exchange constant J for the two-dimensional system does not change, the Dzyaloshinskii–Moriya parameter decreases by a factor of N, and the magnetic moment and anisotropy parameter decrease by a factor of N^2. The experimental lattice constant and magnetic parameters correspond to $N = 20$. The system contained $45N \times 45N$ magnetic moments and satisfied periodic boundary conditions. Fig. 4.15 shows the dependence of the energies E_m and E_{sp} of the antiskyrmion in the equilibrium state and at the saddle point at its collapse, respectively, and (inset) the pre-exponential factor in the Arrhenius law on the parameter N. Calculations show that the stability of the antiskyrmion at room temperature is ensured by a high activation energy for collapse, whereas the pre-exponential factor has a characteristic value of $10^{12} s^{-1}$ despite a large number of spins. Thus, energy rather than entropy effects are responsible for a long lifetime of

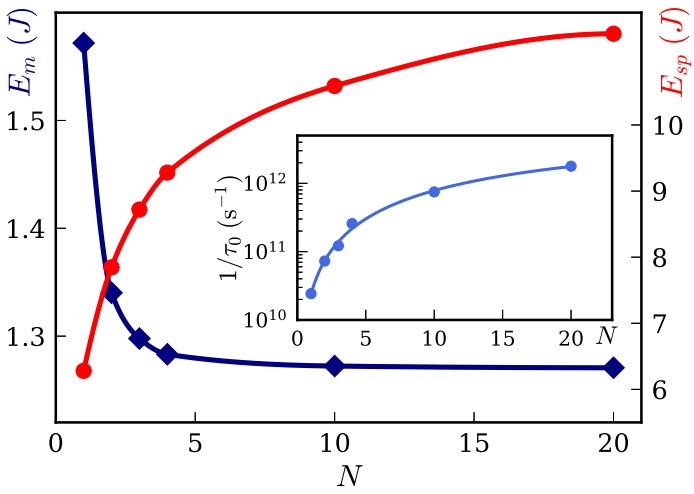

Figure 4.15. Energy of the equilibrium antiskyrmion at the (blue line with diamonds) local minimum E_m and (red line with circles) saddle point E_{sp} at the collapse versus the scaling parameter N. The inset shows the preexponential factor in the Arrhenius law versus N at the parameter $J = 110$ meV.

the antiskyrmion observed in the experiment. Atomic-resolution calculations for the magnetic microsystem with more than a million of degrees of freedom became possible owing to the truncated MEP method (Lobanov et al., 2017) and the recurrent calculation of the determinants of the Hessian of the energy instead of its diagonalization (Lobanov and Uzdin, 2021).

4.4 Antiskyrmion dynamics

In this section we will show the properties of antiskyrmions in both ferromagnetic (FM) and antiferromagnetic (AFM) ultrathin films are related to those of skyrmions by energy-conserving symmetry transformations of the spin configurations and vectors in the Heisenberg-type Hamiltonian. Using this transformation, the dynamics of antiskyrmions can be deduced from those of corresponding skyrmions. Antiskyrmions in FM and AFM materials are shown in Fig. 4.16.

Simulated system. We consider a thin film with perpendicular anisotropy in a magnetic field described by a Heisenberg-type Hamiltonian (1). Depending on the type of DMI, this Hamiltonian can support either Bloch or Néel skyrmions. In the calculations presented here, the DMI vector is taken to point along the bond connecting sites i and j so as to give Bloch type skyrmions. The vector can be written as $\mathbf{D}_{ij} = (\hat{r}_{ij} \cdot \hat{x})\mathbf{D}_1 + (\hat{r}_{ij} \cdot \hat{y})\mathbf{D}_2$ where $\hat{r}_{ij}$ is a unit vector pointing from site i to site j. We note that the dipole-dipole interaction is not included in the Hamiltonian.

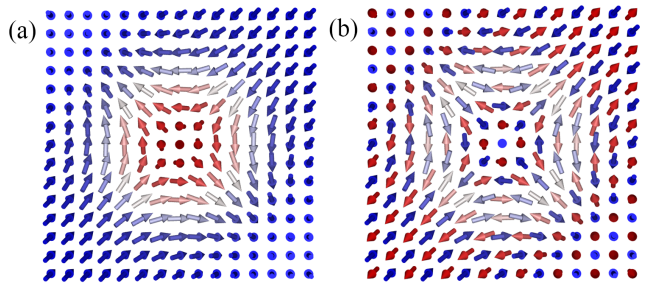

Figure 4.16. Antiskyrmions in (a) ferromagnetic and (b) antiferromagnetic material in the absence of an external magnetic field.

Spin symmetry transformation. To compare skyrmion and antiskyrmion properties we should identify a symmetry transformation converting a skyrmion into a corresponding antiskyrmion while preserving the energy of the system. For simplicity, but without loss of generality, we concentrate on the case of a symmetric antiskyrmion with $\mathbf{D}_1 = (D,0,0)$ and $\mathbf{D}_2 = (0,-D,0)$ in Eq. (1). In this case the spin transformation of skyrmion into antiskyrmion takes the form $(S_x,S_y,S_z) \to (S_x,-S_y,-S_z)$. To keep scalar and cross product in Eq. (1) invariant, we found transformation of material parameters in the following way: $(K_x,K_y,K_z) \to (K_x,-K_y,-K_z)$, $\mathbf{D}_1 = (D,0,0) \to \mathbf{D}_1 = (D,0,0)$, $\mathbf{D}_2 = (0,D,0) \to \mathbf{D}_2 = (0,-D,0)$, and $(H_x,H_y,H_z) \to (H_x,-H_y,-H_z)$. This symmetry transformation can be written in matrix form as $\mathbf{S}' = R\mathbf{S}$ where

$$R = \mathrm{diag}\,(1,-1,-1). \tag{26}$$

The profiles of the antiskyrmion and skyrmion connected by this transformation coincide as can be seen in Fig. 4.17. The transformation R conserves all terms in the Hamiltonian, Eq. (1), as well as the form of the Landau-Lifshitz-Gilbert (LLG) equation of motion without torque terms (see Appendix B). As a result, the lifetime of an antiskyrmion is equal to that of the corresponding skyrmion.

Antiskyrmion in AFM. For comparison, we now consider antiskyrmions in AFM material. To go to the description of AFM from FM, one need to change sign of exchange interaction. As was mentioned in section 4.2, to keep energy constant in case external magnetic field is absent one need also change DM interaction as $\mathbf{D} \to -\mathbf{D}$ and every other spin as $\mathbf{S} \to -\mathbf{S}$. Therefore, the energy of a FM antiskyrmion (Fig. 4.16 (a)) and an AFM antiskyrmion (Fig. 4.16 (b)) is the same and the activation energy for annihilation of FM and AFM antiskyrmions coincide for the corresponding material parameters. However, our calculations show that their lifetimes are somewhat different, by a factor of 6 at $k_BT = J$, because of a difference in the dynamics of skyrmions in FM and AFM materials, leading to a difference in the flux through the transition state.

Antiskyrmion Dynamics. We now consider how the LLG dynamics of an antiskyrmion in FM changes under transformation (26). The equation describing the evolution of the magnetization $\mathbf{S} = \mathbf{S}(\mathbf{r};t)$ under current driven torques (Tatara and

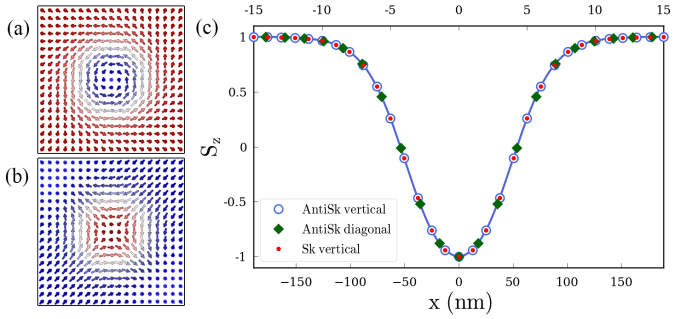

Figure 4.17. Spin textures of (a) skyrmion and (b) antiskyrmion in ferromagnetic material related by the symmetry transformation $(S_x, S_y, S_z) \to (S_x, -S_y, -S_z)$. The images are for the 45 x 45 lattice. (c) Comparison of radial profiles of the antiskyrmion and skyrmion shown in (a) and (b). In the figure, the z-component of the antiskyrmion has been multiplied by -1. Location with respect to the center of the (anti)skyrmion is given in nanometers at the bottom x-axis, while the top x-axis gives the location in terms of the spacing between coarse grained spins.

Kohno, 2004; Thiaville et al., 2005; Ado et al., 2017) is

$$\frac{\partial \mathbf{S}}{\partial t} = \gamma \mu_0 \frac{\delta E(\mathbf{S})}{\delta \mathbf{S}} \times \mathbf{S} - \frac{\alpha}{M_s} \mathbf{S} \times \frac{\partial \mathbf{S}}{\partial t} + \mathbf{T}, \tag{27}$$

where γ is the gyromagnetic ratio, α is the damping constant, M_s the size of the magnetic moment, and $\mathbf{T}$ are the current torques, which are divided in two classes: spin-transfer $\mathbf{T}^{st}$ (STT) and spin-orbit $\mathbf{T}^{so}$ (SOT) torques:

$$\mathbf{T}^{st} = \mathbf{T}^{j} + \beta \mathbf{T}^{e}, \quad \mathbf{T}^{so} = a\mathbf{T}^{a} + b\mathbf{T}^{b} + c\mathbf{T}^{c} + d\mathbf{T}^{d}. \tag{28}$$

where

$$\mathbf{T}^{j} = -(\mathbf{j} \cdot \nabla)\mathbf{S}, \quad \mathbf{T}^{e} = \mathbf{S} \times (\mathbf{j} \cdot \nabla)\mathbf{S} \tag{29}$$

$$\mathbf{T}^{a} = \mathbf{S} \times (\hat{\mathbf{z}} \times \mathbf{j}), \quad \mathbf{T}^{b} = \mathbf{S} \times (\mathbf{S} \times (\hat{\mathbf{z}} \times \mathbf{j})), \tag{30}$$

$$\mathbf{T}^{c} = \mathbf{S} \times (\mathbf{S} \times \hat{\mathbf{z}})(\mathbf{S} \cdot \mathbf{j}), \quad \mathbf{T}^{d} = \mathbf{S} \times \hat{\mathbf{z}}(\mathbf{S} \cdot \mathbf{j}), \tag{31}$$

with a, b, c, d and β being constant that determine the strength of the various torques, and $\mathbf{j}$ is the electrical current.

Under the transformation R, the first two terms on the right-hand side of Eq. (27) remain invariant since $E'[\mathbf{S}'] = E'[R\mathbf{S}] = E[\mathbf{S}]$ (see Appendix B). All SOT are invariant under R if the current is transformed as $\mathbf{j} \mapsto -R\mathbf{j}$ and if only SOT are present, the dynamics of the skyrmion coincides with the dynamics of an antiskyrmion after the transformation. As for STT, they are invariant under R without transformation of the current (see Appendix B) and the dynamics of a skyrmion coincides with the dynamics of an antiskyrmion without any modification of the current.

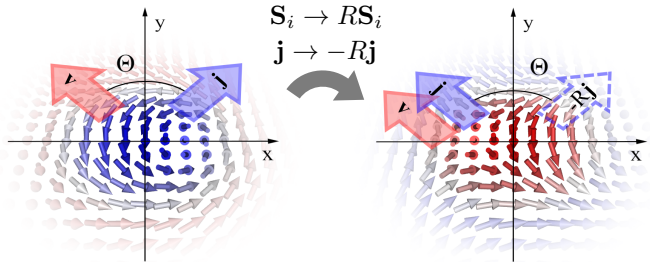

Figure 4.18. Tilted view of skyrmion and antiskyrmion illustrating the effect of the transformation, R, and the possibility of having the direction of spin polarized current coincide with the velocity of the antiskyrmion. Left: Skyrmion traveling with velocity $\mathbf{v}$ *at an angle,* Θ*, the Hall angle (Litzius et al., 2017; Jiang et al., 2017) to the applied current* $\mathbf{j}$*. Right: Antiskyrmion moving along the current* $\mathbf{j}$ *if the angle between* $\mathbf{j}$ *and* $\hat{\mathbf{y}}$ *is* $\Theta/2$*. Only SOT are present in this case.*

If both SOT and STT are simultaneously present, it is impossible to find a current transformation that preserves the LLG dynamics. However, a straightforward procedure can be used to predict the antiskyrmion velocity if the skyrmion velocity is known (Appendix B). Assuming the (anti)skyrmion preserves its shape as it moves, the LLG equation leads to the generalized Thiele equation (Thiele, 1973; Tretiakov et al., 2008; Clarke et al., 2008)

$$\mathbf{G} \times \mathbf{v} - \alpha \mathbf{D} \cdot \mathbf{v} - \mathbf{B} \cdot \mathbf{j} = 0, \tag{32}$$

where $\mathbf{v}$ is the (anti)skyrmion velocity, $\mathbf{G} = (0,0,4\pi Q)$ the gyromagnetic coupling vector, Q the topological charge, $\mathbf{D}$ the dissipative force tensor, and $\mathbf{B}$ the tensor determined by the torques.

Considering the motion of a skyrmion in the presence of SOT and STT, the tensor $\mathbf{B} = \mathbf{B}^{so} + \mathbf{B}^{st}$ spilts into two parts, corresponding to spin-orbit torques $\mathbf{B}^{so}$ and spin-transfer torques $\mathbf{B}^{st}$. Then two velocities can be defined, $\mathbf{v}^{so}(\mathbf{j})$ and $\mathbf{v}^{st}(\mathbf{j})$, corresponding to the skyrmion motion due to only spin-orbit and spin-transfer torques, respectively. If the skyrmion shape is the same for the transport under spin-orbit and spin-transfer torques, the skyrmion velocity under both torques is the superposition $\mathbf{v}_S(\mathbf{j}) = \mathbf{v}^{so}(\mathbf{j}) + \mathbf{v}^{st}(\mathbf{j})$.

We now consider the corresponding antiskyrmion. The shape of a skyrmion and an antiskyrmion is the same if the transformation R is applied. However, the trajectory of the antiskyrmion can be different from that of the skyrmion. The LLG equation for an antiskyrmion gives another Thiele equation with another tensor $\mathbf{B}$ corresponding to modified parameters. Since Thiele equation is linear, its solution with both SOT and STT is a sum of solutions for the separate terms. Therefore, the antiskyrmion velocity is

$$\mathbf{v}_A(\mathbf{j}) = \mathbf{v}^{so}(-R\mathbf{j}) + \mathbf{v}^{st}(\mathbf{j}). \tag{33}$$

The velocity of an antiskyrmion is, therefore, a superposition of the velocity of a skyrmion subjected to the same STT and the velocity of a skyrmion subjected to SOT for a current reflected by $-R$.

This result shows that for a specific angle between the direction of the current and the two axis of the antiskyrmion the skyrmion Hall angle (Litzius et al., 2017; Jiang et al., 2017) is zero, i.e. the antiskyrmion moves in the direction of the current, as demonstrated in Fig. 4.18 for the case when only SOT are present. In AFM there is no skyrmion Hall angle in any case (Barker and Tretiakov, 2016).

5 Conclusion

The possibility of using skyrmions and other topologically protected structures for racetrack memory devices imposes strict conditions on the properties of the corresponding magnetic states. These states must have a small spatial size and be stable with respect to thermal fluctuations at room temperatures, easy change the spatial position under the influence of small currents. The information encoded with their help must be able to quickly write, erase and read. All these requirements make the key problem of the theoretical calculation of the lifetimes of topological magnetic states, taking into account thermal fluctuations, defects in the spatial structure, constricted geometry of the system. It is the lifetimes and rates of magnetic transitions that are a quantitative measure of the stability of topological magnetic structures, which must be assessed when developing any applications.

In the thesis, the activation energy and pre-exponential factor in the Arrhenius expression for the lifetime of a skyrmion is estimated within HTST for a set of decreasing values of the lattice constant while keeping the size of the skyrmion fixed. In the limit of infinitesimal lattice constant, the activation energy reaches a finite value, unlike the topological protection implied by a continuum model. The energy of the transition state approaches the Belavin–Polyakov limit of $4\pi J$ with respect to the ferromagnetic state. The calculated results demonstrate that the entropy term in the pre-exponential factor decreases as the lattice constant is decreased but changes not much then lattice constant decrease in 150 times. The results can also be interpreted in terms of changing skyrmion size for a fixed lattice constant and then demonstrate how the decrease in the pre-exponential factor with increased skyrmion size makes an important contribution to the stability of micrometer skyrmions.

Skyrmions in AFMs and corresponding FMs were shown to be described by similar energy surfaces. Without an applied magnetic field, the energy surfaces coincide exactly. The inclusion of an applied magnetic field for the AFM material is equivalent to a change in the anisotropy in the corresponding FM material without applied field. Therefore, the activation energy for annihilation and the entropy contribution to the pre-exponential factor in the transition rate is exactly the same for AFM and corresponding FM skyrmions. However, the rates are different because the dynamics through the transition state, given by the Landau–Lifshitz equation, is different. The influence of magnetic field on skyrmions in FM and AFM was compared. The rates of skyrmion collapse, escape through the boundary of a track, and detachment from nonmagnetic impurity are calculated as a function of an applied magnetic field for FM and AFM. Magnetic field has a beneficial effect for a skyrmion in the AFM by increasing the rate of detachment as well as by decreasing the rate for decay on the track.

Calculations of the lifetime of large but submicron scale antiskyrmions in Mn–Pt–Sn

tetragonal Heusler material was conducted. The results are consistent with the observed stability at room temperature in recent experiments and show that the long lifetime is due to large activation energy for collapse rather than entropic effects.

Despite the progress made in understanding the mechanisms of stability of topological states due to the use of transition state theory, many questions here remain open and require further research. Among them are the analysis of energy surfaces of three-dimensional structures and transitions between various chiral structures in them, the study of magnetic dipole interaction and calculations of the pre-exponential factor in the Arrhenius law for micron-scale systems with dipole interaction, the study of the issue of creating materials with controlled magnetic parameters.

6 Appendix A: Rates of magnetic transitions

Consider a system consisting of N magnetic moments of the same value μ in the framework of a discrete lattice model corresponding to (1). In what follows, we will mainly take into account only the short-range interaction. The long-range magnetic dipole-dipole interaction will be taken into account by renormalizing the effective anisotropy, although most of the analytical results can also be used when it is taken into account explicitly.

The magnetic configuration is given by the set of all vectors $\mathbf{S_i}$. Let's write energy (1) in a more general form:

$$E[S] = \frac{1}{2} S \cdot QS + S \cdot L \tag{34}$$

Obviously,

$$\frac{\partial E[S]}{\partial S} = QS + L \tag{35}$$

Here L is a vector field, Q is a self-adjoint operator over vector fields. The dynamics of the system is determined by the Landau-Lifshitz equation

$$\frac{dS}{dt} = \frac{\gamma}{\mu} S \times \frac{\partial E[S]}{\partial S}, \tag{36}$$

where the cross product refers to each magnetic moment included in the configuration S.

Substituting the derivative (35) in (36), we obtain the equation of dynamics in the form:

$$\frac{dS}{dt} = \frac{\gamma}{\mu} S \times (QS + L), \tag{37}$$

Further calculations will be carried out in Cartesian coordinates in the tangent space to the manifold $\mathscr{M}$ defined by the condition $\|\mathbf{S_i}\| = 1$.

Consider the state $S = S^0 + \Delta$ in the vicinity of the state S^0. Due to the normalization condition, we get:

$$1 = \mathbf{S}_n^2 = (\mathbf{S}_n^0 + \mathbf{\Delta}_n)^2 = (\mathbf{S}_n^0)^2 + 2\mathbf{S}_n^0 \cdot \mathbf{\Delta}_n + (\mathbf{\Delta}_n)^2.$$

Thus, up to quadratic terms $\mathbf{S}_n^0 \cdot \mathbf{\Delta}_n = 0$ and for all n the vector $\mathbf{\Delta}_n$ belongs to the tangent space to the manifold $\mathscr{M}$. Using coordinates in tangent space, we define curvilinear coordinates near $\mathbf{S^0}$ as follows:

$$\mathbf{S}_n = \frac{\mathbf{S}_n^0 + \mathbf{\Delta}_n}{||\mathbf{S}_n^0 + \mathbf{\Delta}_n||}$$

$$\frac{1}{||\mathbf{S}_n^0 + \mathbf{\Delta}_n||} = \frac{1}{\sqrt{(\mathbf{S}_n^0)^2 + 2\mathbf{S}_n^0\mathbf{\Delta}_n + \mathbf{\Delta}_n^2}} = \frac{1}{\sqrt{1+\mathbf{\Delta}_n^2}} = 1 - \frac{1}{2}\mathbf{\Delta}_n^2 + o(\mathbf{\Delta}_n^2) \quad \text{at } \Delta \to 0$$

$$\mathbf{S}_n = \mathbf{S}_n^0 + \mathbf{\Delta}_n - \frac{1}{2}\mathbf{S}_n^0\mathbf{\Delta}_n^2 + o(\mathbf{\Delta}_n^2) \quad \text{at } \Delta \to 0.$$

Denote by $D = \mathrm{diag}_n\, \mathbf{\Delta}_n^2$. In what follows, we omit the index n. Then

$$S = S^0 + \Delta - \frac{D}{2}S^0 + o(\Delta^2) \quad \text{at } \Delta \to 0.$$

Substituting this expression into (34), we get the energy in local coordinates:

$$E = \frac{1}{2}\left(S^0 + \Delta - \frac{D}{2}S^0\right) Q \left(S^0 + \Delta - \frac{D}{2}S^0\right) + \left(S^0 + \Delta - \frac{D}{2}S^0\right) \cdot L + o(\Delta^2) =$$

$$= E_0 + E_1[\Delta] + \frac{1}{2}E_2[\Delta] + o(\Delta^2), \tag{38}$$

where

$$E_0 = E[S^0] = \frac{1}{2}S^0 Q S^0 + S^0 L - \text{energy in } S^0,$$

$$E_1[\Delta] = \Delta \cdot (QS^0 + L) - \text{energy differential in local coordinates in } S^0, \text{and}$$

$$E_2[\Delta] = \Delta \cdot Q\Delta - DS^0 \cdot (QS^0 + L) \tag{39}$$

is the quadratic form of the Hessian of energy in local coordinates.

The expansion of the energy E allows us to find the stationary point S^0 of the energy. At a stationary point, the energy differential is zero for any increments, so $(QS^0 + L)_n$ is parallel to $\mathbf{S}_n^0$ for all n:

$$\Delta \cdot (QS^0 + L)_n = 0, \quad \Delta \cdot \mathbf{S}_n^0 = 0 \quad \Rightarrow \quad (QS^0 + L)_n \,||\, \mathbf{S}_n^0 \quad \forall n$$

Thus, there are Lagrange multipliers λ_n such that

$$(QS^0 + L)_n = \lambda_n \mathbf{S}_n^0 \quad \forall n \tag{40}$$

Taking into account the normalization condition, the Lagrange multipliers can be found explicitly

$$\lambda_n = \mathbf{S}_n^0 \cdot (QS^0 + L)_n \tag{41}$$

It turns out a nonlinear system of algebraic equations, the solution of which determines the stationary point of energy.

After substituting (41) into (39), the expansion of the energy in powers of Δ at the stationary point S_0 (harmonic approximation) (38) is simplified:

$$E = E_0 + \frac{1}{2}\Delta \cdot Q\Delta - \frac{1}{2}\sum_n \lambda_n \Delta_n^2 + o(\Delta^2) = E_0 + \frac{1}{2}\Delta \cdot H\Delta + o(\Delta^2) \tag{42}$$

Thus, the Hessian of the energy H at the point S_0, restricted to the tangent space, coincides with the matrix Q with the Lagrange multipliers subtracted from the main diagonal.

Let us introduce eigen orthonormal basis for the Hessian H:

$$He^n = \zeta^n e^n, \quad e^n \cdot e^m = \delta_{n,m}.$$

Expanding small increments about the stationary point S^0 in the tangent space $\mathscr{M}$ in this basis

$$\Delta = \sum_{n=1}^{2N} \Delta^n e^n, \tag{43}$$

we obtain the energy in the neighborhood of this point in the form

$$E = E^0 + \frac{1}{2}\sum_{n=1}^{2N} \zeta^n (\Delta^n)^2 + o(\Delta^2). \tag{44}$$

If at the initial moment the system was in a state near the energy minimum S_m, then the probability of finding it in an element of the configuration space dS can be represented as

$$dP = \frac{1}{Z} e^{-\frac{E_m}{k_B T}} dS,$$

where E_m is the minimum energy and the normalization constant is given by:

$$Z = \int e^{-\frac{E_m}{k_B T}} dS. \tag{45}$$

In the approximation (44) we have:

$$Z = e^{-\frac{E_m}{k_B T}} \frac{(2\pi k_B T)^N}{\sqrt{\det H[S_m]}} \tag{46}$$

The number of transitions from the initial to the final state per unit time $k = 1/\tau$ can be estimated as the product of the probability of getting into the neighborhood of the saddle point (transition state) by the rate of leaving it in the direction of the final state:

$$k = \frac{I}{Z} = \frac{1}{Z}\int_{v^\perp > 0} v^\perp(\Delta) e^{-\frac{E^{sp}}{k_B T}} d\Delta, \tag{47}$$

where $v^\perp$ is the velocity component dS/dt orthogonal to the surface passing through the saddle point and separating the initial and final states. The dividing surface is constructed orthogonally to the eigenvector e^1 corresponding to the negative eigenvalue ζ^1. The integral is taken over the part of the dividing surface where the velocity is

directed towards the final state. This velocity can be found from the Landau-Lifshitz equation in the harmonic approximation.

Substituting $S = S^0 + \Delta + o(\Delta)$ into the equation of dynamics (37), we obtain the equation of motion in tangent space:

$$\frac{d}{dt}(\mathbf{S}_n^0 + \mathbf{\Delta}_n + o(\Delta)) = \frac{\gamma}{\mu}(\mathbf{S}_n^0 + \mathbf{\Delta}_n + o(\Delta)) \times (Q(S^0 + \Delta + o(\Delta)) + L)_n$$

$$\frac{d}{dt}(\mathbf{S}_n^0 + \mathbf{\Delta}_n + o(\Delta)) = \frac{\gamma}{\mu}\mathbf{S}_n^0 \times (QS^0 + L)_n + \frac{\gamma}{\mu}[\mathbf{\Delta}_n \times (QS^0 + L)_n + \mathbf{S}_n^0 \times (Q\Delta)_n] + o(\Delta) \tag{48}$$

Let us write the equation of motion (37) for the state S^0:

$$\frac{dS^0}{dt} = \frac{\gamma}{\mu}\mathbf{S}_n^0 \times (QS^0 + L)_n$$

From it, taking into account the equation (40), it follows that S^0 does not change with time: $\frac{dS^0}{dt} = 0$. Thus, the first term on the right side of the equation (48) is equal to zero, while $\frac{d}{dt}\mathbf{\Delta}_n$ remains (on the left side). After substituting the expression (40) into the second term of the right side of the equation, we obtain the dynamics equation up to quadratic terms in the form:

$$\frac{d}{dt}\mathbf{\Delta}_n = \frac{\gamma}{\mu}\mathbf{S}_n^0 \times [(Q - \lambda_n)\mathbf{\Delta}]_n$$

or without the spin index and taking into account $H = Q - \lambda$:

$$\frac{d}{dt}\Delta = \frac{\gamma}{\mu}S^0 \times H\Delta \tag{49}$$

The velocity component orthogonal to the dividing surface is given by the equation

$$v^\perp = \left(\frac{dS}{dt}\right)^\perp = \left(\frac{d}{dt}\Delta\right)^\perp = e^1 \cdot \frac{d}{dt}\Delta = \frac{\gamma}{\mu}e^1 \cdot (S^0 \times H\Delta) \tag{50}$$

Let us substitute into (50) the expansion of the increment Δ by the eigen basis of Hessian H at the saddle point:

$$v^\perp = \frac{\gamma}{\mu}\sum_n \zeta_s^n \Delta^n e^1 \cdot (S^0 \times e^n) = \sum_n a^n \Delta^n \tag{51}$$

where $a^n := \frac{\gamma}{\mu}\zeta_s^n e^1 \cdot (S^0 \times e^n)$ - is the growth rate of the perpendicular component of the velocity $v^\perp$ in the direction of the eigenvector of Hessian of energy e^n when moving from S^0. It's obvious that $a^1 = 0$.

Consider again the frequency of transitions. Substitute the perpendicular component of the velocity (51) and energy decomposition in the transition state (44) $E = E_s + \frac{1}{2}\sum_l \zeta_s^l (\Delta^l)^2$ into the expression for the transition rate (47):

$$I = e^{-\frac{E_s}{k_B T}} \int_{\sum_{n=2}^{2N} a^n \Delta^n > 0 \wedge \Delta^1 = 0} \sum_n a^n \Delta^n \exp\left(-\frac{1}{2k_B T} \sum_l \zeta_s^l (\Delta^l)^2 \right) d\Delta$$

Where E^s - transition state energy. Let's introduce variables $\xi^l = \Delta^l \sqrt{\frac{\zeta_s^l}{2k_B T}}$, then:

$$I = e^{-\frac{E_s}{k_B T}} \int_{\sum_{n=2}^{2N} \frac{a^n \xi^n}{\sqrt{\zeta_s^n}} > 0 \wedge \xi^1 = 0} \sum_{n=2}^{2N} a^n \xi^n \sqrt{\frac{2k_B T}{\zeta_s^n}} \prod_{l=2}^{2N} \sqrt{\frac{2k_B T}{\zeta_s^l}} e^{-(\xi^l)^2} d\xi$$

The product of the exponent contains an expression, which is the square of the length of some vector in the 2N-dimensional configuration space with a minus sign. This length is expressed in terms of the coordinates ξ^l in the $\{e_s^i\}$ basis, but it can be written in any orthonormal basis, and the Jacobian of the transition to a new basis is equal to one. If we choose one of the vectors of this basis along $v^\perp$, then the boundaries of the integration domain will have a simple form, and all integrals can be calculated explicitly. Introducing orthonormal coordinates η such that

$$\eta^1 = \xi^1 \quad \text{and} \quad \eta^2 \sqrt{\sum_{n=2}^{2N} \frac{(a^n)^2}{\zeta_s^n}} = \sum_{n=2}^{2N} \frac{a^n \xi^n}{\sqrt{\zeta_s^n}},$$

We will get

$$I = e^{-\frac{E_s}{k_B T}} \int_{\eta^2 > 0 \wedge \eta^1 = 0} \sqrt{2k_B T} \eta^2 \sqrt{\sum_{n=2}^{2N} \frac{(a^n)^2}{\zeta_s^n}} \prod_{l=2}^{2N} \sqrt{\frac{2k_B T}{\zeta_s^l}} e^{-(\eta^l)^2} d\eta$$

Let's take the integral over all variables:

$$\int_{\mathbb{R}^{2N-2}} \prod_{l=3}^{2N} e^{-(\eta^l)^2} d\eta = \sqrt{\pi}^{2N-2} = \pi^{N-1}$$

$$\int_0^\infty \eta^2 e^{-(\eta^2)^2} d\eta^2 = \frac{1}{2}$$

As a result:

$$I = \frac{1}{2} \pi^{N-1} e^{-\frac{E_s}{k_B T}} \sqrt{2k_B T} \sqrt{\sum_{n=2}^{2N} \frac{(a^n)^2}{\zeta_s^n}} \prod_{l=2}^{2N} \sqrt{\frac{2k_B T}{\zeta_s^l}} = e^{-\frac{E_s}{k_B T}} \frac{(2\pi k_B T)^N}{2\pi} \sqrt{\sum_{n=2}^{2N} \frac{(a^n)^2}{\zeta_s^n}} \left(\prod_{l=2}^{2N} \zeta_s^l \right)^{-\frac{1}{2}} \tag{52}$$

Substituting the expressions (52) and (46) into (47), we obtain an expression for the transition rate:

$$k = \frac{1}{2\pi} \sqrt{\sum_{n=2}^{2N} \frac{(a^n)^2}{\zeta_s^n}} \sqrt{\frac{\det H_m}{\prod_{l=2}^{2N} \zeta_s^l}} e^{-\frac{E_s - E_m}{k_B T}} \tag{53}$$

This expression coincides with that obtained in the article Bessarab et al. (2012).

As mentioned above, we have defined the values of a^n as follows:

$$a^n = \frac{\gamma\zeta_s^n}{\mu} e^1 \cdot (S^0 \times e^n) \tag{54}$$

Let us also give another form of the formula for the transition rate. The states belonging to the MEP and close to the transition state are given by the formula $S^0 + \varepsilon e^1$. These states evolve in accordance with the linearized Landau-Lifshitz equation (49):

$$\varepsilon \frac{d}{dt} e^1 = \varepsilon \frac{\gamma}{\mu} S^0 \times H e^1$$

Substitute into the previous equation $He^1 = \zeta_s^1 e^1$:

$$\frac{d}{dt} e^1 = \frac{\gamma\zeta_s^1}{\mu} S^0 \times e^1 \tag{55}$$

Let's denote by b^n the projection of velocity $\frac{de^1}{dt}$ along the MEP into the eigensubspace of Hessian as

$$b^n := e^n \cdot \frac{d}{dt} e^1$$

Taking into account (55):

$$b^n = \frac{\gamma\zeta_s^1}{\mu} e^n \cdot (S^0 \times e^1) = -\frac{\gamma\zeta_s^1}{\mu} e^1 \cdot (S^0 \times e^n)$$

Then a^n and b^n are connected in the following way:

$$a^n = -\frac{\zeta_s^n}{\zeta_s^1} b^n = \frac{\zeta_s^n}{|\zeta_s^1|} b^n$$

Substituting this expression into (53), we get the equivalent formula for the rate of transition:

$$k = \frac{1}{2\pi} \sqrt{\sum_{n=2}^{2N} \frac{\zeta_s^n}{|\zeta_s^1|} (b^n)^2} \sqrt{\frac{\det H_m}{|\det H_s|}} \exp\left(-\frac{E_s - E_m}{k_B T}\right)$$

The sum over the eigenvalues is the values of the quadratic form of the matrix H on the vector b:

$$\sum_n \zeta_s^n (b^n)^2 = b \cdot Hb$$

The latter expression can be calculated in an arbitrary basis, including the original basis in which the magnetic configuration was given, and thus, it is not necessary to search for all the Hessian eigenvalues. As a result, the transition frequency is given by the following formula

$$k = \frac{1}{2\pi} \sqrt{\frac{b \cdot Hb}{|\zeta_s^1|}} \sqrt{\frac{\det H_m}{\det |H_s|}} \exp\left(-\frac{E_s - E_m}{k_B T}\right)$$

where

$$b^n = \frac{dv_n}{dt} = \frac{\gamma}{\mu}\mathbf{S}_{s,n} \times (H_s v)_n$$

v - unit tangent to the MEP at the saddle point, states S_m and S_s - minimum and saddle point on energy surface, E_m and E_s - corresponding energies, H_m and H_s - Hessians of energy in S_m and S_s.

7 Appendix B: General equations for ferromagnetic system

Consider a magnetic system defined by directions $\mathbf{S}_n$ of magnetic moments located at points $\mathbf{r}_n$. Energy of the state $\mathbf{S}$ consists of contributions of Heisenberg exchange with constants J_{mn}, Dzyaloshinskii-Moriya interaction with vectors $\mathbf{D}_{mn}$, anisotropies with axes $\mathbf{K}_l$ and strengths K_l, and Zeeman energy for external magnetic field $\mathbf{B}_n$:

$$\begin{aligned} E[S] = &- \sum_{m \neq n} (J_{mn} \mathbf{S}_m \cdot \mathbf{S}_n + \mathbf{D}_{mn} \mathbf{S}_m \times \mathbf{S}_n) \\ &- \sum_l K_l \sum_n (\mathbf{K}_l \cdot \mathbf{S}_n)^2 - \sum_n \mathbf{B}_n \cdot \mathbf{S}_n. \end{aligned}$$

Dynamics of the system is defined by the Landau-Lifshitz-Gilbert equation with torques $\mathbf{T}$:

$$\frac{d\mathbf{S}_n}{dt} = \gamma \mathbf{S}_n \times \frac{\partial E}{\partial \mathbf{S}_n} + \alpha \mathbf{S}_n \times \frac{d\mathbf{S}_n}{dt} + \mathbf{T}_n,$$

where γ is the gyromagnetic ratio, α is the damping factor. The torques in general may contains following contributions:

$$\begin{gathered} \mathbf{T}_n = a\mathbf{T}_n^a + b\mathbf{T}_n^b + c\mathbf{T}_n^c + d\mathbf{T}_n^d + \mathbf{T}_n^j + \beta \mathbf{T}_n^e, \\ \mathbf{T}_n^a = \mathbf{S}_n \times (\hat{\mathbf{z}} \times \mathbf{j}_n), \quad \mathbf{T}_n^b = \mathbf{S}_n \times (\mathbf{S}_n \times (\hat{\mathbf{z}} \times \mathbf{j}_n)), \\ \mathbf{T}_n^c = \mathbf{S}_n \times (\mathbf{S}_n \times \hat{\mathbf{z}})(\mathbf{S}_n \cdot \mathbf{j}_n), \quad \mathbf{T}_n^d = \mathbf{S}_n \times \hat{\mathbf{z}}(\mathbf{S}_n \cdot \mathbf{j}_n), \\ \mathbf{T}_n^j = -\mathbf{j} \cdot \frac{\partial \mathbf{S}_n}{\partial \mathbf{r}}, \quad \mathbf{T}_n^e = \mathbf{S}_n \times (\mathbf{j} \cdot \frac{\partial \mathbf{S}_n}{\partial \mathbf{r}}) \end{gathered}$$

where $\hat{\mathbf{z}}$ is the direction of Oz axis, $\mathbf{j}$ is the current, and $a,\ b,\ c,\ d$ and β being constants that determine the strength of the various torques. Since we deal with the lattice model, the gradient $\partial \mathbf{S} / \partial \mathbf{r}$ is estimated using finite differences over adjacent nodes:

$$\mathbf{j} \cdot \frac{\partial \mathbf{S}_n}{\partial \mathbf{r}} = \mathbf{j} \cdot \left. \frac{\partial \mathbf{S}}{\partial \mathbf{r}} \right|_{\mathbf{r}=\mathbf{r}_n} = \sum_d \mathbf{j}_d \sum_m \mu_{nm,d} \mathbf{S}_m,$$

where constants $\mu_{nm,d}$ depend on the lattice structure and positions $\mathbf{r}$ of moments. All torques can be grouped to spin-orbit torques $\mathbf{T}^{so}$ and spin-transfer torques $\mathbf{T}^{st}$:

$$\mathbf{T}^{so} = a\mathbf{T}^a + b\mathbf{T}^b + c\mathbf{T}^c + d\mathbf{T}^d, \quad \mathbf{T}^{st} = \mathbf{T}^j + \beta \mathbf{T}^e.$$

We show below that all spin-orbit torques transform in the same way, whereas the spin-transfer torques change differently under the skyrmion to antiskyrmion transformation.

Correspondence between antiskyrmions and skyrmions

Let us consider transformation R acting on magnetization $\mathbf{S}$ as a rotation of π around the Ox axis:

$$R(S_x, S_y, S_z) = (S_x, -S_y, -S_z).$$

If the skyrmion is located in the x-y plane, then R applied to each $\mathbf{S}_n$ transforms it into antiskyrmion and vice-versa. We will place a tilda above symbols if they correspond to an antiskyrmion. The symbols without tilda are used for the skyrmion. The above mentioned correspondence between antiskyrmion and skyrmions means that $\tilde{\mathbf{S}}_n = R\mathbf{S}_n$. Our aim is to prove that under a proper choice of parameters of antiskyrmion, the energies and dynamics of antiskyrmion and skyrmion coincide. More precisely:

(i) the energy of transformed state $\tilde{\mathbf{S}}$ with transformed parameters

$$\tilde{\mathbf{D}}_{mn} = R\mathbf{D}_{mn}, \quad \tilde{\mathbf{K}}_j = R\mathbf{K}_j, \quad \tilde{\mathbf{B}}_n = R\mathbf{B}_n,$$

coincides with the energy of $\mathbf{S}$ with original parameters without hats;

(ii) the transformed state $\tilde{\mathbf{S}}$ satisfies LLG equation with the transformed parameters

$$\tilde{\mathbf{j}} = -R\mathbf{j},$$

where the current $\tilde{\mathbf{j}}$ is substituted for $\mathbf{j}$ for spin-orbit torques and is preserved for spin-transfer torques.

The derivation below is based on the following facts.

Assertion 1. $R(\mathbf{a}\times\mathbf{b}) = (R\mathbf{a})\times(R\mathbf{b})$ for all vectors $\mathbf{a}$ and $\mathbf{b}$.

Proof. Indeed, for arbitrary orthogonal transformation R:

$$R(\mathbf{a}\times\mathbf{b}) = (\det R)(R\mathbf{a})\times(R\mathbf{b}).$$

Since R preserves orientation, we obtain the desired property. An alternative proof using coordinates:

$$R(\mathbf{a}\times\mathbf{b}) = \begin{vmatrix} \hat{\mathbf{x}} & -\hat{\mathbf{y}} & -\hat{\mathbf{z}} \\ a_x & a_y & a_z \\ b_x & b_y & b_z \end{vmatrix} = \begin{vmatrix} \hat{\mathbf{x}} & \hat{\mathbf{y}} & \hat{\mathbf{z}} \\ a_x & -a_y & -a_z \\ b_x & -b_y & -b_z \end{vmatrix} = (R\mathbf{a})\times(R\mathbf{b}),$$

where we multiplied to last columns by -1. **QED**

Assertion 2. $\mathbf{a}\cdot\mathbf{b} = (R\mathbf{a})\cdot(R\mathbf{b})$ for all vectors $\mathbf{a}$ and $\mathbf{b}$.

First substitute $\tilde{\mathbf{S}}$ to the modified energy:

$$\tilde{E}[\tilde{\mathbf{S}}] = -\sum_{m\neq n}(J_{mn}\tilde{\mathbf{S}}_m\cdot\tilde{\mathbf{S}}_n + \tilde{\mathbf{D}}_{mn}\cdot\tilde{\mathbf{S}}_m\times\tilde{\mathbf{S}}_n) - \sum_l K_l\sum_n(\tilde{\mathbf{K}}_l\cdot\tilde{\mathbf{S}}_n)^2 - \sum_n\tilde{\mathbf{B}}_n\cdot\tilde{\mathbf{S}}_n.$$

Writing R explicitly:

$$\tilde{E}[\tilde{\mathbf{S}}] = -\sum_{m\neq n}(J_{mn}R\mathbf{S}_m\cdot R\mathbf{S}_n + R\mathbf{D}_{mn}\cdot(R\mathbf{S}_m\times R\mathbf{S}_n)) - \sum_l K_l\sum_n(R\mathbf{K}_l\cdot R\mathbf{S}_n)^2 - \sum_n R\mathbf{B}_n\cdot R\mathbf{S}_n.$$

Using Assertion 1:

$$\tilde{E}[\tilde{\mathbf{S}}] = -\sum_{m\neq n}(J_{mn}R\mathbf{S}_m\cdot R\mathbf{S}_n + R\mathbf{D}_{mn}\cdot R(\mathbf{S}_m\times\mathbf{S}_n)) - \sum_l K_l\sum_n (R\mathbf{K}_l\cdot R\mathbf{S}_n)^2 - \sum_n R\mathbf{B}_n\cdot R\mathbf{S}_n.$$

Due to Assertion 2:

$$\tilde{E}[\tilde{\mathbf{S}}] = -\sum_{m\neq n}(J_{mn}\mathbf{S}_m\cdot\mathbf{S}_n + \mathbf{D}_{mn}\cdot(\mathbf{S}_m\times\mathbf{S}_n)) - \sum_l K_l\sum_n (\mathbf{K}_l\cdot\mathbf{S}_n)^2 - \sum_n \mathbf{B}_n\cdot\mathbf{S}_n = E[\mathbf{S}].$$

Hence energy of every skyrmion matches energy of the corresponding antiskyrmion.

To proceed further we have to check how the transformation R affects gradients.

Assertion 3. $\frac{\partial E[\mathbf{S}]}{\partial \mathbf{S}} = R\frac{\partial E[\mathbf{S}]}{\partial R\mathbf{S}}$ for arbitrary functional E and vector $\mathbf{S}$.

Proof The assertion follows from the chain rule for differentiation. It can be also checked directly. We know the gradient explicitly:

$$\frac{\partial E[\mathbf{S}]}{\partial \mathbf{S}_n} = -\sum_{m\neq n}(J_{mn}\mathbf{S}_m + \mathbf{D}_{mn}\times\mathbf{S}_m) - 2\sum_l K_l\mathbf{K}_l(\mathbf{K}_l\cdot\mathbf{S}_n) - \mathbf{B}_n.$$

Substituting $\tilde{\mathbf{S}}_n = R\mathbf{S}_n$ for $\mathbf{S}_n$, we get

$$\frac{\partial E[\tilde{\mathbf{S}}]}{\partial \tilde{\mathbf{S}}_n} = -\sum_{m\neq n}(J_{mn}\tilde{\mathbf{S}}_m + \mathbf{D}_{mn}\times\tilde{\mathbf{S}}_m) - 2\sum_l K_l\mathbf{K}_l(\mathbf{K}_l\cdot\tilde{\mathbf{S}}_n) - \mathbf{B}_n.$$

Substituting antiskyrmion parameters:

$$\frac{\partial \tilde{E}[\tilde{\mathbf{S}}]}{\partial \tilde{\mathbf{S}}_n} = -\sum_{m\neq n}(J_{mn}\tilde{\mathbf{S}}_m + \tilde{\mathbf{D}}_{mn}\times\tilde{\mathbf{S}}_m) - 2\sum_l K_l\tilde{\mathbf{K}}_l(\tilde{\mathbf{K}}_l\cdot\tilde{\mathbf{S}}_n) - \tilde{\mathbf{B}}_n.$$

Using Assertion 1 and Assertion 2:

$$\frac{\partial \tilde{E}[\tilde{\mathbf{S}}]}{\partial \tilde{\mathbf{S}}_n} = R(-\sum_{m\neq n}(J_{mn}\mathbf{S}_m + \mathbf{D}_{mn}\times\mathbf{S}_m) - 2\sum_l K_l\mathbf{K}_l(\mathbf{K}_l\cdot\mathbf{S}_n) - \mathbf{B}_n) = R\frac{\partial E[\mathbf{S}]}{\partial \mathbf{S}_n},$$

where we recognized the expression for $\partial E/\partial \mathbf{S}_n$ provided above. Since $\tilde{E}[\tilde{\mathbf{S}}] = E[\mathbf{S}]$, the last identity coincide with Assertion 3. **QED**

To relate dynamics of anti- and skyrmions we apply R to the Landau-Lifshitz equation:

$$R\frac{d\mathbf{S}_n}{dt} = \gamma R(\mathbf{S}_n\times\frac{\partial E[\mathbf{S}]}{\partial \mathbf{S}_n}) + \alpha R(\mathbf{S}_n\times\frac{d\mathbf{S}_n}{dt}) + R\mathbf{T}_n[\mathbf{S}].$$

In virtue of Assertion 1,

$$\frac{dR\mathbf{S}_n}{dt} = \gamma(R\mathbf{S}_n)\times(R\frac{\partial E[\mathbf{S}]}{\partial \mathbf{S}_n}) + \alpha(R\mathbf{S}_n)\times\frac{dR\mathbf{S}_n}{dt} + R\mathbf{T}_n[\mathbf{S}].$$

Using Assertion 3:

$$\frac{dR\mathbf{S}_n}{dt} = \gamma(R\mathbf{S}_n) \times (R^2 \frac{\partial E[\mathbf{S}]}{\partial R\mathbf{S}_n}) + \alpha(R\mathbf{S}_n) \times \frac{dR\mathbf{S}_n}{dt} + R\mathbf{T}_n[\mathbf{S}].$$

Since $R^2 = \mathrm{Id}$:

$$\frac{d\tilde{\mathbf{S}}_n}{dt} = \gamma\tilde{\mathbf{S}}_n \times \frac{\partial E[\mathbf{S}]}{\partial \tilde{\mathbf{S}}_n} + \alpha\tilde{\mathbf{S}}_n \times \frac{d\tilde{\mathbf{S}}_n}{dt} + R\mathbf{T}_n[\mathbf{S}].$$

We already know that $E[\mathbf{S}] = \tilde{E}[\tilde{\mathbf{S}}]$, hence the Landau-Lifschitz-Gilbert equation for $\mathbf{S}$ coincides with the Landau-Lifshitz equation for $\tilde{\mathbf{S}}$ with modified energy $\tilde{E}$, except possibly the term with torques $R\mathbf{T}_n[\mathbf{S}]$. We are going to check that $R\mathbf{T}_n[\mathbf{S}] = \tilde{\mathbf{T}}_n[\tilde{\mathbf{S}}]$, where the operator $\tilde{\mathbf{T}}$ coincide with $\mathbf{T}$, except of the possible substitution $\mathbf{j} \mapsto \tilde{\mathbf{j}} = -R\mathbf{j}$. We examine each torque independently:

$$\begin{aligned} R\mathbf{T}^a_n[\mathbf{S}] &= R(\mathbf{S}_n \times (\hat{\mathbf{z}} \times \mathbf{j}_n)) = (R\mathbf{S}_n) \times R(\hat{\mathbf{z}} \times \mathbf{j}_n) \\ &= (R\mathbf{S}_n) \times ((R\hat{\mathbf{z}}) \times (R\mathbf{j}_n)) = \tilde{\mathbf{S}}_n \times (\hat{\mathbf{z}} \times (-R\mathbf{j}_n)) \\ &= \tilde{\mathbf{S}}_n \times (\hat{\mathbf{z}} \times \tilde{\mathbf{j}}_n) = \tilde{\mathbf{T}}^a_n[\tilde{\mathbf{S}}]. \end{aligned}$$

Other three torques transform in the same way:

$$\begin{aligned} R\mathbf{T}^b_n[\mathbf{S}] &= R(\mathbf{S}_n \times (\mathbf{S}_n \times (\hat{\mathbf{z}} \times \mathbf{j}_n))) = \tilde{\mathbf{S}}_n \times R(\mathbf{S}_n \times (\hat{\mathbf{z}} \times \mathbf{j}_n)) \\ &= \tilde{\mathbf{S}}_n \times (\tilde{\mathbf{S}}_n \times R(\hat{\mathbf{z}} \times \mathbf{j}_n)) = \tilde{\mathbf{S}}_n \times (\tilde{\mathbf{S}}_n \times (\hat{\mathbf{z}} \times (-R\mathbf{j}_n))) \\ &= \tilde{\mathbf{S}}_n \times (\tilde{\mathbf{S}}_n \times (\hat{\mathbf{z}} \times \tilde{\mathbf{j}}_n)) = \tilde{\mathbf{T}}^b_n[\tilde{\mathbf{S}}]. \end{aligned}$$

$$\begin{aligned} R\mathbf{T}^c_n[\mathbf{S}] &= R(\mathbf{S}_n \times (\mathbf{S}_n \times \hat{\mathbf{z}})(\mathbf{S}_n \cdot \mathbf{j}_n)) = \tilde{\mathbf{S}}_n \times R(\mathbf{S}_n \times \hat{\mathbf{z}})(\mathbf{S}_n \cdot \mathbf{j}_n) \\ &= \tilde{\mathbf{S}}_n \times (\tilde{\mathbf{S}}_n \times (-\hat{\mathbf{z}}))(\tilde{\mathbf{S}}_n \cdot R\mathbf{j}_n) = \tilde{\mathbf{S}}_n \times (\tilde{\mathbf{S}}_n \times \hat{\mathbf{z}})(\tilde{\mathbf{S}}_n \cdot \tilde{\mathbf{j}}_n) = \tilde{\mathbf{T}}^c_n[\tilde{\mathbf{S}}]. \end{aligned}$$

$$R\mathbf{T}^d_n[\mathbf{S}] = R(\mathbf{S}_n \times \hat{\mathbf{z}}(\mathbf{S}_n \cdot \mathbf{j}_n)) = \tilde{\mathbf{S}}_n \times (-\hat{\mathbf{z}})(R\mathbf{S}_n \cdot R\mathbf{j}_n) = \tilde{\mathbf{S}}_n \times \hat{\mathbf{z}}(\tilde{\mathbf{S}}_n \cdot \tilde{\mathbf{j}}_n) = \tilde{\mathbf{T}}^d_n[\tilde{\mathbf{S}}].$$

That is substituting $\tilde{\mathbf{j}}$ for $\mathbf{j}$ in spin-orbit torques $\tilde{\mathbf{T}}^{so}$ for antiskyrmion, we obtain the same dynamics as for the skyrmion. Let us take a look at two last torques. To compute them we need to know how R affects gradient of the vector field $\mathbf{S}$.

Assertion 4.

$$R(\mathbf{j} \cdot \frac{\partial \mathbf{S}}{\partial \mathbf{r}}) = \mathbf{j} \cdot \frac{\partial R\mathbf{S}}{\partial \mathbf{r}}$$

Proof. From the finite difference approximation to the gradient we get

$$R(\mathbf{j} \cdot \frac{\partial \mathbf{S}}{\partial \mathbf{r}}) = R\sum_d \mathbf{j}_d \sum_m \mu_{nm,d}\mathbf{S}_m = \sum_d \mathbf{j}_d \sum_m \mu_{nm,d} R\mathbf{S}_m = \mathbf{j} \cdot \frac{\partial (R\mathbf{S})}{\partial \mathbf{r}}.$$

QED

Using Assertion 4, we can compute last two torques:

$$R\mathbf{T}_n^j[\mathbf{S}] = R(-\mathbf{j}\cdot\frac{\partial \mathbf{S}}{\partial \mathbf{r}}) = -\mathbf{j}\cdot\frac{\partial R\mathbf{S}}{\partial \mathbf{r}} = \tilde{\mathbf{T}}_n^j[\tilde{\mathbf{S}}],$$

and the last one:

$$R\mathbf{T}_n^e[\mathbf{S}] = R(\mathbf{S}_n\times(\mathbf{j}\cdot\frac{\partial \mathbf{S}_n}{\partial \mathbf{r}})) = \tilde{\mathbf{S}}_n\times R(\mathbf{j}\cdot\frac{\partial \mathbf{S}_n}{\partial \mathbf{r}}) = \tilde{\mathbf{S}}_n\times(\mathbf{j}\cdot\frac{\partial \tilde{\mathbf{S}}_n}{\partial \mathbf{r}}) = \tilde{\mathbf{T}}_n^e[\tilde{\mathbf{S}}].$$

In other words, without modification of current in spin-transfer torques dynamics of skyrmion and antiskyrmion are the same.

Conclusion. The mapping $\mathbf{S}_n \mapsto \tilde{\mathbf{S}}_n = R\mathbf{S}_n$ transforms skyrmion into antiskyrmion. Under appropriate substitution of parameters

$$\mathbf{D}_{mn} \mapsto \tilde{\mathbf{D}} = R\mathbf{D}_{mn}, \quad \mathbf{K}_j \mapsto \tilde{\mathbf{K}}_j = R\mathbf{K}_j, \quad \mathbf{B}_n \mapsto \tilde{\mathbf{B}}_n = R\mathbf{B}_n,$$

the transformation preserves energy. If there are only spin-orbit torques, under appropriate correction of currents

$$\mathbf{j} \mapsto \tilde{\mathbf{j}} = -R\mathbf{j}.$$

the transformation R preserves dynamics. All parameters not mentioned in the substitutions should not be modified. If LLG equation contains only spin-transfer torques, the dynamics is preserved without correction of the current. If both spin-orbit and spin-transfer torques are taken into account, than there is no way to correct current to preserve dynamics. Below we provide a simple procedure on how to compute antiskyrmion velocity, if one knows the velocity of corresponding skyrmion.

Thiele equation and velocity of antiskyrmion

Let us assume that the magnetic moments $\mathbf{S}_n$ are located so close to each other that we can use continuous variable $\mathbf{r}$ to describe the moment by its position $\mathbf{r}_n$. Further assuming that while skyrmion (or antiskyrmion) moves it preserves its shape, its magnetization profile as a function of time can be calculated as $\mathbf{S}(\mathbf{r};t) = \phi(\mathbf{r}-\mathbf{R}(t))$, where ϕ defines the shape, and $\mathbf{R}$ is the skyrmion center. According to Landau-Lifshitz-Gilbert equation:

$$\nabla\phi(\mathbf{r}-\mathbf{R})\cdot\mathbf{v} = \gamma\phi(\mathbf{r}-\mathbf{R})\times\frac{\partial E}{\partial \mathbf{S}}[\phi(\mathbf{r}-\mathbf{R})]$$
$$+\alpha\phi(\mathbf{r}-\mathbf{R})\times\nabla\phi(\mathbf{r}-\mathbf{R})\cdot\mathbf{v} + \mathbf{T}[\phi(\mathbf{r}-\mathbf{R})],$$

where $\mathbf{v} = \frac{d}{dt}\mathbf{R}$. After integrating the equation over all spins, the variable $\mathbf{r}$ is eliminated from the equation, and we obtain Thiele equation Thiele (1973); Tretiakov et al. (2008); Clarke et al. (2008):

$$\mathbf{G}\times\mathbf{v} - \alpha\mathbf{D}\cdot\mathbf{v} - \mathbf{B}\cdot\mathbf{j} = 0,$$

where $\mathbf{G} = (0,0,4\pi Q)$ is the gyromagnetic coupling vector, Q is the topological charge, $\mathbf{D}$ is the dissipative force tensor, and the tensor $\mathbf{B}$ is determined by the torques.

Let us consider motion of skyrmion in the presence of spin-orbit torques and spin-transfer torques, than tensor $\mathbf{B} = \mathbf{B}^{so} + \mathbf{B}^{st}$ spilts into two parts, corresponding to spin-orbit torques $\mathbf{B}^{so}$ and spin-transfer torques $\mathbf{B}^{st}$. Then we define two velocities $\mathbf{v}^{so}$ and $\mathbf{v}^{st}$ corresponding to the skyrmion motion due to only spin-orbit and spin-transfer torques, respectively:

$$\mathbf{G} \times \mathbf{v}^{so} - \alpha \mathbf{D} \cdot \mathbf{v}^{so} - \mathbf{B}^{so} \cdot \mathbf{j} = 0,$$

$$\mathbf{G} \times \mathbf{v}^{st} - \alpha \mathbf{D} \cdot \mathbf{v}^{st} - \mathbf{B}^{st} \cdot \mathbf{j} = 0.$$

These velocities depend on the current, i. e. $\mathbf{v}^{so}(\mathbf{j})$ and $\mathbf{v}^{st}(\mathbf{j})$. If the skyrmion shape is the same for the transport under spin-orbit and spin-transfer torques, the skyrmion velocity under both torques is their superposition: $\mathbf{v}(\mathbf{j}) = \mathbf{v}^{so}(\mathbf{j}) + \mathbf{v}^{st}(\mathbf{j})$.

Now we consider antiskyrmion, corresponding to the discussed above skyrmion:

$$\tilde{\mathbf{S}}(\mathbf{r}) = R\phi(\mathbf{r} - \tilde{\mathbf{R}}).$$

We know that the shapes of skyrmion and antiskyrmion are matched up to the transformation R, however trajectory $\tilde{\mathbf{R}}$ of the antiskyrmion may be different. Landau-Lifshitz-Gilbert equation for antiskyrmion gives us another Thiele equation with possibly another tensors corresponding to modified parameters, the modified parameters are marked by hat as above. We already proved that the solution of LLG equation for skyrmions and antiskyrmions with modified parameters is the same up to the transformation R, hence solution to Thiele equation must also coincide:

$$\tilde{\mathbf{G}} \times \mathbf{v}^{so}(\tilde{\mathbf{j}}) - \alpha \tilde{\mathbf{D}} \cdot \mathbf{v}^{so}(\tilde{\mathbf{j}}) - \tilde{\mathbf{B}}^{so} \cdot \tilde{\mathbf{j}} = 0,$$

$$\tilde{\mathbf{G}} \times \mathbf{v}^{st}(\mathbf{j}) - \alpha \tilde{\mathbf{D}} \cdot \mathbf{v}^{st}(\mathbf{j}) - \tilde{\mathbf{B}}^{st} \cdot \mathbf{j} = 0.$$

Since Thiele equation is linear, its solution with both SOT and STT is a sum of solutions for separate SOT and STT Thiele equations. Therefore, the antiskyrmion velocity is

$$\mathbf{v}(\mathbf{j}) = \mathbf{v}^{so}(-R\mathbf{j}) + \mathbf{v}^{st}(\mathbf{j}).$$

In other words, the velocity of antiskyrmion is a superposition of skyrmion velocity subjected to the same spin-transfer torques and skyrmion velocity subjected to the spin-orbit torques for reflected by R current.

References

Ado, I. A., Tretiakov, O. A., and Titov, M. (2017). Microscopic theory of spin-orbit torques in two dimensions. *Physical Review B*, 95:094401.

Barker, J. and Tretiakov, O. A. (2016). Static and dynamical properties of antiferromagnetic skyrmions in the presence of applied current and temperature. *Physical Review Letters*, 116(14):147203.

Belavin, A. A. and Polyakov, A. M. (1975). Metastable states of two-dimensional isotropic ferromagnets. *JETPL*, 22:245.

Bessarab, P. F., Müller, G. P., Lobanov, I. S., Rybakov, F. N., Kiselev, N. S., Jónsson, H., Uzdin, V. M., Blügel, S., Bergqvist, L., and Delin, A. (2018). Lifetime of racetrack skyrmions. *Scientific Reports*, 8:3433.

Bessarab, P. F., Uzdin, V. M., and Jónsson, H. (2012). Harmonic transition-state theory of thermal spin transitions. *Physical Review B - Condensed Matter and Materials Physics*, 85(18):184409.

Bessarab, P. F., Uzdin, V. M., and Jónsson, H. (2013a). Potential energy surfaces and rates of spin transitions. *Zeitschrift fur Physikalische Chemie*, 227(11):1543–1557.

Bessarab, P. F., Uzdin, V. M., and Jónsson, H. (2013b). Size and shape dependence of thermal spin transitions in Nanoislands. *Physical Review Letters*, 110(2):020604.

Bessarab, P. F., Uzdin, V. M., and Jónsson, H. (2014). Calculations of magnetic states and minimum energy paths of transitions using a noncollinear extension of the Alexander-Anderson model and a magnetic force theorem. *Physical Review B - Condensed Matter and Materials Physics*, 89:214424.

Bessarab, P. F., Yudin, D., Gulevich, D. R., Wadley, P., Titov, M., and Tretiakov, O. A. (2019). Stability and lifetime of antiferromagnetic skyrmions. *Physical Review B*, 99:140411.

Bogdanov, A. and Yablonskii, D. (1989). Thermodynamically stable "vortices" in magnetically ordered crystals. The mixed state of magnets. *Sov. Phys. JETP*, 68:101–103.

Bordács, S., Butykai, A., Szigeti, B. G., White, J. S., Cubitt, R., Leonov, A. O., Widmann, S., Ehlers, D., Nidda, H. A. V., Tsurkan, V., Loidl, A., and Kézsmárki, I. (2017). Equilibrium skyrmion lattice ground state in a polar easy-plane magnet. *Scientific Reports*, 7(1):7584.

Boulle, O., Vogel, J., Yang, H., Pizzini, S., Chaves, D. D. S., Locatelli, A., Menteş, T. O., Sala, A., Buda-Prejbeanu, L. D., Klein, O., Belmeguenai, M., Roussigné, Y., Stashkevich, A., Chérif, S. M., Aballe, L., Foerster, M., Chshiev, M., Auffret, S., Miron, I. M., and Gaudin, G. (2016). Room-temperature chiral magnetic skyrmions in ultrathin magnetic nanostructures. *Nature Nanotechnology*, 11(5):449–454.

Büttner, F., Lemesh, I., and Beach, G. S. D. (2018). Theory of isolated magnetic

skyrmions: From fundamentals to room temperature applications. *Scientific Reports*, 8(1):4464.

Camosi, L., Rougemaille, N., Fruchart, O., Vogel, J., and Rohart, S. (2018). Micromagnetics of antiskyrmions in ultrathin films. *Physical Review B*, 97:134404.

Caretta, L., Mann, M., Büttner, F., Ueda, K., Pfau, B., Günther, C. M., Hessing, P., Churikova, A., Klose, C., Schneider, M., Engel, D., Marcus, C., Bono, D., Bagschik, K., Eisebitt, S., and Beach, G. S. (2018). Fast current-driven domain walls and small skyrmions in a compensated ferrimagnet. *Nature Nanotechnology*, 13(12):1154–1160.

Clarke, D. J., Tretiakov, O. A., Chern, G. W., Bazaliy, Y. B., and Tchernyshyov, O. (2008). Dynamics of a vortex domain wall in a magnetic nanostrip: Application of the collective-coordinate approach. *Physical Review B - Condensed Matter and Materials Physics*, 78:134412.

Coffey, W. T., Garanin, D. A., and McCarthy, D. J. (2001). Crossover formulas in the Kramers theory of thermally activated escape rates-application to spin systems. *Advances in Chemical Physics*, 117:483–765.

Cortés-Ortuño, D., Wang, W., Beg, M., Pepper, R. A., Bisotti, M. A., Carey, R., Vousden, M., Kluyver, T., Hovorka, O., and Fangohr, H. (2017). Thermal stability and topological protection of skyrmions in nanotracks. *Scientific Reports 2017 7:1*, 7:1–13.

Desplat, L., Suess, D., Kim, J. V., and Stamps, R. L. (2018). Thermal stability of metastable magnetic skyrmions: Entropic narrowing and significance of internal eigenmodes. *Physical Review B*, 98(13):134407.

Duine, R. A., Lee, K. J., Parkin, S. S., and Stiles, M. D. (2018). Synthetic antiferromagnetic spintronics. *Nature Physics 2018 14:3*, 14:217–219.

Dzyaloshinsky, I. (1958). A thermodynamic theory of "weak" ferromagnetism of antiferromagnetics. *Journal of Physics and Chemistry of Solids*, 4(4):241–255.

E, W., Ren, W., and Vanden-Eijnden, E. (2002). String method for the study of rare events. *Physical Review B - Condensed Matter and Materials Physics*, 66(5):052301.

Fert, A., Reyren, N., and Cros, V. (2017). Magnetic skyrmions: Advances in physics and potential applications. *Nature Reviews Materials*, 2(7):17031.

Fert, A. R. (1991). Magnetic and transport properties of metallic multilayers. *Materials Science Forum*, 59-60:439–480.

Fiedler, G., Fidler, J., Lee, J., Schrefl, T., Stamps, R. L., Braun, H. B., and Suess, D. (2012). Direct calculation of the attempt frequency of magnetic structures using the finite element method. *Journal of Applied Physics*, 111:093917.

Finocchio, G., Büttner, F., Tomasello, R., Carpentieri, M., and Kläui, M. (2016). Magnetic skyrmions: From fundamental to applications. *Journal of Physics D: Applied Physics*, 49(42):423001.

Golub, G. H. and Loan, C. F. V. (2013). Matrix computations. *JHU press*, 3.

Heil, B., Rosch, A., and Masell, J. (2019). Universality of annihilation barriers of large magnetic skyrmions in chiral and frustrated magnets. *Physical Review B*, 100(13):134424.

Heinze, S., Bergmann, K. V., Menzel, M., Brede, J., Kubetzka, A., Wiesendanger, R., Bihlmayer, G., and Blügel, S. (2011). Spontaneous atomic-scale magnetic skyrmion lattice in two dimensions. *Nature Physics*, 7(9):713–718.

Heistracher, P., Abert, C., Bruckner, F., Vogler, C., and Suess, D. (2018). GPU-accelerated atomistic energy barrier calculations of skyrmion annihilations. *IEEE Transactions on Magnetics*, 54(11):7206105.

Henkelman, G. and Jónsson, H. (1999). A dimer method for finding saddle points on high dimensional potential surfaces using only first derivatives. *Journal of Chemical Physics*, 111(15):7010–7022.

Henkelman, G., Uberuaga, B. P., and Jónsson, H. (2000). Climbing image nudged elastic band method for finding saddle points and minimum energy paths. *Journal of Chemical Physics*, 113(22):9901–9904.

Hoffmann, M., Müller, G. P., and Blügel, S. (2020). Atomistic perspective of long lifetimes of small skyrmions at room temperature. *Physical Review Letters*, 124(24):247201.

Huang, S., Zhou, C., Chen, G., Shen, H., Schmid, A. K., Liu, K., and Wu, Y. (2017). Stabilization and current-induced motion of antiskyrmion in the presence of anisotropic dzyaloshinskii-moriya interaction. *Physical Review B*, 96:144412.

Hänggi, P., Talkner, P., and Borkovec, M. (1990). Reaction-rate theory: Fifty years after Kramers. *Reviews of Modern Physics*, 62(2):251–341.

Ivanov, A., Bessarab, P. F., Uzdin, V. M., and Jónsson, H. (2017). Magnetic exchange force microscopy: Theoretical analysis of induced magnetization reversals. *Nanoscale*, 9(35):13320–13325.

Ivanov, A. V., Dagbartsson, D., Tranchida, J., Uzdin, V. M., and Jónsson, H. (2020). Efficient optimization method for finding minimum energy paths of magnetic transitions. *Journal of Physics Condensed Matter*, 32(34).

Jena, J., Göbel, B., Ma, T., Kumar, V., Saha, R., Mertig, I., Felser, C., and Parkin, S. S. (2020). Elliptical bloch skyrmion chiral twins in an antiskyrmion system. *Nature Communications 2020 11:1*, 11:1–9.

Jiang, W., Zhang, X., Yu, G., Zhang, W., Wang, X., Jungfleisch, M. B., Pearson, J. E., Cheng, X., Heinonen, O., Wang, K. L., Zhou, Y., Hoffmann, A., and Velthuis, S. G. T. (2017). Direct observation of the skyrmion Hall effect. *Nature Physics*, 13(2):162–169.

Kang, W., Huang, Y., Zhang, X., Zhou, Y., and Zhao, W. (2016). Skyrmion-Electronics: An Overview and Outlook. *Proceedings of the IEEE*, 104(10):2040–2061.

Krause, S., Herzog, G., Stapelfeldt, T., Berbil-Bautista, L., Bode, M., Vedmedenko, E. Y., and Wiesendanger, R. (2009). Magnetization reversal of nanoscale islands: How size and shape affect the arrhenius prefactor. *Physical Review Letters*, 103:127202.

Kuchkin, V. M. and Kiselev, N. S. (2020). Turning a chiral skyrmion inside out. *Physical Review B*, 101:064408.

Legrand, W., Maccariello, D., Ajejas, F., Collin, S., Vecchiola, A., Bouzehouane, K., Reyren, N., Cros, V., and Fert, A. (2020). Room-temperature stabilization of antiferromagnetic skyrmions in synthetic antiferromagnets. *Nature Materials*, 19(1):34–42.

Litzius, K., Lemesh, I., Krüger, B., Bassirian, P., Caretta, L., Richter, K., Büttner, F., Sato, K., Tretiakov, O. A., Förster, J., Reeve, R. M., Weigand, M., Bykova, I., Stoll, H., Schütz, G., Beach, G. S., and Klaüi, M. (2017). Skyrmion Hall effect revealed by direct time-resolved X-ray microscopy. *Nature Physics*, 13(2):170–175.

Lobanov, I., Potkina, M., Jónsson, H., and Uzdin, V. (2017). Truncated minimum energy

path method for finding first order saddle points. *Nanosystems: Physics, Chemistry, Mathematics*, 8(5):586–595.

Lobanov, I. S., Jónsson, H., and Uzdin, V. M. (2016). Mechanism and activation energy of magnetic skyrmion annihilation obtained from minimum energy path calculations. *Physical Review B*, 94(17):174418.

Lobanov, I. S. and Uzdin, V. M. (2021). The lifetime of micron scale topological chiral magnetic states with atomic resolution. *Computer Physics Communications*, 269.

Malottki, S. V., Dupé, B., Bessarab, P. F., Delin, A., and Heinze, S. (2017). Enhanced skyrmion stability due to exchange frustration. *Scientific Reports*, 7(1):12299.

Moriya, T. (1960). Anisotropic superexchange interaction and weak ferromagnetism. *Physical Review*, 120(1):91–98.

Moskalenko, M., Bessarab, P. F., Uzdin, V. M., and Jónsson, H. (2016). Qualitative insight and quantitative analysis of the effect of temperature on the coercivity of a magnetic system. *AIP Advances*, 6(2):025213.

Mühlbauer, S., Binz, B., Jonietz, F., Pfleiderer, C., Rosch, A., Neubauer, A., Georgii, R., and Böni, P. (2009). Skyrmion lattice in a chiral magnet. *Science*, 323:915–919.

Müller, G. P., Bessarab, P. F., Vlasov, S. M., Lux, F., Kiselev, N. S., Blügel, S., Uzdin, V. M., and Jónsson, H. (2018). Duplication, collapse, and escape of magnetic skyrmions revealed using a systematic saddle point search method. *Physical Review Letters*, 121(19):197202.

Nagaosa, N. and Tokura, Y. (2013). Topological properties and dynamics of magnetic skyrmions. *Nature Nanotechnology*, 8(12):899–911.

Nayak, A. K., Kumar, V., Ma, T., Werner, P., Pippel, E., Sahoo, R., Damay, F., Rößler, U. K., Felser, C., and Parkin, S. S. (2017). Magnetic antiskyrmions above room temperature in tetragonal Heusler materials. *Nature*, 548(7669):561–566.

Olsen, R. A., Kroes, G. J., Henkelman, G., Arnaldsson, A., and Jónsson, H. (2004). Comparison of methods for finding saddle points without knowledge of the final states. *Journal of Chemical Physics*, 121(20):9776–9792.

Paul, S., Haldar, S., von Malottki, S., and Heinze, S. (2020). Role of higher-order exchange interactions for skyrmion stability. *Nature Communications*, 11(1):4756.

Peng, L., Takagi, R., Koshibae, W., Shibata, K., Nakajima, K., hisa Arima, T., Nagaosa, N., Seki, S., Yu, X., and Tokura, Y. (2020). Controlled transformation of skyrmions and antiskyrmions in a non-centrosymmetric magnet. *Nature Nanotechnology 2020 15:3*, 15:181–186.

Rohart, S., Miltat, J., and Thiaville, A. (2016). Path to collapse for an isolated Néel skyrmion. *Physical Review B*, 93(21):214412.

Romming, N., Hanneken, C., Menzel, M., Bickel, J. E., Wolter, B., Bergmann, K. V., Kubetzka, A., and Wiesendanger, R. (2013). Writing and deleting single magnetic skyrmions. *Science*, 341(6146):636–639.

Romming, N., Kubetzka, A., Hanneken, C., Bergmann, K. V., and Wiesendanger, R. (2015). Field-dependent size and shape of single magnetic skyrmions. *Physical Review Letters*, 114(17):177203.

Rybakov, F. N., Borisov, A. B., Blügel, S., and Kiselev, N. S. (2015). New type of stable particlelike states in chiral magnets. *Physical Review Letters*, 115.

Suess, D., Vogler, C., Bruckner, F., and Abert, C. (2018). A repulsive skyrmion chain as a guiding track for a racetrack memory. *AIP ADVANCES*, 8:115301.

Tatara, G. and Kohno, H. (2004). Theory of current-driven domain wall motion: Spin transfer versus momentum transfer. *Physical Review Letters*, 92:086601.

Thiaville, A., García, J. M., Dittrich, R., Miltat, J., and Schrefl, T. (2003). Micromagnetic study of bloch-point-mediated vortex core reversal. *Phys. Rev. B*, 67:094410.

Thiaville, A., Nakatani, Y., Miltat, J., and Suzuki, Y. (2005). Micromagnetic understanding of current-driven domain wall motion in patterned nanowires. *Europhysics Letters*, 69:990.

Thiele, A. A. (1973). Steady-state motion of magnetic domains. *Physical Review Letters*, 30:230.

Tretiakov, O. A., Clarke, D., Chern, G. W., Bazaliy, Y. B., and Tchernyshyov, O. (2008). Dynamics of domain walls in magnetic nanostrips. *Physical Review Letters*, 100:127204.

Uzdin, V. M., Potkina, M. N., Lobanov, I. S., Bessarab, P. F., and Jónsson, H. (2018a). The effect of confinement and defects on the thermal stability of skyrmions. *Physica B: Condensed Matter*, 549:6–9.

Uzdin, V. M., Potkina, M. N., Lobanov, I. S., Bessarab, P. F., and Jónsson, H. (2018b). Energy surface and lifetime of magnetic skyrmions. *Journal of Magnetism and Magnetic Materials*, 459:236–240.

Varentcova, A. S., von Malottki, S., Potkina, M. N., Kwiatkowski, G., Heinze, S., and Bessarab, P. F. (2020). Toward room-temperature nanoscale skyrmions in ultrathin films. *npj Computational Materials*, 6:1–11.

Vedmedenko, E. Y., Udvardi, L., Weinberger, P., and Wiesendanger, R. (2007). Chiral magnetic ordering in two-dimensional ferromagnets with competing Dzyaloshinsky-Moriya interactions. *Physical Review B - Condensed Matter and Materials Physics*, 75(10):104431.

Voter, A. F. (1985). A monte carlo method for determining free-energy differences and transition state theory rate constants. *The Journal of Chemical Physics*, 82:1890.

Wang, X. S., Yuan, H. Y., and Wang, X. R. (2018). A theory on skyrmion size. *Communications Physics*, 1(1):1–7.

Woo, S., Litzius, K., Krüger, B., Im, M. Y., Caretta, L., Richter, K., Mann, M., Krone, A., Reeve, R. M., Weigand, M., Agrawal, P., Lemesh, I., Mawass, M. A., Fischer, P., Kläui, M., and Beach, G. S. (2016). Observation of room-temperature magnetic skyrmions and their current-driven dynamics in ultrathin metallic ferromagnets. *Nature Materials*, 15(5):501–506.

Woo, S., Song, K. M., Zhang, X., Zhou, Y., Ezawa, M., Liu, X., Finizio, S., Raabe, J., Lee, N. J., Kim, S. I., Park, S. Y., Kim, Y., Kim, J. Y., Lee, D., Lee, O., Choi, J. W., Min, B. C., Koo, H. C., and Chang, J. (2018). Current-driven dynamics and inhibition of the skyrmion Hall effect of ferrimagnetic skyrmions in GdFeCo films. *Nature Communications*, 9(1):959.

Yang, Y. (2001). Solitons in field theory and nonlinear analysis. *Springer*, pages 43–48.

Zhang, S., Petford-Long, A. K., and Phatak, C. (2016). Creation of artificial skyrmions and antiskyrmions by anisotropy engineering. *Scientific Reports 2016 6:1*, 6:1–10.

Article I

Lifetime of skyrmions in discrete systems with infinitesimal lattice constant

Potkina M. N., Lobanov I.S., Jónsson H., Uzdin V. M.

JMMM. **549**, 168974 (2022)

Graphical Abstract

Lifetime of skyrmions in discrete systems with infinitesimal lattice constant

M.N. Potkina, I.S. Lobanov, H. Jónsson, V.M. Uzdin

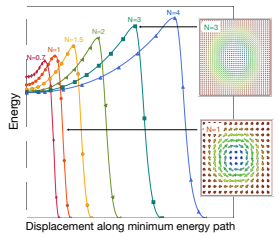

Highlights

Lifetime of skyrmions in discrete systems with infinitesimal lattice constant

M.N.Potkina, I.S. Lobanov, H. Jónsson, V.M. Uzdin

- The lifetime of skyrmions is estimated within the framework of the harmonic transition-state theory
- Collapse inside the sample and escape through the boundary are considered.
- Pre-exponential factors and activation barriers are calculated for systems with different lattice constants corresponding to the same continuous micromagnetic model.
- The manifestation of topological protection of chiral magnetic structures in discrete systems is shown.

Lifetime of skyrmions in discrete systems with infinitesimal lattice constant

M.N.Potkina[a,b,c], I.S. Lobanov[a,b], H. Jónsson[c], V.M. Uzdin[a,b]

[a]*Department of Physics, St. Petersburg State University, St.Petersburg, 198504, St.Petersburg, Russia*
[b]*Department of Physics, ITMO University, St.Petersburg, 197101, Russia*
[c]*Science Institute and Faculty of Physical Sciences, University of Iceland, Reykjavik, VR-III, 107, Iceland*

Abstract

Topological protection of chiral magnetic structures is investigated by taking a two-dimensional magnetic skyrmion as an example. The skyrmion lifetime is calculated based on harmonic transition state theory for a discrete lattice model using various values of the ratio of the lattice constant and the skyrmion size. Parameters of the system corresponding to exchange, anisotropy and Dzyaloshinsky-Moriya interaction are chosen in such a way as to keep the energy and size of the skyrmion unchanged for small values of the lattice constant, using scaling relations derived from continuous micromagnetic description. The number of magnetic moments included in the calculations reaches more than a million. The results indicate that in the limit of infinitesimal lattice constant, the energy barrier for skyrmion collapse approaches the Belavin-Polyakov lower bound of the energy of a topological soliton in the σ-model, the entropy contribution to the pre-exponential factor in the Arrhenius rate expression for collapse approaches a constant and the skyrmion lifetime can, for large enough number of spins, correspond to thermally stable skyrmion at room temperature even without magnetic dipole-dipole interaction.

Keywords: chiral magnet, skyrmion, topological protection, lifetime
PACS: 75.25.+z

Preprint submitted to Journal of Magnetism and Magnetic Materials November 24, 2021

1. Introduction

Topological chiral magnetic structures, such as magnetic skyrmions, are promising information carriers in future generations of racetrack memory, logical and neuromorphic devices [1, 2, 3]. For such applications, thermal stability is a fundamental issue as thermal fluctuations and external disturbances can lead to structural breakdown and loss of the information encoded in the magnetic configurations. The theoretically predicted stability of topological magnetic systems is associated with the existence of a nonzero topological charge, an integer that cannot change under continuous variation of the magnetization. Magnetic skyrmion and homogeneous ferromagnetic states have different topological charges and, therefore, cannot be transformed into each other by continuous magnetization transformation [4]. In real materials, magnetic moments are localized at discrete sites of the crystal lattice, and the topological arguments do, strictly speaking, not apply. Instead, one might expect to find finite energy barriers between states with different topological charges and if they are large enough the states can be protected against destruction by thermal fluctuations. However, estimates of the energy barrier for the collapse of the small skyrmions in PdFe/Ir(111) [5, 6, 7] and Co/Pt [8], which have diameter 1-10 nm, are below 150 meV. This is of similar magnitude as energy barriers for magnetization reversal in small Fe islands on W(110) surface, where no topological change is involved [9, 10]. The lifetime of nanoscale skyrmions studied so far appears to be of the same order of magnitude as that of non-topological magnetic structures of the same size. This means that despite the apparent topological protection, small skyrmions are quite unstable and can hardly exist at room temperature.

Theoretical model calculations of skyrmion lifetime have, however, shown that it is in principle possible to identify material parameters giving stable skyrmions at room temperature. Parameter values can be found that lead to large enough energy barrier for skyrmion collapse and small enough prefactor in the Arrhenius expression for the lifetime [11]. The question remains whether materials can be found that correspond to these parameter values. The manipulation of magnetic properties at atomic scale is a challenging task and the possible range for parameter values in quite narrow. On the micron scale for large skyrmions, effective parameters can be modified more easily. For example, in layered structures containing ferromagnetic (FM) layers and hard metal layers with large spin-orbit interaction, the effective Dzyaloshinsky-Moriya interaction (DMI) can be varied in a con-

trolled way by the choice of materials and layer thickness. In such structures, skyrmion states have been found to be stable even above room temperature [12, 13]. Such modification of effective parameters that can lead to increased skyrmion stability is not directly related to topological protection. Moreover, as the number of magnetic moments in the skyrmion increases, the magnetic dipole interaction becomes more important and some have argued that it is the dipole interaction that is responsible for the observed stability of micron-scale skyrmions [14]. Whether it is possible to have stability at room temperature in thin layers with negligible dipole interaction is still an open question. Furthermore, for skyrmions in antiferro- and ferrimagnets [15], as well as in synthetic antiferromagnets [16], where the magnetic dipole-dipole interaction is suppressed, the mechanism of stabilization still needs to be elucidated.

The stability of magnetic states depends not only on the activation energy of the transitions the system can undergo from these states but also on the pre-exponential factor in the Arrhenius expression for the rate of the magnetic transitions which depends on the the shape of the energy surface in the vicinity of the initial and transition states [17, 18]. The role of the pre-exponential factor increases with increasing temperature. According to recent theoretical studies, [11] this can be used to create small 2D skyrmions that are stable at room temperature, although materials with the parameters proposed in [11] have not yet been found. A change in the pre-exponential factor by more than 30 orders of magnitude for small changes in the magnetic field has been reported from experimental measurements [19].

When the size of a skyrmion is increased, the direction of neighboring magnetic moments becomes more similar and the continuous magnetization model becomes more appropriate for describing the system. How does topological protection present in continuous models manifest itself in the limit of infinitesimal lattice constant in discrete models? What limit does the energy barrier for skyrmion annihilation and the skyrmion lifetime approach when the ratio of the lattice constant and the skyrmion radius becomes infinitesimal? These questions are addressed in the present article. We calculate the energy of the skyrmion state, the minimum energy path between the metastable skyrmion and the homogeneous FM state, and the activation energy of the skyrmion collapse as well as escape through a boundary for a gradually decreasing lattice constants while the skyrmion radius is kept constant. The pre-exponential factor in the Arrhenius for the life time is estimated within the harmonic approximation to transition state theory (HTST) [17]

for several values of the lattice constant. All parameters of the system, such as the exchange and anisotropy constants as well as the DMI are chosen in such a way as to keep the size of the skyrmion and its energy unchanged for small enough lattice constant. The parameter values for the discrete lattice model are scaled with the lattice constant in such a way as to be consistent with the same continuous micromagnetic model. The calculated results can be interpreted either in terms of trends when the lattice constant is decreased and the skyrmion size remains the same, or in terms of increased skyrmion size if the lattice constant is taken to be the same.

The article is organized as follows. First, in section 2. the model and the computational methodology is described. Then, in section 3, the results are presented along with discussions. Conclusions are given in section 4.

2. Model and methods

In this section the Hamiltonian of the systems studied is defined and the computational methods used to estimate the energy barrier and pre-exponential factor in the Arrhenius expression for the life time described.

2.1. Model

The energy of the magnetic system is described by a Heisenberg-type expression for the energy of a two-dimensional (2D) square lattice

$$E[\mathbf{S}] = -\sum_{<j,k>} (J_{jk}\mathbf{S}_j \cdot \mathbf{S}_k + \mathbf{D}_{j,k} \cdot (\mathbf{S}_j \times \mathbf{S}_k)) - K\sum_j S_{j,z}^2 - \mu\sum_j \mathbf{B} \cdot \mathbf{S}_j, \quad (1)$$

where $\mathbf{S}_i$ is a unit vector giving the direction of the magnetic moment at site i, μ is the value of magnetic moments taken to be the same on all sites, J is the exchange parameter that is non-zero only for nearest-neighbour sites, and K is anisotropy parameter. The DMI vector $\mathbf{D}_{j,k}$ is taken to lie in the plane of the lattice and point in the direction along the vector connecting atomic sites j and k, thereby stabilizing a Bloch-type skyrmion. Formally, the lattice constant does not enter in eqn. (1), but when the same system is described with higher resolution, i.e. smaller lattice constant, the parameter values corresponding to this system need to be changed in a certain way. In order to achieve this, a connection between the Heisenberg-type model and a micromagnetic model with continuous distribution of magnetisation is used.

There, the energy with respect to the homogeneous FM state can be written as

$$E = \int \omega(\mathbf{r}) d^2\mathbf{r}, \tag{2}$$

where

$$\omega(\mathbf{r}) = \mathcal{A}\|\nabla\mathbf{S}(\mathbf{r})\|^2 - \mathcal{D}(\mathbf{S}(\mathbf{r}) \cdot \mathrm{rot}\mathbf{S}(\mathbf{r})) - \mathcal{K}(\mathbf{K^0} \cdot \mathbf{S}(\mathbf{r})) - \mathcal{M}(\mathbf{B} \cdot \mathbf{S}(\mathbf{r})) \tag{3}$$

The integration is taken over the whole $\mathbb{R}^2$ space. The exchange stiffness $\mathcal{A}$, DMI density $\mathcal{D}$, anisotropy density $\mathcal{K}$ and magnetization $\mathcal{M}$ are proportional to the exchange parameter J_{jk}, modulus of the DMI vector $\mathbf{D}_{j,k}$, anisotropy constant K and μ in (1), respectively. The coefficients of proportionality depend on the type of crystal lattice, number of exchange parameters used in lattice model, *etc.* While the correspondence between continuous and lattice models is ambiguous in that different lattice parameters can correspond to a given micromagnetic model, the scaling of parameters in the discrete model is determined uniquely and depends only on the dimensionality of the system. For a 2D system, micromagnetic parameter values can be converted into parameter values for a discrete model of a square lattice with lattice constant h by

$$J = 2\mathcal{A}, \quad D = h\mathcal{D}, \quad K = h^2\mathcal{K}, \quad \mu = h^2\mathcal{M}.$$

This gives a scaling law for the values of the parameters as the lattice constant is changed in such a way that correspondence is maintained to the same micromagnetic model

$$D\,(h/N) = \frac{D(h)}{N}, \quad K\,(h/N) = \frac{K(h)}{N^2}, \quad \mu\,(h/N) = \frac{\mu(h)}{N^2} \tag{4}$$

while J is independent of N. Within this framework, calculations were performed for the following set of dimensionless parameters and $N = 1$: $D/J = 0.35$, $K/J = 0.16$, $\mu B/J = 0.02$. The cell size, $l = 30$ (30×30 spins subject to periodic boundary conditions) was chosen to be sufficiently large compared to the skyrmion size to prevent the influence of boundary conditions on the state of the skyrmion. In what follows, we will refer to N as the scaling parameter, which denotes how the lattice constant is scaled.

In addition to the extended 2D system, calculations are also presented for a magnetic track with finite width in one dimension. Periodic boundary conditions are then only applied in the direction of the track while free boundaries are then used in the perpendicular direction, along the edges of

the track. The escape of the skyrmion through the edge of the track is studied also as a function of N.

2.2. Methodology

The lifetime of the skyrmion state is estimated within the framework of HTST for magnetic degrees of freedom [17]. Within this approximation, the lifetime, τ, has an Arrhenius dependence on temperature

$$\tau = \tau_0 e^{\Delta E/k_B T} \tag{5}$$

where ΔE is the activation energy given by the energy difference between the saddle point and the initial state, T is the absolute temperature and τ_0 is the pre-exponential factor related to the entropy difference between the transition state and the initial state, as well as the flux through the transition state. In a continuum description of the system, a smooth transformation of the magnetization connecting the skyrmion and FM states does not exist since these states have different topological charge [4]. However, for a discrete lattice description, such a magnetic transition is possible for any lattice constant, but there can be a significant energy barrier for annihilation making the skyrmion state stable for practical purposes. The question addressed here is how the activation energy and the pre-exponential factor depend on the scaling factor, especially in the limit of infinitesimal lattice constant which is the closest a discrete model comes to the continuum model.

To study this dependence, the minimum energy path (MEP) between the skyrmion and the FM state is calculated. The point of highest energy along the MEP, a first order saddle point on the multidimensional energy surface given by eq. (1), minus the initial state energy gives the activation energy for the transition. For $N = 1$ the dimensionality of the energy surface is already high, 1800, and it increases as the square of the scaling parameter, N^2. For small N, the MEP can easily be calculated using the geodesic nudged elastic band method [20, 21]. When N becomes large, this, however, becomes a computationally demanding task. Since the shape of the path is known it is possible to focus only on the region around the maximum and thereby reduce the effort significantly [22]. In this way calculations can be carried out for large values of N, even larger than $N = 100$.

In HTST, the energy surface near the initial state and near the saddle point on the energy surface corresponding to the transition state is approximated by a quadratic expansions. Zero modes corresponding to degrees of

freedom for which the energy does not change significantly need to be treated separately. The expression for the attempt frequency $f_0 = 1/\tau_0$ is [17, 23]

$$f_0 = \frac{1}{2\pi}(2\pi k_B T)^{\frac{(P_{sk}-P_{sp})}{2}} \frac{V_{sp}}{V_{sk}} \sqrt{\sum_{j=2}^{D-P_{sp}} b_j^2 \epsilon_{sp,j} \frac{\prod_{j=1}^{D-P_{sk}} \sqrt{\epsilon_{sk,j}}}{\prod_{j=2}^{D-Psp} \sqrt{\epsilon_{sp,j}}}} \tag{6}$$

Here $\epsilon_{sk,j}$ and $\epsilon_{sp,j}$ are the eigenvalues of the Hessian matrix for the initial skyrmion state and at the saddle point, respectively, V_{sk} and V_{sp} give the volume corresponding to zero modes while P_{sk} and P_{sp} the number of such modes. The summation for the saddle point does not include the negative eigenvalue $\epsilon_{sp,1}$ and starts at $j = 2$. The number D in the upper limit of the summations is equal to the dimension of the energy surface $2N^2I^2$. The variables b_j denote the expansion coefficients for the unstable mode at the saddle point derived from the linearized Landau-Lifshitz equation of motion. More precisely $b_j = \frac{\gamma}{\mu}(\mathbf{e}_{sp,1} \cdot [\mathbf{S}_{sp} \times \mathbf{e}_{sp,j}])$, where γ is the gyromagnetic ratio, μ the length of the magnetic moments, $\mathbf{e}_{sp,1}$ and $\mathbf{e}_{sp,j}$ are the unit vectors along the first eigenvalue (normal to dividing surface) and the j-th eigenvector of the Hessian at the saddle point, and $\mathbf{S}_{sp}$ corresponds to the spin configuration at the saddle point [24].

First, consider the entropic contribution to the expression for f_0 with the product of square roots of the positive eigenvalues of the Hessian in the numerator (for skyrmion state) and denominator (for transition state)(6). These expressions can be rewritten as

$$\prod_i^{D^*} \sqrt{\epsilon_i} = \exp\left(\frac{1}{2}\sum_i^{D^*} \ln \epsilon_i\right) = \left[\exp\left(\frac{1}{D^*}\sum_i^{D^*} \frac{1}{2} \ln \epsilon_i\right)\right]^{D^*} \tag{7}$$

The upper limit D^* in eq. (7) takes into account the absence of zero modes at the saddle point and in the skyrmion state, as well as the negative eigenvalue at the saddle point.

Recently, another algorithm for calculating the entropic contribution to the pre-exponential factor has been presented [24]. This contribution can be written via determinants of the Hessian at the minimum and saddle point. An algorithm for calculating these determinants without searching for eigenvalues of the Hessian but using recursive relations makes use of the sparse

structure of the Hessian matrix for energy in the Heisenberg-like energy expression when only short-range interactions are included. The method makes it possible to calculate determinants for systems containing millions of magnetic moments. This makes it possible to calculate the pre-exponential factor and estimate the lifetimes of micron-scale topological structures with atomic resolution [25].

3. Results and discussion

Results are presented from calculations of both activation energy and pre-exponential factor in the Arrhenius expression for the life time of the skyrmion. Two annihilation mechanisms are considered, radial collapse within an extended 2D system and escape through the edge of a track with finite width.

3.1. Activation energy

Figure 1 shows the computed MEPs for radial skyrmion collapse for several values of N. The path length represents the total change in orientation of all the spins and therefore increases with N since a larger number of spins then forms the skyrmion structure. The energy of the initial skyrmion state first decreases with N, but already at $N > 2$ the change becomes insignificant. The energy maximum along the MEP increases with scaling parameter and is still increasing for $N = 4$. But, calculations for much larger values of N show that at $N \approx 100$ and larger the maximum energy changes insignificantly and approaches the lower bound of the energy of a topological soliton given by the σ-model [26]. This can be understood from the fact that, according to the scaling relations in eq. (4), all the parameters of the expression for the energy in eq. (1), with the exception of the exchange parameter J, tend to zero with increasing N. Nevertheless, the contribution of various terms in eq. (1) to the energy of the skyrmion state does not change since the number of magnetic moments that form the skyrmion also increases with increasing N. However, the number of lattice sites corresponding to noncollinear ordering at the saddle point is much smaller than that of the skyrmion and it increases relatively slowly with increasing N. Therefore, the transition state for large N is a topological soliton that can be described within the σ-model [27] which only includes exchange interaction. In the continuous σ-model the energy E of any structure with topological charge q satisfies the inequality $E \geqslant 4\pi Jq$ [26]. Consequently, the energy barrier for the nucleation of

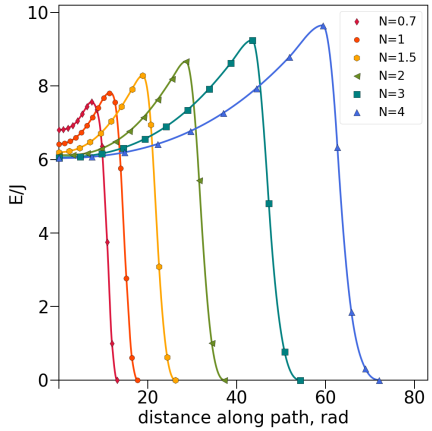

Figure 1: Minimum energy path for radial skyrmion collapse calculated for several values of the scaling parameter. The activation energy for collapse increases as the lattice constant is decreased over this range of small values of N but reaches a large N saturation limit at $N \approx 100$ where the energy maximum is $4\pi J$ with respect to the ferromagnetic state which is taken to give the zero of energy in each case.

a structure with $q = 1$ cannot be lower than $4\pi J$. Our calculations show that the energy barrier is nearly equal to this value for large N and that the barrier for the nucleation of a skyrmion from the FM state in the continuous case can be estimated from the soliton energy in the σ-model. The collapse of a skyrmion passes through a state corresponding to this solution with a small radius (infinitesimal in the continuous limit).

For a track of finite width, a skyrmion can also be eliminated by escape through the boundary [6, 28, 29]. This mechanism corresponds to another path on the energy surface. Figure 2 shows the MEP for skyrmion escape

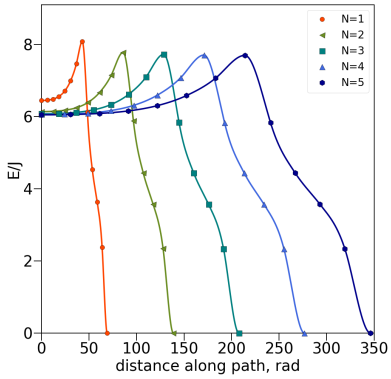

Figure 2: Minimum energy path for skyrmion escape through the boundary of a track with finite width for several values of the scaling parameter, N. The activation energy reaches a limiting, constant value for small values of N. The zero of energy is taken to be that of the final ferromagnetic state.

through the sample boundary for several values of the scaling parameter. The width of the track for $N = 1$ corresponds to 30 atomic rows, about 3 times larger than the size of the skyrmion, wide enough for the boundaries not to have significant effect on the skyrmion state. The energy barrier

for escape first decreases slightly with N but then remains constant. Thus, the activation energy for this skyrmion annihilation mechanism is nearly independent of scaling for $N > 2$. Unlike the collapse mechanism, escape can be described with a micromagnetic model [30].

3.2. Pre-exponential factor

Figure 3 shows calculated eigenvalues of the Hessian arranged in increasing order. The horizontal axis gives the number of the eigenvalue in this sequence divided by the total number of eigenvalues, i/D^*. This is a monotone function, $\epsilon_i(i/D^*)$, on the interval $[0, 1]$, defined for a discrete set of points.

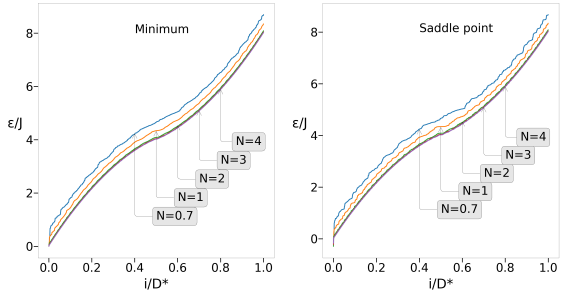

Figure 3: Eigenvalues of the Hessian matrix for the initial skyrmion state (left) and at the saddle point corresponding to the transition state (right) as a function of i/D^*, where i is a number of the eigenvalue when they are arranged in increasing order. D^* is the total number of positive eigenvalues. The value of the scaling parameter N for each curve is shown.

As N is increased, additional eigenvalues are introduced and the scaled index i/D^* becomes more densely distributed over the interval $[0, 1]$. As N goes to infinity, the eigenvalues approach a limiting function $\epsilon(x)$. In figure 3 the left and right panels correspond to the initial skyrmion state and transition state respectively. In both cases, convergence has been achieved for practical purposes already at $N = 2$.

In the limit of large N, the expression in parentheses in the exponent in eq. (7) can be regarded as a Riemann sum for a definite integral over the function $\ln \epsilon(x)$ and, therefore,

$$\frac{1}{D^*} \sum_{i}^{D^*} \frac{1}{2} \ln \epsilon_i \overset{D^* \to \infty}{\longrightarrow} \frac{1}{2} \int_0^1 \ln \epsilon(x) dx. \tag{8}$$

An expression of the form (8) enters both in the numerator (6) at the point corresponding to the skyrmion state, as well as into the denominator of eq. (6) at the saddle point.

If the integrals over $\ln \epsilon(x)$ at the minimum and at the saddle point are different, an exponential dependence of the entropic contribution to f_0 on the scaling parameter N is obtained. For relatively small value of D^*, the density of the eigenvalues of the Hessian has been analyzed previously [31], where the importance of accurate consideration of close to zero eigenvalues was emphasized. The case of large D^* is computationally challenging since the calculation of the function $\epsilon(x)$ presupposes the knowledge of all eigenvalues of a matrix with a rank of several million with high accuracy already for $N \approx 100$.

The results presented here show that the entropy term in the pre-exponential factor for the lifetime, τ_0, first increases as the scaling parameter N increases, but then approaches a constant value for $N > 30$. The increase in the entropy factor corresponds to five orders of magnitude while the dynamic term, containing the b_j in eq. (6), changes by less than one order of magnitude. A strong increase in the pre-exponential factor with increasing skyrmion size explains the possible stability of micrometer skyrmions at room temperature even without taking into account the magnetic dipole interaction and can be considered as a manifestation of topological stabilization in the limit of an infinitesimal lattice constant.

The pre-exponential factor corresponding to skyrmion escape through the boundary also changes with the scaling parameter N, but only by two orders of magnitude, and already for $N > 4$ it is practically constant. In contrast to the case of collapse in an extended system, the escape involves unequal number of zero modes at the minimum and at the saddle point (two for the skyrmion but only one for the transition state). The pre-exponential factor is, therefore, temperature dependent. The variation of the lifetime due to escape with N is much smaller than for skyrmion collapse inside the sample.

4. Conclusions

The activation energy and pre-exponential factor in the Arrhenius expression for the life time of a skyrmion is estimated within HTST for a set of decreasing values of the lattice constant while keeping the size of the skyrmion fixed. In the limit of infinitesimal lattice constant, the activation energy reaches a finite value, unlike the topological protection implied by a continuum model. The energy of the transition state approaches the Belavin-Polyakov limit of $4\pi J$ with respect to the ferromagnetic state. An efficient method for calculating the pre-exponential factor for transitions in large systems is used where the eigenvalues of the Hessian need not be evaluated. The calculated results demonstrate that the entropy term in the pre-exponential factor decreases as the lattice constant is decreased but also approaches a constant value. The results can also be interpreted in terms of changing skyrmion size for a fixed lattice constant and then demonstrate how the decrease in the pre-exponential factor with increased skyrmion size makes an important contribution to the stability of micrometer skyrmions even in the absence of magnetic dipole interaction.

Acknowledgments

This work was supported by Russian Science Foundation (Grant 19-42-06302), the Icelandic Research Fund, and the Research Fund of the University of Iceland.

References

[1] G. Finocchio, F. Büttner, R. Tomasello, M. Carpentieri, M. Kläui, Magnetic skyrmions: from fundamental to applications, J. Phys. D: Appl. Phys. 49 (2016) 423001.

[2] A. Fert, N. Reyren, V. Cros, Magnetic skyrmions: advances in physics and potential applications, Nat. Rev. Mat. 2 (2017) 17031.

[3] K. Everschor-Sitte, J. Masell, R. M. Reeve, M. Kläui, Perspective: Magnetic skyrmions—overview of recent progress in an active research field, J. Appl. Phys. 124 (2018) 240901.

[4] N. Nagaosa, Y. Tokura, Topological properties and dynamics of magnetic skyrmions, Nat. Nanotech. 8 (2013) 899.

[5] J. Hagemeister, N. Romming, K. von Bergmann, E. Y. Vedmedenko, R. Wiesendanger, Stability of single skyrmionic bits, Nat. Commun. 6 (2015) 8455.

[6] P. F. Bessarab, G. P. Müller, I. S. Lobanov, F. N. Rybakov, N. S. Kiselev, H. Jónsson, V. M. Uzdin, S. Blügel, L. Bergqvis, A. Delin, Lifetime of racetrack skyrmion, Sci. Rep. 8 (2018) 3433.

[7] V. M. Uzdin, M. N. Potkina, I. S. Lobanov, H. Jónsson, Energy surface and lifetime of magnetic skyrmions, J. Magn. Magn. Mat. 459 (2018) 236.

[8] I. S. Lobanov, H. Jónsson, V. M. Uzdin, Mechanism and activation energy of magnetic skyrmion annihilation obtained from minimum energy path calculations., Phys. Rev B. 94 (2016) 174418.

[9] S. Krause, G. Herzog, T. Stapelfeldt, L. Berbil-Bautista, M. Bode, E. Y. Vedmedenko, R. Wiesendanger, Magnetization reversal of nanoscale islands: How size and shape affect the arrhenius prefactor, Phys. Rev. Lett. 103 (2009) 127202.

[10] P. F. Bessarab, V. M. Uzdin, H. Jónsson, Size and shape dependence of thermal spin transitions in nanoislands, Phys. Rev. Lett. 110 (2013) 020604.

[11] A. S. Varentcova, S. von Malottki, M. N. Potkina, G. Kwiatkowski, S. Heinze, P. F. Bessarab, Toward room-temperature nanoscale skyrmions in ultrathin films, npj Comp. Mat. 6 (2020) 193.

[12] S. Woo, K. Litzius, B. Krüger, M.-Y. Im, L. Caretta, K. Richter, M. Mann, A. Krone, R. Reeve, M. Weigand, P. Agrawal, I. Lemesh, M.-A. Mawass, F. P., M. Kläui, G. Beach, Observation of room-temperature magnetic skyrmions and their current-driven dynamics in ultrathin metallic ferromagnets, Nat. Mater. 15 (2016) 501.

[13] A. Soumyanarayanan, M. Raju, A. L. G. Oyarce, A. K. C. Tan, M.-Y. Im, A. P. Petrović, P. H, K. Khoo, M. Tran, C. K. Gan, F. Ernult, C. Panagopoulos, Tunable room-temperature magnetic skyrmions in ir/fe/co/pt multilayers, Nat. Mater. 16 (2017) 898.

[14] F. Büttner, I. Lemesh, G. S. Beach, Theory of isolated magnetic skyrmions: From fundamentals to room temperature applications, Sci. Rep. 8 (2018) 4464.

[15] M. N. Potkina, I. S. Lobanov, H. Jónsson, V. M. Uzdin, Skyrmions in antiferromagnets: Thermal stability and the effect of external field and impurities, J. Appl. Phys. 127 (2020) 213906.

[16] W. Legrand, D. Maccariello, F. Ajejas, S. Collin, A. Vecchiola, K. Bouzehouane, N. Reyren, V. Cros, A. Fert, Room-temperature stabilization of antiferromagnetic skyrmions in synthetic antiferromagnets, Nat. Mat. 19 (2020) 34.

[17] P. F. Bessarab, V. M. Uzdin, H. Jónsson, Harmonic transition-state theory of thermal spin transitions, Phys. Rev. B. 85 (2012) 184409.

[18] W. T. Coffey, D. A. Garanin, D. J. McCarthy, Crossover formulas in the kramers theory of thermally activated escape rates—application to spin systems, Adv. Chem. Phys. 117 (2001) 483.

[19] J. Wild, T. N. Meier, S. Pöllath, M. Kronseder, A. Bauer, A. Chacon, M. Halder, M. Schowalter, A. Rosenauer, J. Zweck, J. Müller, Entropy-limited topological protection of skyrmions, Sci. Adv. 3 (2017) e1701704.

[20] P. F. Bessarab, V. M. Uzdin, H. Jónsson, Method for finding mechanism and activation energy of magnetic transitions, applied to skyrmion and antivortex annihilation, Comp. Phys. Comm. 196 (2015) 335.

[21] A. V. Ivanov, D. Dagbartsson, J. Tranchida, V. M. Uzdin, H. Jónsson, Efficient optimization method for finding minimum energy paths of magnetic transitions, J. Phys. Cond. Mat. 32 (2020) 345901.

[22] I. S. Lobanov, M. N. Potkina, H. Jónsson, V. M. Uzdin, Truncated minimum energy path method for finding first order saddle points, Nanosystems: phys., chem., math. 8 (2017) 586.

[23] A. Ivanov, P. Bessarab, V. J. Uzdin, H. Jónsson, Magnetic exchange force microscopy: Theoretical analysis of induced magnetization reversals, Nanoscale 9 (2017) 13320.

[24] I. S. Lobanov, V. Uzdin, The lifetime of big size topological chiral magnetic states. estimation of the pre-exponential factor in the arrhenius law, IarXiv:2008.06754 [cond-mat.mtrl-sci] (2020).

[25] M. N. Potkina, I. S. Lobanov, O. A. Tretiakov, H. Jónsson, V. M. Uzdin, Stability of long-lived antiskyrmions in mn-pt-sn tetragonal heusler material, Phys. rev. B 102 (2020) 134430.

[26] A. A. Belavin, A. M. Polyakov, Metastable states of two-dimensional isotropic ferromagnets, Sov. Phys. JETP Lett. 22 (1975) 245.

[27] Y. Yang, Solitons in field theory and nonlinear analysis, Springer Science & Business Media, 2001.

[28] V. M. Uzdin, M. N. Potkina, I. S. Lobanov, P. F. Bessarab, H. Jónsson, The effect of confinement and defects on the thermal stability of skyrmions, Physica B. 549 (2018) 6.

[29] D. Cortés-Ortuño, W. Wang, M. Beg, R. A. Pepper, M.-A. Bisotti, R. Carey, M. Vousden, T. Kluyver, O. Hovorka, H. Fangohr, Thermal stability and topological protection of skyrmions in nanotracks, Sci. Rep. 7 (2017) 4060.

[30] D. Suess, C. Vogler, F. Bruckner, C. Abert, A repulsive skyrmion chain as a guiding track for a racetrack memory, AIP Advances. 8 (2018) 115301.

[31] L. Desplat, D. Suess, J. V. Kim, R. Stamps, Thermal stability of metastable magnetic skyrmions: Entropic narrowing and significance of internal eigenmodes, Phys. Rev. B. 98 (2018) 13407.

Article II

Skyrmions in antiferromagnets: Thermal stability and the effect of external field and impurities

Potkina M. N., Lobanov I.S., Jónsson H., Uzdin V. M.

J. Appl. Phys. **127**, 213906 (2020)

Skyrmions in antiferromagnets: thermal stability and the effect of external field and impurities

Maria N. Potkina,[1,2,3] Igor S. Lobanov,[2,3] Hannes Jónsson,[1,4,a)] and Valery M. Uzdin[2,3]
[1)] *Science Institute and Faculty of Physical Sciences, University of Iceland, 107 Reykjavík, Iceland*
[2)] *Dept. of Physics, St. Petersburg State University, St. Petersburg, 198504, Russia*
[3)] *ITMO University, 197101 Saint Petersburg, Russia*
[4)] *Dpt. of Applied Physics, Aalto University, FI-00076 Espoo, Finland*

Calculations of skyrmions in antiferromagnets (AFMs) are presented, and their properties compared with skyrmions in corresponding ferromagnets (FMs). The rates of skyrmion collapse and escape through the boundary of a track, as well as the binding to and collapse at a non-magnetic impurity, are calculated as a function of applied magnetic field. The activation energy for skyrmion annihilation is the same in AFMs and corresponding FMs in the absence of an applied magnetic field. The pre-exponential factor in the Arrhenius rate law is, however, different because skyrmion dynamics is different in the two systems. An applied magnetic field has opposite effects on skyrmions in the two types of materials. In AFMs the rate of collapse of skyrmions as well as the rate of escape through the edge of a magnetic strip decreases slightly with increasing field, while these rates increase strongly for a skyrmion in the corresponding FMs when the field is directed antiparallel to the magnetization in the center of the skyrmion. A non-magnetic impurity is less likely to trap a skyrmion in AFMs especially in the presence of a magnetic field. This, together with the established fact that a spin polarized current moves skyrmions in AFMs in the direction of the current, while in FMs skyrmions move at an angle to the current, demonstrates that skyrmions in AFMs have several advantageous properties over skyrmions in FMs for memory and spintronic devices.

I. INTRODUCTION

Topological magnetic chiral structures are of interest as a manifestation of topology in fundamental physics, as well as in connection with applications such as the development of a new generation of magnetic storage and data processing devices.[1–3] Magnetic skyrmions have been observed in various thin layers of ferromagnets (FMs) adsorbed on a surface of a heavy metal,[4] in multilayer systems[5] and in materials with broken inversion symmetry.[6] Skyrmions can be characterized by topological charge, which is an integer that cannot be changed by a continuous transformation of magnetization. A skyrmion state and a ferromagnetic state have different topological charges and therefore cannot be transformed from one to another in a continuous medium. In that sense, a skyrmion is topologically protected. However, when the magnetic moments are localized at sites of a discrete lattice, there is a finite activation barrier for the collapse of a skyrmion and its lifetime becomes shorter the higher the temperature is.[7,8]

Skyrmions could be used as magnetic bits in racetrack memory with high density, speed and energy efficiency. However, small skyrmions in FMs with diameter of 10 to 20 nm have been found to be stable only at low temperature[9] while skyrmions that are stable at room temperature are large, with diameter exceeding 50 nm.[10] The stray field of large skyrmions leads to complicated skyrmion interactions and sets a limit to their density. Skyrmions can be moved by a spin polarized current but in a FM the direction of movement is at an angle to the current, the so-called Hall angle.[11] This can lead to the escape of skyrmions through the boundary of the track. Some of these problems may be overcome by using other materials or topological magnetic structures. Accordingly, skyrmions in antiferromagnets (AFMs) and ferrimagnets,[12,13] as well as antiskyrmions,[14] have recently attracted increased attention.

Skyrmions in AFMs can have several advantages over skyrmions in FMs but they are hard to detect. Recently, however, skyrmions that are stable at room temperature have been observed in a synthetic antiferromagnet based on Pt/Co/Ru multilayers. This system consist of several FM layers with antiparallel magnetization separated by metal spacers. The skyrmions in this type of structure have been detected using magnetic force microscopy.[15] Skyrmions have also recently been observed in ferrimagnetic materials.[16,17] At a certain temperature, the magnetization of the two sublattices of the ferrimagnet is compensated and the properties of the skyrmions are then similar to the properties of a skyrmion in an AFM. Below and above the compensation temperature, skyrmions in a ferrimagnet can be detected by the same methods as in FM.

The observation and control of skyrmions in AFM materials is a challenging task that has to be solved for their utilization. The magnetic moment associated with a skyrmion in an AFM is small and methods typically used to register skyrmions in FM materials do not work. The core of a skyrmion in an AFM looks like the AFM material outside it but the domain wall at the boundary can be detected for example using spin polarized scanning tunneling microscopy because the direction of the magnetic moments inside the domain wall is different. AFM skyrmions can be obtained in ferrimagnetic materials near the temperature of compensation.[16] Below and above this temperature, the skyrmion posses some magnetic moment which can be measured. Therefore, local perturbation such as a variation in the temperature can make the skyrmion visible. Also, sublattices in ferrimagnets contain atoms of different chemical elements. Therefore, element specific methods such as

[a)] Electronic mail: hj@hi.is

element-specific scanning transmission X-ray microscopy[17] can be used to detect topological structures without net magnetization. Finally, topological Hall effect for AFM and FM skyrmions is quite different and could be used for detection and manipulation of skyrmions.[18]

Theoretical arguments for the existence of vortex structures in easy-axis gyrotropic antiferrimagnets were given by Bogdanov *et al.* within the framework of continuum micromagnetic theory.[19,20] Skyrmion-like objects in continuum models were also predicted in a certain subclass of antiferromagnetic materials.[21]

More recently, theoretical analysis of skyrmions in a continuum representation of an AFM material has been presented by Keesman *et al.*[25] The ground state was determined using Monte Carlo simulations and the results compared to theoretical analysis. For finite systems, a phase that shows similarities with skyrmions was identified in between the spin flop and the spiral phases.

Zhang *et al.*[26] carried out micromagnetic lattice simulations and mapped out a phase diagram for AFM skyrmions as function of the exchange stiffness, Dzyaloshinskii-Moriya (DM) and perpendicular anisotropy constants, and demonstrated two approaches for creating an AFM skyrmion. Jin *et al.*[27] analyzed the dynamics of a skyrmion in AFM and showed that the minimum driving current density is about two orders of magnitude smaller than for a FM skyrmion, the velocity is significantly larger and the movement is in the direction of the current (while skyrmions in FM move at an angle with respect to the current). Theoretical studies have also been carried out of the dynamics of AFM skyrmions in the presence of an inhomogeneous distribution of magnetic anisotropy,[22] temperature gradients,[23] and defects.[24]

Barker and Tretiakov, and Bessarab *et al.*[28,29] analyzed the dynamics of a skyrmion in AFM as well as the effect of temperature on its size and phase stability. The activation energy for collapse of the skyrmion was evaluated and the lifetime of the skyrmion estimated to be on the order of milliseconds for a temperature range of 50 K to 65 K and a certain set of parameter values. However, from these calculations it could not be concluded whether compact AFM skyrmions are possible at room temperature.

In the present article, the properties of skyrmions in AFMs are compared with the properties of skyrmions in corresponding FMs. By reversing the sign of the exchange and DM parameters and flipping every other spin, one system is mapped onto the other and the energy surfaces characterizing these two systems are shown to be identical in the absence of a magnetic field. The extensive knowledge that has already been obtained on skyrmions in FM can, therefore, be used to predict properties of skyrmions in AFMs. The activation energy for the various skyrmion annihilation processes is the same in the absence of an applied field, but the dynamics of skyrmions in AFMs is different from that in FMs so the pre-exponential factor in the Arrhenius rate law is different. In the presence of an applied magnetic field, the activation energy for the annihilation of a skyrmion in AFM is close to that of a skyrmion in the corresponding FM with modified anisotropy parameter and zero field. A non-magnetic impurity tends to bind the skyrmion and increase the rate of collapse, but the effect of an applied magnetic field is opposite for AFM and the corresponding FM. Numerical calculations of these processes are presented below for a characteristic AFM film.

II. MODEL

We consider a system of magnetic moments localized at the nodes of a square lattice track in the x-y plane. The width of the track is 60 lattice sites along the y-direction with free boundary conditions at the edges. The simulation cell contains also 60 lattice sites along the x-direction but with periodic boundary conditions applied there. In this two-dimensional (2D) model, each spin represents a column of spins, with effective parameters chosen to represent a three-dimensional film.

The energy of the system is given by a generalized Heisenberg model:

$$E = -\sum_{<i,j>} (J_{ij}\mathbf{S}_i \cdot \mathbf{S}_j + \mathbf{D}_{ij} \cdot (\mathbf{S}_i \times \mathbf{S}_j)) - \sum_j (K(\mathbf{S}_j \cdot \mathbf{e}_z)^2 + \mu \mathbf{B} \cdot \mathbf{S}_j) \quad (1)$$

where $\mathbf{S}_j$ is a unit vector pointing in the direction of the magnetic moment on atom j, the sum over $< i, j >$ is taken over all pairs of nearest neighbor atoms, J_{ij} is the Heisenberg exchange parameter, $\mathbf{D}_{ij}$ is the DM vector, K is the constant of easy axis anisotropy (along z-direction, $K > 0$), $\mathbf{B}$ is applied magnetic field with magnitude $B = |\mathbf{B}|$ and μ is the magnitude of the magnetic moments. For FM $J_{ij} > 0$ and for AFM $J_{ij} < 0$.

The Hamiltonian used here is equivalent to the one used by Zhang *et al.*[26] in their study of the phase diagram and in the calculations presented below we choose parameter values that are representative for a metastable skyrmion state: $|J| = 4.97 \cdot 10^{-21}$ J, $K = 0.8 \cdot 10^{-21}$ J, $D = 1.76 \cdot 10^{-21}$ J (or $|J| = 31$ meV, $K = 5$ meV, $D = 11$ meV). This corresponds to $D/|J| \approx 0.35$, $K/|J| \approx 0.16$.

Note that dipole-dipole interaction is not included in the Hamiltonian. For skyrmions in FM with a radius 50 nm or larger this interaction can play a significant role[2] but can, to first approximation, be taken into account effectively by modifying the anisotropy.[30] However, for AFM the dipole-dipole interaction is almost completely suppressed and can be neglected even for micron-scale structures.

The AFM lattice can be divided into two square checkerboard-like sub-lattices labeled a and b and can be mapped into the FM lattice by reversing the direction of magnetic moments in one of the sub-lattices $\mathbf{S}_i^a \mapsto -\mathbf{S}_i^a$. If at the same time the Hamiltonian parameters are changed as $J_{ij} \mapsto -J_{ij}$, $\mathbf{D}_{ij} \mapsto -\mathbf{D}_{ij}$ the AFM is mapped into a corresponding FM with the same energy if there is no applied magnetic field, $B = 0$. The energy surface, i.e. the variation of the energy as a function of the orientation of all the spins, is exactly the same for the AFM as for the corresponding FM.

The effect of an external magnetic field on the transformation between a skyrmion in FM and a skyrmion in AFM has been presented on the basis of a continuum model.[25] Denoting by $\mathbf{L}$ the staggered magnetization and by $\mathbf{M}$ the total magnetization, the energy density $\omega(\mathbf{r})$ for AFM can be written as:

$$\omega(\mathbf{r}) = -\frac{\mathscr{J}}{2}(\|\nabla\mathbf{L}\|^2 + 8\|\mathbf{M}\|^2) - M_s B M_z - \mathscr{K} {L_z}^2 + \mathscr{D}\mathbf{L}\cdot\mathrm{rot}\mathbf{L}$$

Here, $\mathscr{J}$, $\mathscr{K}$ and $\mathscr{D}$ are the densities corresponding to the energy parameters in Eqn. (1), and M_s is the magnetization. The continuous vector fields $\mathbf{L}$ and $\mathbf{M}$ can be related to the spin orientation $\mathbf{S}_j$ on the lattice as follows: $\mathbf{L} = (\mathbf{S}^a - \mathbf{S}^b)/2$, $\mathbf{M} = (\mathbf{S}^a + \mathbf{S}^b)/2$. Here, $\mathbf{S}^a$ and $\mathbf{S}^b$ correspond to the values of $\mathbf{S}$ on the two sub-lattices.

By minimizing $\omega(\mathbf{r})$ with respect to $\mathbf{M}$ under the condition $\mathbf{M}\cdot\mathbf{L} = 0$, the following expression for the energy density of a (meta)stable skyrmion state is obtained as a function of only the staggered component:

$$\omega(\mathbf{r}) = -\frac{\mathscr{J}}{2}\|\nabla\mathbf{L}\|^2 + \frac{(M_s B)^2}{16|\mathscr{J}|}(L_z^2 - 1) - \mathscr{K} {L_z}^2 + \mathscr{D}\mathbf{L}\cdot\mathrm{rot}\mathbf{L}$$

When $B = 0$, this expression coincides with $\omega(\mathbf{r})$ for FM with magnetization $\mathbf{L}$. If $\mathbf{B} \neq 0$ the staggered magnetization in an AFM state coincides with the magnetization in a FM state without magnetic field but with modified anisotropy

$$K \mapsto K - \frac{(M_s B)^2}{16|\mathscr{J}|} \tag{2}$$

Therefore, there is a one-to-one correspondence between (meta)stable states in AFM and in the corresponding FM. The energy of a skyrmion in AFM is affected by the application of an external magnetic field in the same way as the change in the anisotropy constant given by Eqn. (2). While the transformation described by Eqn. (2) is obtained for a continuum model, it also gives a good approximation for a discrete, atomic scale model, not only for the skyrmion state but for the whole path for skyrmion annihilation, as will be demonstrated below.

Both directions of the field perpendicular to the plane of the lattice are equivalent for a skyrmion in an AFM, but they lead to a different effect on a skyrmion in an FM. If the field is directed along the magnetization of the ferromagnet, it reduces the radius of the FM skyrmion. In the calculations presented here, this will be the direction of the applied magnetic field. If the field is directed in the opposite way, the size of the FM skyrmion increases and it easily becomes unstable with respect to a spiral structure. In the system studied numerically below, a field of just $\mu B/|J| = -0.0012$ is sufficient to produce spiral structure. In experimental studies of skyrmions in FMs, the field is invariably directed along the magnetization of the ferromagnet.

III. METHODOLOGY

The focus of the work presented here is an analysis of the various annihilation processes of skyrmions in AFMs and comparison with skyrmions in corresponding FMs. Also, the binding to and dissociation from a non-magnetic impurity is calculated. The energy as a function of all the variables representing degrees of freedom in the system, for example the angles describing the orientation of the magnetic moments, is referred to as the energy surface characterizing the system. We, however, use Cartesian coordinates of the magnetic moments and Lagrange multipliers to keep the magnitude of each magnetic moment constant in the calculations presented below. Metastable states are characterized by local energy minima on this energy surface and the stable state by the global minimum. A transition from one state to another is characterized by the minimum energy path (MEP) connecting the initial and final state minima. The MEP for a magnetic transition can be found using the geodesic nudged elastic band method.[31] For large systems with many degrees of freedom it can be helpful to take advantage of previous knowledge of the saddle point and the shape of the MEP in its vicinity to reduce the computational effort.[32] The activation energy for a transition can be estimated from the highest energy along the MEP. A maximum along the MEP corresponds to a first order saddle point on the energy surface.[33]

The rate of a transitions in a magnetic system, such as a skyrmion annihilation process, can be estimated using the harmonic approximation to transition state theory (HTST) for magnetic systems.[33,34] The transition state is then taken to be a hyperplane going through the first order saddle point with normal vector pointing along the direction of the eigenvector corresponding to the negative eigenvalue of the Hessian at the saddle point, H^{sp}. The energy surfaces defined by the Hamiltonian in Eqn. (1) for an AFM material and the corresponding FM material coincide in the absence of an applied magnetic field. The activation energy for collapse is, therefore, the same for the two types of skyrmions if B=0.

HTST predicts an Arrhenius-type rate law for transitions between magnetic states

$$k = \nu_0 \exp\left(\frac{-\Delta E}{k_B T}\right).$$

The activation energy, ΔE, equals the energy at the (highest) maximum along the MEP minus the energy at the minimum corresponding to the initial state. The pre-exponential factor can be written as[34]

$$\nu_0 = \frac{\lambda\Omega_0}{2\pi} \tag{3}$$

where the factor Ω_0 is a ratio of determinants of the Hessian at the initial state minimum, H^{min}, and at the saddle point, H^{sp}, i.e.

$$\Omega_0 = \frac{\sqrt{\det H^{min}}}{\sqrt{|\det H^{sp}|}}. \tag{4}$$

It is connected with the ratio of the entropy of the initial state and the transition state. The factor λ is connected with dynamics of the system and relates to the flux through the transition state. An explicit expression for the rate constant has previously been given in terms of eigenvalues and eigenvectors

of the Hessian at the saddle point.[33,34] But, here λ is written in a basis invariant form as

$$\lambda = \sqrt{\frac{\mathbf{b}\cdot H^{sp}\mathbf{b}}{|\zeta|}}, \quad \text{with } \mathbf{b} = \frac{\gamma\zeta}{\mu}\mathbf{S}^{sp}\times\mathbf{e}, \tag{5}$$

where $\mathbf{S}^{sp}$ is the spin configuration at the saddle point and $\mathbf{e}$ is the eigenvector corresponding to the negative eigenvalue of H^{sp} (a unit tangent vector to the MEP at the saddle point). This expression for λ is easier to evaluate numerically since it can be computed in spin-related basis without the evaluation of the eigenvectors of H^{sp}. Also, λ can then be interpreted without referring to the dividing surface. Indeed, $\mathbf{b}\cdot H^{sp}\mathbf{b}$ is the value of the Hessian in the direction $\mathbf{b}$. The velocity is zero at $\mathbf{S}^{sp}$ since the gradient is zero, but the velocity at other points along the MEP is not zero, and in the vicinity of the saddle point the velocity is equal to $\mathbf{b}$ times the distance from the saddle point. This means that the value of $\mathbf{b}\cdot H^{sp}\mathbf{b}$ can be interpreted as the curvature of the energy surface at the saddle point in the direction of $\mathbf{b}$.

When several different transitions are possible from a given initial state, as for example the different annihilation processes considered here for the skyrmion, then the lifetime of the initial state can be obtained from the inverse of the sum of the rate constant of the various transitions $\tau = 1/\sum_i k_i$. The lifetime of the skyrmion can thus be obtained from the sum of the rate of collapse (i.e. annihilation within the track) and escape through the boundary of the track. In the presence of an impurity, there are additional processes such as binding to the impurity and possible collapse there or detachment from the impurity. The time evolution of such a system where multiple possible transitions take place can be simulated using a kinetic Monte Carlo approach.

The harmonic approximation in HTST does not apply to degrees of freedom for which the energy is nearly constant. For example, a skyrmion can translate almost freely within the track for the system studied here. Such degrees of freedom need to be handled separately in the rate expression. They are often referred to as zero modes. An integration along these modes needs to be performed to obtain the corresponding entropy.[8,35] This gives the volume of the subspace corresponding to the zero-modes. As a result, Ω_0 has an additional factor $Z = (2\pi k_B T)^{\frac{n_{min}-n_{sp}}{2}} V_{sp}/V_{min}$, where n_{sp}, V_{sp} and n_{min}, V_{min} give the number of zero modes and the corresponding volumes at the saddle point and at the initial state minimum, respectively. We make here the assumption that the skyrmion can translate freely inside the track and also at the saddle point for collapse (i.e. there are two zero modes in both the initial state and transition state, n_{min}=n_{sp}=2), while it can translate freely only in one direction at the saddle point for escape (n_{min}=2, n_{sp}=1).

The transformation of exchange $J \to -J$ and DM interaction $D \to -D$ with simultaneous change of anisotropy and external magnetic field in accordance with Eqn. (2) and $B \to 0$ conserves the shape of energy surface. Therefore, the entropy factor Ω_0 is the same for the skyrmion collapse in AFM and the corresponding FM. However λ which is connected with the linearized Landau-Lifschitz equation in the neighborhood of the saddle point is different for skyrmions in AFMs and the corresponding FMs, as illustrated below.

We note that in an alternative approach for estimating the transition rate based on the Kramers-Langer approximation,[36] λ is the positive eigenvalue of the Landau-Lifschitz-Gilbert equation, linearized around the saddle point. It characterizes the unstable barrier-crossing mode.[37]

IV. RESULTS

We now present results of numerical calculations for the model and parameter values specified above.

A. Effect of applied field on skyrmion size

Fig. 1 shows how an applied magnetic field affects the radius of a skyrmion in the AFM and in the corresponding FM. The radius is defined here as the distance from the center to the region where the magnetic moments have no out of plane component. The size of the skyrmion changes in opposite ways in the two cases. While the radius of the skyrmion in the FM decreases when the field is directed against the moment in the center of the skyrmion, the radius of the skyrmion in AFM increases for either direction of the field perpendicular to the plane. The effect is larger for the skyrmion in FM and it becomes unstable in a field of B=0.07 $|J|/\mu$. However, the increase in the size of the skyrmion in AFM leads to increased stability.

B. Rates of annihilation processes

Fig. 2 shows MEPs for the collapse of a skyrmion in AFM and the corresponding FM with and without applied magnetic field. Not only are the relaxed skyrmions equivalent in the two materials in the absence of an applied magnetic field, but this applies as well to the whole MEP. The activation energy for collapse is exactly the same. For parameters chosen here ($|J| \approx 31$ meV, $K \approx 5$ meV, $D \approx 11$ meV, $\mu = 8\ \mu_B$) the activation energy for collapse of the skyrmion is 124 meV when B=0. This value of the magnetic moment in the 2D representation of the film could correspond to a 4 atomic layer film where each atom has a magnetic moment of 2 μ_B.

When a magnetic field is applied, the skyrmion in AFM becomes more stable and the MEP for collapse longer. Nearly the same effect on the path is obtained by modifying the anisotropy constant and setting the magnetic field to zero. For example, the application of a field of B=0.3 $|J|/\mu$ is nearly equivalent to reducing the anisotropy constant from K=0.16 $|J|$ to 0.154 $|J|$ in accordance with Eqn. (2). The total displacement along the path and activation energy for annihilation are quite similar in the two cases. The field increases the radius of the skyrmion in AFM by a third and the activation energy for annihilation increases by about a third making the skyrmion in AFM more stable.

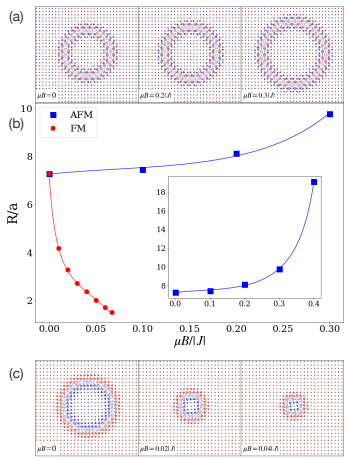

FIG. 1. (a): AFM skyrmion in a magnetic field of $B = 0$, 0.2 and 0.3 $|J|/\mu$. The color (red vs. blue) indicates the direction of the out-of-plane component of the magnetic vector and the color intensity the magnitude. (b): Radius (in units of lattice parameter, a) of a skyrmion as a function of applied magnetic field in the AFM (blue) and the corresponding FM (red) where the sign of the exchange coupling parameter, J, and the Dzyaloshinskii-Moriya parameter, D, has been reversed. In a field of 0.07 $|J|/\mu$, the FM skyrmion becomes unstable, but the AFM skyrmion is stable, even for significantly larger field (see inset for extended scale). While the radius of the skyrmion in an FM shrinks with applied field, it increases in an AFM. (c): FM skyrmion in a magnetic field of $B = 0$, 0.02 and 0.04 $|J|/\mu$. Same color code as in top panel but smaller field.

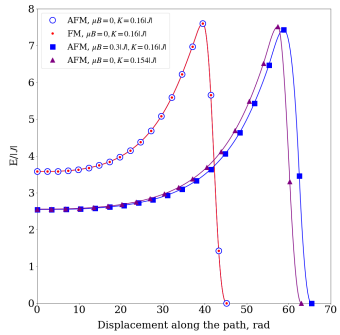

FIG. 2. Minimum energy path for the collapse of a skyrmion in the AFM (blue) and in the corresponding FM (red) where the sign of the exchange coupling parameter, J, and the Dzyaloshinskii-Moriya parameter, D, have been reversed. In the absence of an external magnetic field (dots and circles), the paths are identical for the two materials. In a field of B=0.3 $|J|/\mu$, the activation energy for collapse is increased for a skyrmion in AFM and the path lengthens (squares), but for the FM skyrmion the activation energy drops significantly as can be seen from the large increase in the rate shown in Fig. 3(a). An application of a field of B=0.3 $|J|/\mu$ in the AFM has a similar effect as a slight reduction of the anisotropy constant from K=0.16 $|J|$ to 0.154 $|J|$ in the absence of an applied field (triangles), where again the path is the same for the two types of materials.

The value of the pre-exponential factor of the rate constant for skyrmion collapse is $1.0 \cdot 10^4\ s^{-1}$ for AFM and $\nu_0 = 3.3 \cdot 10^3\ s^{-1}$ for the corresponding FM.

The effect of an applied field on the rate of collapse inside the track and escape through the boundary of the track can be seen in Fig. 3. For the FM, the rate of both mechanisms increases strongly with the field. While escape has higher rate constant for small field, a crossover between the two mechanisms occurs at a field of B=0.02 $|J|/\mu$ and the rate constant for collapse inside the track becomes larger than escape through the edge for higher values of the field. The field has the opposite effect on the rate constants in the AFM as they become smaller when the field is increased, consistent with the increased activation energy shown in Fig. 2. However, the cause of the drop in the value of the rate constants is not only because of the increase in the activation energy but also a decrease in the pre-exponential factor, ν_0, as can be seen from Fig. 3(b). This reflects a decrease in the entropy of the transition state with respect to the entropy of the initial state. It can be understood from the fact that the larger the skyrmion is, the larger its vibrational entropy is. As the field increases, the skyrmion in AFM becomes larger, thus increasing the entropy of the initial state. But, at the transition state the skyrmion is reduced to a critical size that depends less on the applied field. So, the entropy of the transition state increases less with the field than the entropy of the initial state.

A more likely annihilation mechanism at zero magnetic field for this set of parameter values is an escape of the skyrmion through the edge of the track. Even if the relative number of sites adjacent to the edge and the number of sites in the interior of the track is taken into account, the probability of escape through the edge of the track is much more likely than collapse. This means that additional effort, such as insertion of material with other magnetic characteristics at the boundary, or pinning of skyrmions by defects such as a nar-

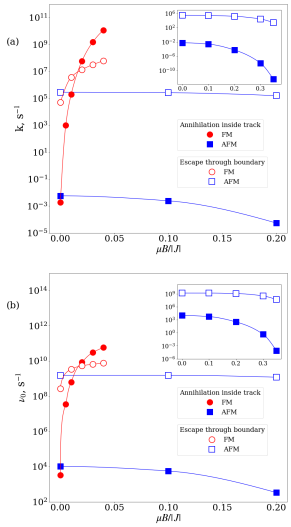

FIG. 3. (a): Rate constant for the escape of a skyrmion through a boundary of the track and collapse inside the track as a function of applied magnetic field at a temperature of 100 K. For a skyrmion in the AFM (blue) the effect of the field is weak, but for a skyrmion in the corresponding FM (red) the rate of annihilation increases dramatically as the strength of the applied field increases and a crossover occurs between collapse and escape, the former becoming more likely for large field. (b): Pre-exponential factor, ν_0 for the rate constants illustrated in (a). A similar variation with the field strength is seen, a decrease for the AFM but a large increase for the corresponding FM. Insets: Scale extended to larger field strength.

row strip with a different materials parameter[38] are necessary to keep the skyrmion inside the track.

While the activation energy for collapse is exactly the same for a skyrmion in the AFM and in the corresponding FM when there is no applied field, the pre-exponential factor in the rate expression is different. The reason is that the Landau-Lifschitz dynamics of the skyrmion in the transition state is different in the two materials. Fig. 4 shows the contributions of the various eigenmodes $\mathbf{e}_k$: $f_k = \mathbf{e}_k \cdot (\mathbf{S}^{sp} \times \mathbf{e})$ to the factor λ in the pre-exponential (see Eqn. (5)). The eigenvectors $\mathbf{e}_k$ are numbered in increasing order of the corresponding eigenvalues. The calculated results show that small eigenvalues give the major contribution for the transition state for skyrmion collapse in the FM (note the logarithmic scale), whereas the full range of eigenvalues contributes in the AFM. As a result, the value of the pre-exponential factor for the collapse of a skyrmion in the AFM and the corresponding FM turn out to differ.

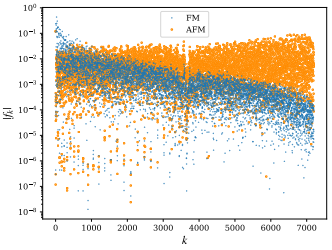

FIG. 4. The contribution f_k of the 7199 positive eigenmodes of the Hessian at the saddle point for skyrmion collapse to the factor λ in the pre-exponential factor of the rate constant (see Eqn. (5)). The x-axis gives the number of the eigenvalue arranged in increasing order. Small eigenvalues give the major contribution for the transition state of skyrmion collapse in the FM (note the logarithmic scale), whereas the full range of eigenvalues contributes in the AFM. The dynamical contribution to the pre-exponential factor is different for the two because the Landau-Lifshitz dynamics are different.

C. Non-magnetic impurity

An important issue for practical applications of magnetic skyrmions is the effect of impurities in the magnetic material. The effect of a non-magnetic impurity on the stability and pinning of a skyrmion in FM has been presented previously.[39] Fig. 5 shows the minimum energy path for the attachment of a skyrmion in AFM to a non-magnetic substitutional atom and subsequent collapse of the skyrmion. There is a small activation energy barrier for attaching to the defect, but once that has been overcome the energy drops below that of a free skyrmion. The optimal configuration is obtained when the non-magnetic atom is located in the region where the magnetic moments have no out-of-plane component, see Fig. 5. This defines the optimal distance between the impurity and the center of the skyrmion. The skyrmion can rotate freely around the impurity as long as the distance to the impurity remains constant. This motion involves no change in the energy of the system (see the long stretch between points 3 and 4 in Fig. 5).

There is still a large probability that the skyrmion detaches from the impurity because the energy barrier is rather small. The impurity, however, also increases greatly the probability

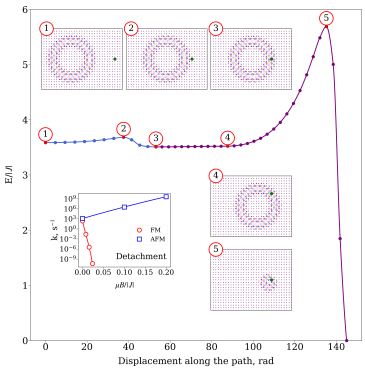

FIG. 5. Minimum energy path for the attachment of a skyrmion to a non-magnetic impurity atom in the AFM and subsequent collapse there. The lowest energy spin configuration is when the defect is located in a region of the skyrmion where the magnetic moments have no out-of-plane component. The skyrmion can rotate without changing the energy as long as the impurity remains at the same distance from the center (compare points 3 and 4). Inset graph: Rate constant for the detachment from the impurity as a function of applied magnetic field strength at T=3 K. The skyrmion detaches more readily from an impurity in the AFM than in the corresponding FM, and this difference becomes greater as the field strength increases. In the AFM, the rate constant for dissociation from the impurity is always larger than the rate constant for collapse even for large applied field. Insets 1-5: Configurations of the magnetic vectors at the various labeled points along the minimum energy path.

of collapse as the activation energy drops to a half compared to that of a free skyrmion, as can be seen by comparing Fig. 5 with Fig. 2. The impurity stabilizes the contracted skyrmion at the transition state more than the relaxed skyrmion in the initial state, thereby lowering the activation energy. Correspondingly, the lifetime drops if the skyrmion is bound to the impurity. An applied field has a beneficial effect for a skyrmion in the AFM by increasing the rate of detachment (see inset in Fig. 5) as well as by increasing the energy barrier for collapse, as shown in Fig. 2.

V. DISCUSSION

Skyrmions in AFMs and corresponding FMs can be described by similar energy surfaces. Without an applied magnetic field the energy surfaces coincide exactly. The inclusion of an applied magnetic field for the AFM material is equivalent to a change in in the anisotropy in the corresponding FM material without applied field. Therefore, the activation energy for annihilation and the entropy contribution to the pre-exponential factor Ω_0 in the transition rate is exactly the same for AFM and corresponding FM skyrmions. However, the rates are different because the dynamics through the transition state, given by the Landau-Lifschitz equation, is different. The calculated results presented here illustrate this for an example system. This result is in agreement with recently reported mean switching time by coherent rotation of AFM nanoparticles in the superparamagnetic limit, which have shown different pre-exponential factor for AFM and FM single-domain particles.[40]

The effect of a non-magnetic impurity is found to be quite different for a skyrmion in the AFM than in the corresponding FM, especially in the presence of an applied field. Recently, dynamical modeling of the movement of the skyrmion inside a track and its collision with hole defects was reported.[41] Depending on the strength of the applied current and the type of collision, a skyrmion in an AFM can be captured, scattered or completely destroyed by the hole. Evidently, these phenomena are connected with the energy barriers and pre-exponential factors presented above.

The key question is whether it is possible to find an AFM where skyrmions are stable enough at room temperature. The equivalence of the energy surfaces for skyrmions in AFM and in the corresponding FM gives hope that this is possible, because stable skyrmions in FM materials at room temperature have been reported experimentally.[1,3,10] FM skyrmions that have been studied experimentally, even those which exist in ultra thin magnetic films on a surface of a heavy metal,[4] contain several magnetic atomic layers. If the thickness of the film is much less than the size of the skyrmion then the structure can be considered as a quasi 2D system. Such skyrmions are tubes with the same magnetic structure in each atomic layer.[42,43] In this approach, a column of magnetic moments is represented by a macrospin with effective parameters within the 2D model. Parameters of the Hamiltonian in Eqn. (1), such as J, K, D and μ, are then to a first approximation proportional to the thickness of the magnetic film whereas the skyrmion radius and in-plane structure do not depend on the thickness. Evidently, if the sign of the exchange and DM interaction between magnetic moments in neighboring layers is changed as well as the directions of the magnetic moments, the same energy surface for AFM and FM is obtained as in the 2D case. For AFM, the vector L should be considered instead of local moments, but the effective parameters of the Hamiltonian will, to first approximation, be proportional to the AFM film thickness as in the case of FM films.

Density functional theory (DFT) calculations have given estimates of the parameter J characterizing the exchange interaction between nearest neighbor magnetic moments around 10 meV.[44] If the magnetic film contains several atomic layers, this parameter can be proportionally larger. As for FM materials, the parameter values for an AFM film scale with the thickness of the magnetic layer. The value of the exchange parameter J, anisotropy parameter K, and even magnetic moment μ (a macrospin representation) can be proportional to the number of magnetic layers. Note that the effective magnetic moment in the AFM case corresponds to the value of

staggered magnetization **L**. Thus the effective values of the parameters in the 2D Hamiltonian Eqn. (1) can be much larger than values of the interactions between local magnetic moments calculated by the DFT method.[8,44] Note, however, that the DM interaction in a quasi-2D system is associated with the presence of a heavy metal with large spin orbit interaction and this effect decays rapidly away from the interface. The DM parameter is then not proportional to the thickness of the film. Nevertheless recent calculations[45] show that in an amorphous ferrimagnetic GdCo film on Pt, the skyrmion assumes a columnar configuration that extends uniformly across the film thickness of 10 nm despite having near zero DM interaction far away from the interface. Effective DM interaction is still enough to stabilize the skyrmion tube.

The properties of a skyrmion in an AFM is related here to the properties of a skyrmion in a corresponding FM by a transformation of the relevant parameters in the Hamiltonian and the orientation of the spins. Similar analysis can be carried out for other topological magnetic textures. For example, the properties of an antiskyrmion in a FM have been analyzed by spin transformation that converts it to a skyrmion in the FM and corresponding changes in the parameters in the Hamiltonian if there are no spin-orbit and spin-transfer torques. This means that the lifetime of the antiskyrmion is exactly the same as for the skyrmion if the DM vector is transformed accordingly. Moreover, by applying this transformation to the Landau-Lifshitz-Gilbert equation of motion one can predict the direction of the current for which the angle between current and antiskyrmion movement equals zero.[46]

The data that support the findings of this study are available from the corresponding author upon a reasonable request.

ACKNOWLEDGMENTS

This work was supported by the Icelandic Research Fund, the Research Fund of the University of Iceland, the Russian Foundation of Basic Research (grants RFBR 18-02-00267 and 19-32-90048) and the Foundation for the Advancement of Theoretical Physics and Mathematics “BASIS” under Grant No. 19-1-1-12-1.

[1] A. Fert, N. Reyren, and V. Cros, Nature Reviews Materials **2**, 17031 (2017).
[2] F. Büttner, I. Lemesh, and G. S. D. Beach, Scientific Reports **8**, 4464 (2018).
[3] K. Everschor-Sitte, J. Masell, R. Reeve, and M. Kläui, Journal of Applied Physics **124**, 240901 (2018).
[4] S. Heinze, K. von Bergmann, M. Menzel, J. Brede, A. Kubetzka, R. Wiesendanger, G. Bihlmayer, and S. Blügel, Nat. Phys. **7**, 713 (2011).
[5] S. Woo, K. Litzius, B. Kruger, M.-Y. Im, L. Caretta, K. Richter, M. Mann, A. Krone, R. M. Reeve, M. Weigand, P. Agrawal, I. Lemesh, M.-A. Mawass, P. Fischer, M. Klaui, and G. S. D. Beach, Nature Mater. **15**, 501 (2016).
[6] Y. Tokunaga, X. Z. Yu, J. S. White, H. M. Rnnow, D. Morikawa, Y. Taguchi, and Y. Tokura, Nature Communications **6**, 7638 (2015).
[7] V. M. Uzdin, M. N. Potkina, I. S. Lobanov, P. F. Bessarab, and H. Jónsson, J. Magn. Magn. Mat. **459**, 236 (2018).
[8] P. F. Bessarab, G. P. Müller, I. S. Lobanov, F. N. Rybakov, N. S. Kiselev, H. Jónsson, V. M. Uzdin, S. Blügel, L. Bergqvist, and A. Delin, Sci. Rep. **8**, 3433 (2018).
[9] R. Wiesendanger, Reviews Materials **1**, 16044 (2016).
[10] A. Soumyanarayanan, M. Raju, A. G. Oyarce, *et al.*, Nature Materials **16**, 898 (2017).
[11] K. Litzius, I. Lemesh, B. Krüger, P. Bassirian, L. Caretta, K. Richter, F. Büttner, K. Sato, O. A. Tretiakov, J. Förster, R. M. Reeve, M. Weigand, I. Bykova, H. Stoll, G. Schütz, G. S. D. Beach, and M. Kläui, Nature Phys. **13**, 170 (2017).
[12] L. Smejkal, Y. Mokrousov, B. Yan, and A. H. MacDon- ald, Nature Communications 14, 242 (2018).
[13] O. Gomonay, T. Jungwirth, and J. Sinova, Phys. Rev. Lett. **117**, 017202 (2016).
[14] A. K. Nayak, V. Kumar, T. Ma, P. Werner, E. Pippel, R. Sahoo, F. Damay, U. K. Rößler, C. Felser, and S. S. P. Parkin, Nature **548**, 561 (2017).
[15] W. Legrand, D. Maccariello, F. Ajejas, S. Collin, A. Vecchiola, K. Bouzehouane, N. Reyren, V. Cros, and A. Fert, Nature Materials **19**, 34 (2020).
[16] L. Caretta, M. Mann, F. Büttner, K. Ueda, B. Pfau, C. M. Günther, P. Hessing, A. Churikova, C. Klose, M. Schneider, E. D., C. Marcus, B. D., B. K., S. Eisebitt, and G. S. D. Beach, Nature Nanotechnology **13**, 1154 (2018).
[17] S. Woo, K. M. Song, X. Zhang, Y. Zhou, M. Ezawa, X. Liu, S. Finizio, J. Raabe, N. J. Lee, S.-I. Kim, S.-Y. Park, Y. Kim, J.-Y. Kim, D. Lee, O. Lee, J. W. Choi, B.-C. Min, H. C. Koo, and J. Chang, Nature Communications **9**, 959 (2018).
[18] P. M. Buhl, F. Freimuth, S. Blügel, and Y. Mokrousov, Phys. Status Solidi RRL **11**, 1700007 (2017).
[19] A. N. Bogdanov and D. A. Yablonskii, Sov. Phys. JETP **68**, 101 (1989); Sov. Phys. JETP **68**, 142 (1989).
[20] A. N. Bogdanov and A. A. Shestakov, Low Temp. Phys. **25**, 76 (1999).
[21] A. N. Bogdanov, U. K. Rösler, M. Wolf and K.-H. Müller, Phys. Rev. B **66**, 214410 (2002).
[22] L. Shen, J. Xia, G. Zhao, X. Zhang, M. Ezawa, O. A. Tretiakov, X. Liu and Y. Zhou, Phys. Rev. B **98**, 134448 (2018).
[23] X. Liang, G. Zhao, L. Shen, J. Xia, L. Zhao, X. Zhang and Y. Zhou, Phys. Rev. B **100**, 144439 (2019).
[24] R. Khoshlahni, A. Qaiumzadeh, A. Bergman and A. Brataas, Phys. Rev. B **99**, 054423 (2019).
[25] R. Keesman, M. Raaijmakers, A. E. Baerends, G. T. Barkema, and R. A. Duine, Phys. Rev. B **94**, 054402 (2016).
[26] X. Zhang, Y. Zhou, and M. Ezawa, Scientific Reports **6**, 24795 (2016).
[27] C. Jin, C. Song, J. Wang, and Q. Liu, Applied Physics Letters **109**, 182404 (2016).
[28] J. Barker and O. A. Tretiakov, Phys. Rev. Lett. **116**, 147203 (2016).
[29] P. Bessarab, D. Yudin, D. Gulevich, P. Wadley, M. Titov, and O. A. Tretiakov, Phys. Rev. B **99**, 140411 (2019).
[30] I. S. Lobanov, H. Jónsson, and V. M. Uzdin, Phys. Rev. **B 94**, 174418 (2016).
[31] P. F. Bessarab, V. M. Uzdin, and H. Jónsson, Comput. Phys. Commun. **196**, 335 (2015).
[32] I. S. Lobanov, M. N. Potkina, H. Jónsson, and V. M. Uzdin, Nanosystems: Physics, Chemistry, Mathematics **8**, 586 (2017).
[33] P. F. Bessarab, V. M. Uzdin and H. Jónsson, Zeitschrift fur Physikalische Chemie **227**, 1543 (2013).
[34] P. F. Bessarab, V. M. Uzdin, and H. Jónsson, Phys. Rev. B **85**, 184409 (2012).
[35] A. Ivanov, P. F. Bessarab, V. M. Uzdin and H. Jónsson, Nanoscale **9**, 13320 (2017).
[36] W. T. Coffey, D. A. Garanin, and D. J. McCarthy, Advances in Chemical Physics **117**, 483 (2001).
[37] L. Desplat, D. Suess, J.-V. Kim, and R. Stamp, Phys. Rev. B **98**, 134407 (2018).
[38] D. Stosic, J. Mulkers, B. Van Waeyenberge, T. B. Ludermir, and M. V. Milosević, Phys.Rev.B **95**, 214418 (2017).
[39] V. M. Uzdin, M. N. Potkina, I. S. Lobanov, P. F. Bessarab, and H. Jónsson, Physica B **549**, 6 (2018).
[40] L. Rózsa, S. Selzer, T. Birk, U. Atxitia, and U. Nowak, Phys. Rev. B **100**, 064422 (2019).
[41] R. L. Silva, R. C. Silva, A. Pereira, and W. A. Moura-Melo, J. Phys.: Condens. Matter **31**, 225802 (2019).
[42] H. R. O. Sohn, S. M. Vlasov, V. M. Uzdin, A. O. Leonov, and I. I. Smalyukh, Phys. Rev. B **100**, 104401 (2019).
[43] S. M. Vlasov, V. M. Uzdin, and A. O. Leonov, J. Phys.: Condens. Matter **32**, 185801 (2020).

[44] S. von Malottki, B. Dupé, P. F. Bessarab, A. Delin, and S. Heinze, Scientific Reports **7**, 12299 (2017).
[45] C. T. Ma, Y. Xie, H. Sheng, A. Ghosh, and S. J. Poon, Scientific Reports **9**, 9964 (2019).
[46] M. N. Potkina, I. S. Lobanov, O. A. Tretiakov, H. Jónsson, and V. M. Uzdin, arxiv.org/abs/1906.06383 (2019).

Article III

Stability of long-lived antiskyrmions in the Mn-Pt-Sn tetragonal Heusler material

Potkina M. N., Lobanov I.S., Tretiakov O. A., Jónsson H., Uzdin V. M.

Phys. Rev. B **102**, 134430 (2020)

PHYSICAL REVIEW B **102**, 134430 (2020)

Stability of long-lived antiskyrmions in the Mn-Pt-Sn tetragonal Heusler material

M. N. Potkina,[1,2,3] I. S. Lobanov,[2,3] O. A. Tretiakov,[4] H. Jónsson,[1,5] and V. M. Uzdin[2,3]
[1]*Science Institute and Faculty of Physical Sciences, University of Iceland, 107 Reykjavík, Iceland*
[2]*Department of Physics, St. Petersburg State University, 198504 St. Petersburg, Russia*
[3]*Faculty of Physics and Engineering, ITMO University, 197101 St. Petersburg, Russia*
[4]*School of Physics, The University of New South Wales, Sydney 2052, Australia*
[5]*Department of Applied Physics, Aalto University, FIN-00076 Espoo, Finland*

(Received 15 August 2020; revised 28 September 2020; accepted 1 October 2020; published 26 October 2020)

The lifetime of antiskyrmions at room temperature in an Mn–Pt–Sn tetragonal Heusler material has been calculated using an atomic scale representation including nearly a million spins. The evaluation of the pre-exponential factor in the Arrhenius rate expression for this large system is made possible by implementation of harmonic transition state theory that avoids evaluation of the eigenvalues of the Hessian matrix. The parameter values in the extended Heisenberg Hamiltonian, including anisotropic Dzyaloshinskii-Moriya interaction, are chosen to reproduce experimental observations [Nayak *et al.*, Nature (London) **548**, 561 (2017)], in particular, the 150-nm diameter. The calculated results are consistent with the long lifetime observed in the laboratory and this exceptional stability of the antiskyrmions is found to result from large activation energy for collapse due to strong exchange coupling while the pre-exponential factor in the Arrhenius expression for the lifetime is found to have a typical magnitude of 10^{-12} s, despite the large number of spins. The long lifetime is, therefore, found to result from energetic effects rather than entropic effects in this system.

DOI: 10.1103/PhysRevB.102.134430

I. INTRODUCTION

Skyrmions and antiskyrmions are localized magnetic states that have been proposed as elements in future spintronics devices [1–3]. Along with interesting transport properties, such states can exhibit particlelike behavior and carry a topological charge that enhances their stability with respect to the uniform ferromagnetic or antiferromagnetic states. A key issue is the lifetime of (anti)skyrmions and its dependence on temperature and applied magnetic field. The challenge is to find or design materials where such magnetic states are sufficiently stable at ambient temperature and still small enough to be used in high density spintronic devices. Figure 1 shows the spin configuration of an antiskyrmion as well as that of a skyrmion.

So far, stability at room temperature has mainly been obtained for large skyrmions with a diameter of 50 nm or more [4,5]. It is important to understand what determines the lifetime in order to guide the search for materials where smaller (anti)skyrmions are sufficiently stable at room temperature. From recent experimental studies of skyrmions in $Fe_{1-x}Co_xSi$, a large, destabilizing entropic contribution which reduces the lifetime of skyrmions has been reported [6]. On the other hand, theoretical studies have found that isolated skyrmions can be stabilized by entropic contributions [7–11]. The question we address here is whether this is also the case for the recently observed stable antiskyrmions in acentric tetragonal Heusler compounds [12]. The diameter of these antiskyrmions is large, 150 nm, but it may be possible to modify materials parameters in some way to obtain smaller antiskyrmions that are still stable at room temperature. Antiskyrmions offer some advantage over skyrmions in that they can under some conditions move in the direction of an applied spin polarized current, while skyrmions necessarily move at an angle [13].

Skyrmions have been studied for several systems and recent reviews have summarized results obtained [3,4]. The annihilation of a skyrmion can occur through various mechanisms, in particular collapse in the interior of the sample [14–17] and escape through the boundary of the magnetic domain [16–18]. Two skyrmions can also merge to form a single skyrmion (and the reverse can also occur, i.e., a division of a skyrmion into two) [19]. The calculated lifetime estimates have taken into account the influence of a magnetic field [18], point defects [17], and the width of the track where the skyrmion resides [17]. Calculations have also been carried out for skyrmions in antiferromagnets [20,21]. Recent calculations have addressed how the various materials parameters, such as the Dzyaloshinskii-Moriya interaction (DMI) and anisotropy constants affect the activation energy for the collapse of a skyrmion [7]. The results show that the activation energy is not simply a function of the size of the skyrmion although the two tend to be correlated.

Fewer studies have been carried out on antiskyrmions. They are stabilized by anisotropic Dzyaloshinskii-Moriya interaction (DMI) while isotropic DMI stabilizes skyrmions [12,22]. Some aspects of antiskyrmions in systems with anisotropic DMI have been studied theoretically [13,23–25]. Antiskyrmions can also be stabilized by the magnetostatic interactions, for example, in ion-irradiated Co/Pt multilayer films [26]. Antiskyrmions have, furthermore, been discussed

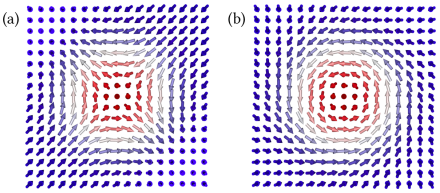

FIG. 1. (a) Antiskyrmion. (b) Bloch skyrmion. The color (red vs blue) indicates the direction of the out-of-plane component of the magnetic vector and the intensity of the color indicates the magnitude.

in relation to skyrmion-antiskyrmion pair production [27–29], in particular, in frustrated ferromagnetic films [30–32]. Monte Carlo simulations using parameters estimated from electronic density functional theory calculations have been used to simulate both skyrmions and antiskyrmions in the Pd/Fe/Ir(111) system and the predicted spin-polarized scanning tunneling microscopy images found to be similar [33]. Antiskyrmions as well as skyrmions in ferromagnetic films have been simulated using the micromagnetic approximation and the effect of the dipole-dipole interaction shown to provide larger stabilization for antiskyrmions [34]. The energy barrier for collapse cannot, however, be evaluated within the micromagnetic approximation since the collapse mechanism involves a singularity that requires a discrete lattice representation.

It is of great interest for potential spintronic applications to carry out more studies of antiskyrmions. Only a few calculations of antiskyrmions have been reported so far, and they have mainly focused on stabilization by frustrated exchange rather than the anisotropic DMI [31,35,36]. Simulation studies of the factors that affect thermal stability have, furthermore, been limited so far to rather small skyrmions that are unstable at room temperature. An important challenge is to extend the simulation methodology in order to make it applicable to large enough lattices to accurately represent the large (anti)skyrmions that have been found experimentally to be stable at room temperature.

In this paper, the stability of antiskyrmions is evaluated using an atomic scale representation and harmonic transition state theory. The calculations reproduce large antiskyrmions observed in the Mn–Pt–Sn inverse Heusler compound [12]. The long lifetime at room temperature is found to be due to high energy barrier for collapse resulting mainly from strong exchange interaction. The pre-exponential factor which includes the entropic effects is, however, found to be of a typical magnitude, 10^{-12} s, despite the large number of spins involved.

II. SIMULATED SYSTEM

The system is described by a Heisenberg-type Hamiltonian

$$\mathcal{H} = -\sum_{\langle i,j\rangle}[J\mathbf{S}_i\cdot\mathbf{S}_j + \mathbf{D}_{ij}\cdot(\mathbf{S}_i\times\mathbf{S}_j)] - \sum_i\left[\mu\mathbf{B}\cdot\mathbf{S}_i + KS_{i,z}^2\right]. \tag{1}$$

Here, J is the exchange constant for the nearest neighbor magnetic moments ($J > 0$), $\mathbf{D}_{ij}$ is the Dzyaloshinskii-Moriya vector lying in the plane of the sample (x-y plane), K is the uniaxial anisotropy constant, $\mathbf{B}$ is the magnetic field, and $\mathbf{S}_i$ is the vector of unit length in the direction of the magnetic moment at site i of a square lattice. The summation $\langle i, j\rangle$ runs over pairs of nearest-neighbor sites. We note that the dipole-dipole interaction is not included in the Hamiltonian in the present calculations. Free boundary conditions are used resulting in an energy barrier for the escape of the antiskyrmion through the boundary and eliminating translational invariance that would lead to zero modes. Such modes require special treatment in the lifetime calculation [37].

Depending on the type of DMI, this Hamiltonian can give rise to skyrmions (Bloch or Néel) or antiskyrmions. If the DMI vector points along the bond connecting sites i and j, a Bloch type skyrmion [shown in Fig. 1(b)] can form. The vector can be written as $\mathbf{D}_{ij} = (\hat{r}_{ij}\cdot\hat{x})\mathbf{D}_1 + (\hat{r}_{ij}\cdot\hat{y})\mathbf{D}_2$ where $\hat{r}_{ij}$ is a unit vector pointing from site i to site j. An anisotropic DMI with $\mathbf{D}_1 = (D, 0, 0)$ and $\mathbf{D}_2 = (0, -D, 0)$ in Eq. (1) supports a symmetric antiskyrmion [shown in Fig. 1(a)] [23,38].

The parameters in the extended Heisenberg Hamiltonian are chosen here to mimic the Mn–Pt–Sn inverse Heusler compound where antiskyrmions have been observed over long time scale at room temperature [12]. The diameter of an antiskyrmion in this material has been measured to be approximately 150 nm, corresponding to 230 lattice constants, and accurate atomic scale modeling therefore requires a square lattice containing at least 900 × 900 lattice points, i.e., nearly a million spins. In order to evaluate the activation energy and estimate the lifetime of the antiskyrmion, it is necessary to use a discrete atomic lattice, rather than the continuum approximation invoked in micromagnetic simulations.

The parameters in the Hamiltonian used here are chosen to be consistent with the previously determined micromagnetic model parameters for this system [12]. There, the antiskyrmions at $T = 300$ K were modeled using the following parameter values: exchange stiffness $A = 1.2\times10^{-10}$ J/m, Dzyaloshinskii-Moriya parameter $d = 6\times10^{-3}$ J/m^2, saturation magnetization $M_s = 445$ kA/m, external field $B =$ 0.29 T, zero anisotropy, and an in-plane lattice constant of $a =$ 0.63 nm and out-of-plane lattice constant of $c =$ 1.22 nm. These micromagnetic parameter values are converted to parameters for the atomic scale lattice Hamiltonian as $J = 2cA = 1830$ meV, $D = acd = 29$ meV, $K = 0$, and $\mu = a^2cM_s = 1.37$ meV/T. We note, however, that the micromagnetic simulations can only be used to determine these quantities relative to the exchange parameter, J, so our calculations are carried out in terms of scaled parameters $D/J =$ 0.016 and $\mu/J = 7.5\times10^{-4}$ T^{-1}.

III. CALCULATIONS OF THE LIFETIME

The lifetime of a magnetic state can generally be described by an Arrhenius rate law, $\tau = \tau_0\exp(E_a/k_BT)$, where E_a is the activation energy for the annihilation event and τ_0 is the so-called pre-exponential factor. The two parameters, τ_0 and E_a, can be estimated using the harmonic approximation to transition state theory (HTST) for magnetic degrees of freedom [39,40]. It is based on an analysis of the

multidimensional energy surface of the system, describing how the energy depends on the angular variables specifying the direction of all the magnetic moments in the system. In the case of interest, the antiskyrmion corresponds to a local minimum on the energy surface, whereas the homogeneous ferromagnetic phase corresponds to the global minimum. The activation energy for annihilation can be estimated as the highest rise in energy along the minimum energy path (MEP) connecting the antiskyrmion minimum to the ferromagnetic minimum. The point of highest energy on the MEP corresponds to a first order saddle point on the energy surface. The MEP can be found using the geodesic nudged elastic band method [14]. The computational effort is reduced here by making use of prior knowledge about the shape of the MEP and by focusing only on a small part of the MEP near the maximum [41].

In HTST, the pre-exponential factor τ_0 is related to the relative vibrational entropy of the initial and transition states as well as the flux through the transition state. The vibrational entropy is estimated by approximating the energy surface in the vicinity of the local minimum and the saddle point as quadratic functions to obtain the frequencies of the vibrational modes. The vibrational entropy of a state is then given by the product of the vibrational frequencies for that state. Normally this involves evaluating the eigenvalues of the Hessian matrix [39], but for large systems, this becomes a challenging calculation. Below, we briefly describe a more efficient method for evaluating τ_0 that does not require the evaluation of the eigenvalues and makes it possible to carry out calculations for the large system studied here. Additional information about the method can be found in Ref. [42]. The lowest couple of eigenvalues of the Hessian are still calculated explicitly using the Lanczos method to ensure that only one negative eigenvalue is found at the obtained saddle point and to test for the possible presence of zero modes.

An atomic scale simulation of such a large system is computationally challenging because of the large number of variables. In order to reduce computational effort, we use the following scaling method. A sequence of calculations is carried out for systems with decreasing in-plane lattice constant, a, and increasing number of spins in such a way as to keep the values of the parameters corresponding to the micromagnetic model constant. Letting $a_N = a_1/N$ denote the in-plane lattice constant after N iterations and referring to the relationship between micromagnetic model parameters, which are kept constant, and atomic lattice parameters, which depend on the lattice constant, the following scaling relationships are obtained: $D_N = D_1/N$ and $\mu_N = \mu_1/N^2$ while the exchange constant J is unchanged as it is independent of a. The number of spins is $45N \times 45N$, starting from $N = 1$, and eventually reaching the 900×900 when $N = 20$ giving spacing between sites that corresponds to the lattice constant of the Mn–Pt–Sn inverse Heusler compound. The calculation for an MEP for a given N starts from an initial guess obtained from the calculation with $N - 1$. The minimum energy path, as well as initial and saddle point configurations, for $N = 1$ are presented in Fig. 2. Figure 3 shows the spin configurations corresponding to the first three values of N.

The pre-exponential factor is evaluated separately for each N but without having to determine the eigenvalues of the Hessian as has been done in previous calculations [39,40]. It is difficult to obtain high enough accuracy for the eigenvalues when the number of spins is so large. Since the dipole-dipole interaction is not included here explicitly, only the nearest neighbors interact making it possible to write the Hessian matrix in a block tri-diagonal form and thereby evaluate the determinant of the Hessian. The pre-exponential factor is then evaluated from the determinant directly without having to determine the eigenvalues. It can be written as

$$\tau_0 = \frac{2\pi}{\lambda \Omega_0}, \tag{2}$$

where the factor Ω_0 is a ratio of determinants of the Hessian at the initial state minimum $H^{\min}$ and at the saddle point H^{sp},

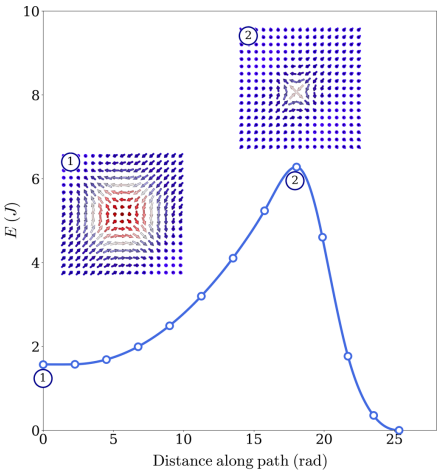

FIG. 2. Minimum energy path for the collapse of an antiskyrmion in a system when $N = 1$, i.e., containing 45×45 spins. The initial state and saddle point spin configurations are shown in insets (only part of the simulated system is shown). The final state at a distance of around 25 radians is the ferromagnetic state. The distance along the path is the sum of the geodesic displacements corresponding to changes in the orientation of all the magnetic vectors in the system.

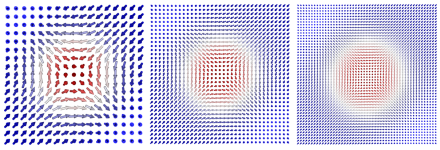

FIG. 3. Antiskyrmion configuration for $N = 1$ (left), 2 (middle), and 3 (right). The color (red vs blue) indicates the direction of the out-of-plane component of the magnetic vector and the intensity of the color indicates the magnitude.

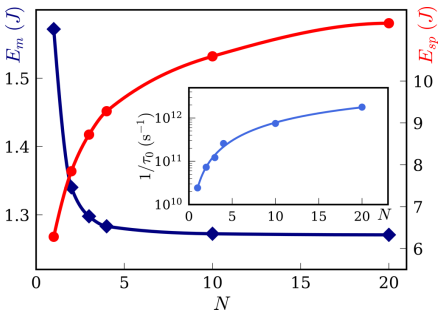

FIG. 4. Antiskyrmion energy at the local minimum, E_m (blue line with diamonds), and at the saddle point for collapse, E_{sp} (red line with circles), as a function of the scaling parameter N. The inset shows the pre-exponential factor in the Arrhenius rate law for antiskyrmion collapse as a function of N assuming $J = 110$ meV. The lattice parameter in the coarse grained simulation model corresponds that of the Mn–Pt–Sn inverse Heusler compound [12] when $N = 20$.

i.e.,

$$\Omega_0 = \frac{\sqrt{\det H^{\min}}}{\sqrt{|\det H^{sp}|}}. \tag{3}$$

It is connected with the ratio of the entropy of the initial state and the entropy of the transition state, both evaluated within the harmonic approximation. The factor λ is connected with the dynamics of the system through the transition state and is evaluated from a basis invariant expression as

$$\lambda = \sqrt{\frac{\mathbf{b}\cdot H^{sp}\mathbf{b}}{|\zeta|}}, \quad \text{with } \mathbf{b} = \frac{\gamma\zeta}{\mu}\mathbf{S}^{sp}\times\mathbf{e}, \tag{4}$$

where $\mathbf{S}^{sp}$ is the spin configuration at the saddle point, ζ the negative eigenvalue of H^{sp}, $\mathbf{e}$ the corresponding eigenvector (a unit tangent vector to the MEP at the saddle point), and γ the gyromagnetic ratio. This expression for λ can be evaluated numerically even for large systems since it can be computed in spin-related basis without the evaluation of the whole set of eigenvectors and eigenvalues of H^{sp} [21].

Figure 4 shows the energy of the antiskyrmion with respect to the uniform ferromagnetic state and the energy of the saddle point as a function of the scaling parameter N. The energy at the local minimum corresponding to the antiskyrmion almost reaches a constant as the parameter N is increased, while the energy of the saddle point is still increasing at $N = 20$. The lattice effects are still strong at $N = 20$ and the Belavin-Polyakov limit [43] of $4\pi J$ has not yet been reached. For the full 900×900 lattice corresponding to $N = 20$, the antiskyrmion energy is found to be $E_m/J = 1.27$ and the saddle point energy $E_{sp}/J = 11.38$. Thus, the energy barrier for the collapse of the antiskyrmion is $E_a/J = 10.11$. (See Ref. [44] for an animation of the MEP for antiskyrmion collapse when $N = 1$).

The largest uncertainty lies in the value of the exchange parameter, J. The value of exchange stiffness used in the micromagnetic modeling of Nayak *et al.* [12] corresponds to $J = 1830$ meV for the lattice representation. Even for a much smaller value of $J = 110$ meV, the activation energy for collapse is large, ca. 1 eV. However, the pre-exponential factor turns out to have a typical value of 10^{-12} s (see inset in Fig. 4). Together, these values give a lifetime of a month at room temperature. A larger value of J would give even longer lifetime. This high stability is in good agreement with the reported experimental observations [12]. The reason for the long lifetime is the large activation energy for the collapse of the antiskyrmion in this material while the pre-exponential factor, which is related to entropic effects, has a value that is similar to what has been calculated previously for the collapse of small skyrmions [18].

IV. CONCLUSIONS

Calculations of the lifetime of large but submicron scale antiskyrmions in Mn–Pt–Sn tetragonal Heusler material are presented. The results are consistent with the observed stability at room temperature in recent experiments [12] and show that the long lifetime is due to large activation energy for collapse rather than entropic effects. Since the atomic scale representation of this system requires roughly a million spins, the calculations are challenging and are made possible by using a scaling approach to evaluate the activation energy and an improved method for evaluating the pre-exponential factor in the Arrhenius rate expression. The latter is possible because the dipole-dipole interaction is not included here. Previous studies using the micromagnetic approach have shown that the dipole-dipole interaction makes antiskyrmions more stable with respect to skyrmions [34]. The rate of collapse cannot, however, be evaluated from micromagnetic simulations but we expect that the inclusion of dipole-dipole interaction would further increase the activation energy while not affecting the value of the pre-exponential factor significantly.

ACKNOWLEDGMENTS

This work was supported by the Icelandic Research Fund, the Research Fund of the University of Iceland, and the Russian Science Foundation (Grant 19-42-06302). The calculations were carried out at the Icelandic Research High Performance Computing facility.

[1] N. S. Kiselev, A. N. Bogdanov, R. Schäfer, and U. K. Rössler, Chiral skyrmions in thin magnetic films: new objects for magnetic storage technologies? J. Phys. D: Appl. Phys. **44**, 392001 (2011).

[2] A. Fert, V. Cros, and J. Sampaio, Skyrmions on the track, Nat. Nanotechnol. **8**, 152 (2013).

[3] A. Fert, N. Reyren, and V. Cros, Magnetic skyrmions: advances in physics and potential applications, Nat. Rev. Mater. **2**, 17031 (2017).

[4] K. Everschor-Sitte, J. Masell, R. M. Reeve, and M. Kläui, Perspective: Magnetic skyrmions – Overview of recent progress in an active research field, J. Appl. Phys. **124**, 240901 (2018).

[5] A. Soumyanarayanan, M. Raju, A. L. Oyarce, T. Gonzalez, K. C. Anthony, M-Y. Im, A. P. Petrović, P. Ho, K. H. Khoo, M. Tran, and C. K. Gan, Tunable room-temperature magnetic skyrmions in Ir/Fe/Co/Pt multilayers, Nat. Mater. **16**, 898 (2017).

[6] J. Wild, T. N. G. Meier, S. Pöllath, M. Kronseder, A. Bauer, A. Chacon, M. Halder, M. Schowalter, A. Rosenauer, J. Zweck, J. Müller, A. Rosch, C. Pfleiderer, and C. H. Back, Entropy-limited topological protection of skyrmions, Sci. Adv. **3**, e1701704 (2017).

[7] A. S. Varentsova, M. N. Potkina, S. von Malottki, S. Heinze, and P. F. Bessarab, Interplay between size and stability of magnetic skyrmions, Nanosystems: Phys. Chem. Math. **9**, 356 (2018).

[8] L. Desplat, D. Suess, J.-V. Kim, and R. L. Stamps, Thermal stability of metastable magnetic skyrmions: Entropic narrowing and significance of internal eigenmodes, Phys. Rev. B **98**, 134407 (2018).

[9] S. von Malottki, P. F. Bessarab, S. Haldar, A. Delin, and S. Heinze, Skyrmion lifetime in ultrathin films, Phys. Rev. B **99**, 060409(R) (2019).

[10] L. Desplat, C. Vogler, J.-V. Kim, R. L. Stamps, and D. Suess, Path sampling for lifetimes of metastable magnetic skyrmions and direct comparison with Kramers' method, Phys. Rev. B **101**, 060403(R) (2020).

[11] M. Hoffmann, G. P. Müller, and Stefan Blügel, Atomistic Perspective of Long Lifetimes of Small Skyrmions at Room Temperature, Phys. Rev. Lett. **124**, 247201 (2020).

[12] A. K. Nayak, V. Kumar, T. Ma, P. Werner, E. Pippel, R. Sahoo, F. Damay, U. K. Rößler, C. Felser, and S. S. P. Parkin, Magnetic antiskyrmions above room temperature in tetragonal Heusler materials, Nature (London) **548**, 561 (2017).

[13] S. Huang, C. Zhou, G. Chen, H. Shen, A. K. Schmid, K. Liu, and Y. Wu, Stabilization and current-induced motion of antiskyrmion in the presence of anisotropic Dzyaloshinskii-Moriya interaction, Phys. Rev. B **96**, 144412 (2017).

[14] P. F. Bessarab, V. M. Uzdin, and H. Jónsson, Method for finding mechanism and activation energy of magnetic transitions applied to skyrmion and antivortex annihilation, Comput. Phys. Commun. **196**, 335 (2015).

[15] I. S. Lobanov, H. Jónsson, and V. M. Uzdin, Mechanism and activation energy of magnetic skyrmion annihilation obtained from minimum energy path calculations, Phys. Rev. B **94**, 174418 (2016).

[16] D. Stosic, J. Mulkers, B. Van Waeyenberge, T. Ludermir, and M. V. Milosević, Paths to collapse for isolated skyrmions in few-monolayer ferromagnetic films, Phys. Rev. B **95**, 214418 (2017).

[17] V. M. Uzdin, M. N. Potkina, I. S. Lobanov, P. F. Bessarab, and H. Jónsson, Energy surface and lifetime of magnetic skyrmions, J. Magn. Magn. Mater. **459**, 236 (2018).

[18] P. F. Bessarab, G. P. Müller, I. S. Lobanov, F. N. Rybakov, N. S. Kiselev, H. Jónsson, V. M. Uzdin, S. Blügel, L. Bergqvist, and A. Delin, Lifetime of racetrack skyrmions, Sci. Rep. **8**, 3433 (2018).

[19] G. P. Müller, P. F. Bessarab, S. M. Vlasov, F. Lux, N. S. Kiselev, V. M. Uzdin, S. Blügel, and H. Jónsson, Duplication Collapse and Escape of Magnetic Skyrmions Revealed Using a Systematic Saddle Point Search Method, Phys. Rev. Lett. **121**, 197202 (2018).

[20] P. F. Bessarab, D. Yudin, D. R. Gulevich, P. Wadley, M. Titov and O. A. Tretiakov, Stability and lifetime of antiferromagnetic skyrmions, Phys. Rev. B **99**, 140411(R) (2019).

[21] M. N. Potkina, I. S. Lobanov, H. Jónsson, and V. M. Uzdin, Skyrmions in antiferromagnets: thermal stability and the effect of external field and impurities, J. Appl. Phys. **127**, 213906 (2020).

[22] O. Meshcheriakova, S. Chadov, A. K. Nayak, U. K. Rößler, J. Kübler, G. André, A. A. Tsirlin, J. Kiss, S. Hausdorf, A. Kalache, W. Schnelle, M. Nicklas, and C. Felser, Large Noncollinearity and Spin Reorientation in the Novel Mn_2RhSn Heusler Magnet, Phys. Rev. Lett. **113**, 087203 (2014).

[23] U. Güngördü, R. Nepal, O. A. Tretiakov, K. Belashchenko, and A. A. Kovalev, Stability of skyrmion lattices and symmetries of quasi-two-dimensional chiral magnets, Phys. Rev. B **93**, 064428 (2016).

[24] M. Hoffmann, B. Zimmermann, G. P. Müller, D. Schürhoff, N. S. Kiselev, C. Melcher, and S. Blügel, Antiskyrmions stabilized at interfaces by anisotropic Dzyaloshinskii-Moriya interactions, Nat. Commun. **8**, 308 (2017).

[25] A. A. Kovalev and S. Sandhoefner, Skyrmions and antiskyrmions in quasi-two-dimensional magnets, Front. Phys. **6**, 98 (2018).

[26] S. Zhang, A. K. Petford-Long and C. Phatak, Creation of artificial skyrmions and antiskyrmions by anisotropy engineering, Sci. Rep. **6**, 31248 (2016).

[27] W. Koshibae and N. Nagaosa, Creation of skyrmions and antiskyrmions by local heating, Nat. Commun. **5**, 5148 (2014).

[28] W. Koshibae and N. Nagaosa, Theory of antiskyrmions in magnets, Nat. Commun. **7**, 10542 (2016).

[29] M. Stier, W. Haüsler, T. Posske, G. Gurski, and M. Thorwart, Skyrmion–Anti-Skyrmion Pair Creation by In-Plane Currents, Phys. Rev. Lett. **118**, 267203 (2017).

[30] L. O. Leonov and M. Mostovoy, Multiply periodic states and isolated skyrmions in an anisotropic frustrated magnet, Nat. Commun. **6**, 8275 (2015).

[31] S. von Malottki, B. Dupé, P. F. Bessarab, A. Delin, and S. Heinze, Enhanced skyrmion stability due to exchange frustration, Sci. Rep. **7**, 12299 (2017).

[32] X. Zhang, J. Xia, Y. Zhou, X. Liu, H. Zhang, and M. Ezawa, Skyrmion dynamics in a frustrated ferromagnetic film and current-induced helicity locking-unlocking transition, Nat. Commun. **8**, 1717 (2017).

[33] B. Dupé, C. N. Kruse, T. Dornheim, and S. Heinze, How to reveal metastable skyrmionic spin structures by spin-polarized scanning tunneling microscopy, New J. Phys. **18**, 055015 (2016).

[34] L. Camosi, N. Rougemaille, O. Fruchart, J. Vogel, and S. Rohart, Micromagnetics of antiskyrmions in ultrathin films, Phys. Rev. B **97**, 134404 (2018).

[35] U. Ritzmann, S. von Malottki, J.-V. Kim, S. Heinze, J. Sinova, and B. Dupé, Trochoidal motion and pair generation in skyrmion and antiskyrmion dynamics under spin–orbit torques, Nat. Electron. **1**, 451 (2018).

[36] L. Desplat, J.-V. Kim, and R. L. Stamps, Paths to annihilation of first- and second-order (anti)skyrmions via (anti)meron nucleation on the frustrated square lattice, Phys. Rev. B **99**, 174409 (2019).

[37] A. Ivanov, P. F. Bessarab, V. M. Uzdin, and H. Jónsson, Magnetic exchange force microscopy: Theoretical analysis of induced magnetization reversals, Nanoscale **9**, 13320 (2017).

[38] A. N. Bogdanov and D. A. Yablonskii, Thermodynamically stable "vortices" in magnetically ordered crystals. The mixed state of magnets, Sov. Phys. JETP **68**, 101 (1989).

[39] P. F. Bessarab, V. M. Uzdin, and H. Jónsson, Harmonic transition state theory of thermal spin transitions, Phys. Rev. B **85**, 184409 (2012).

[40] P. F. Bessarab, V. M. Uzdin, and H. Jónsson, Potential energy surfaces and rates of spin transitions, Z. Phys. Chem. **227**, 1543 (2013).

[41] I. S. Lobanov, M. N. Potkina, H. Jónsson, and V. M. Uzdin, Truncated minimum energy path method for finding first order saddle points, Nanosyst. Phys. Chem. Math. **8**, 586 (2017).

[42] I. S. Lobanov and V. M. Uzdin, The lifetime of big size topological chiral magnetic states. Estimation of the pre-exponential factor in the Arrhenius law, arXiv:2008.06754.

[43] A. A. Belavin and A. M. Polyakov, Metastable states of two-dimensional isotropic ferromagnets, Sov. Phys. JETP Lett. **22**, 245 (1975).

[44] See Supplemental Material at http://link.aps.org/supplemental/10.1103/PhysRevB.102.134430 for an animation of the MEP for the collapse of an antiskyrmion.